2025-11-25

Optimized Control of a Brushless Doubly Fed Reluctance Motor using a Sliding Mode Controller

Singh, Anushree Yogendrapal

UNIVERSITY OF CALGARY

Optimized Control of a Brushless Doubly Fed Reluctance Motor using a Sliding Mode Controller

by

Anushree Singh

A THESIS

SUBMITTED TO THE FACULTY OF GRADUATE STUDIES

IN PARTIAL FULFILMENT OF THE REQUIREMENTS FOR THE

DEGREE OF MASTER OF SCIENCE

GRADUATE PROGRAM IN ELECTRICAL ENGINEERING

CALGARY, ALBERTA

NOVEMBER, 2025

Abstract

Brushless Doubly Fed Reluctance Machines (BDFRMs) have emerged as strong candidates for limited accessibility and sustainable applications such as wind energy conversion systems and variable speed pump drives due to their characteristic advantages such as low maintenance, reduced converter cost, and independence from rare earth magnets. However, the complex nonlinear characteristics of BDFRMs, coupled with the presence of significant current and flux harmonics, make high performance current control particularly challenging.

This thesis proposes the use of a Discrete Time Super Twisting Sliding Mode (DTSTSM) controller under a Field Oriented Control (FOC) framework to address these issues. The DTSTSM controller provides fast dynamic response, improved robustness, and reduced chattering, which are crucial for nonlinear systems like BDFRMs. To ensure optimal performance, the controller parameters are tuned automatically using a Particle Swarm Optimization (PSO) algorithm.

A detailed harmonic analysis of the BDFRM is carried out to study the influence of its inherent nonlinearity on control performance. Experimental validation is conducted using a conventional PI controller for comparison. The results demonstrate that the proposed DTSTSM controller strategy significantly improves current tracking accuracy and dynamic response while maintaining stability under varying operating conditions. This work contributes to the ongoing development of effective control strategies for BDFRMs and promotes their use in clean energy generation and consumption sectors.

Preface

This thesis is an original work by the author. Some parts of the research conducted for this thesis has been previously published in two conference papers:

- A. Singh, F. P. Scalcon and A. M. Knight, "Challenges in the Control of Brushless Doubly Fed Reluctance Machines," 2025 IEEE Industry Applications Society Annual Meeting (IAS), Taipei, Taiwan, 2025, pp. 1-7, doi: 10.1109/IAS62731.2025.11061502.
- A. Singh, F. P. Scalcon and A. M. Knight, "Optimized Discrete-Time Super-Twisting Sliding Mode Control for Brushless Doubly Fed Reluctance Machines," presented at 2025 IEEE Energy Conversion Congress and Exposition (ECCE), Philadelphia, PA, USA, 2025.

Acknowledgements

First and foremost, I would like to express my deepest gratitude to my supervisor, Dr. Andrew M. Knight, for his unwavering support, guidance, and mentorship throughout the course of my Master's research. I am truly grateful for the opportunity to work under his supervision. His patience, kindness, and encouragement gave me the confidence to explore new ideas and persevere through challenges. I have learned immensely from his expertise, and his belief in my potential has played a vital role in my academic journey.

I would also like to sincerely thank the University of Calgary for providing an enriching academic environment that fostered both my personal and professional growth. The financial assistance through scholarships and funding greatly eased my path and enabled me to focus on my research with dedication.

Finally, and most importantly, I wish to acknowledge my mother, who is and will always remain my greatest inspiration. Her unwavering strength, love, and sacrifice have made me who I am today. It is because of her hard work and resilience that I have been able to pursue my dreams. She is the cornerstone of my life, and I dedicate this achievement to her.

To my mother, for her endless love, support, and sacrifices that made this journey possible

Table of Contents

List of Figures

List of Tables

List of Symbols, Abbreviations, and Nomenclature

Symbol	Definition
p_r	Number of rotor poles
p_1	Number of primary winding poles
p_2	Number of secondary winding poles
ω_m	Mechanical rotor speed
ω_1	Primary winding electrical angular frequency
ω_2	Secondary winding electrical angular frequency
f_r	Rotor electrical frequency
d	Direct axis
q	Quadrature axis
$i_{a,b,c}$	Three phase time-varying current
$i_{d,q}$	Time-invariant current in orthogonal $d-q$ rotating reference frame
$i_{\alpha,\beta}$	Time-variant current in orthogonal $\alpha-\beta$ reference frame
$\underline{v}_{1s}$	Primary winding voltage space vector in the stationary reference frame
$\underline{v}_{2s}$	Secondary winding voltage space vector in the stationary reference frame
$\underline{i}_{1s}$	Primary winding current space vector in the stationary reference frame
$\underline{i}_{2s}$	Secondary winding current space vector in the stationary reference frame
$\underline{\lambda}_{1s}$	Primary winding flux linkage space vector in the stationary reference frame
$\underline{\lambda}_{2s}$	Secondary winding flux linkage space vector in the stationary reference frame
r_1	Primary winding phase resistance
r_2	Secondary winding phase resistance
θ_r	Rotor electrical angle

θ_m	Rotor mechanical angle
λ_{1abc}	Primary winding three phase flux linkage
λ_{2abc}	Secondary winding three phase flux linkage
i_{1abc}	Primary winding three phase current
i_{2abc}	Secondary winding three phase current
v_{1abc}	Primary winding three phase voltage
v_{2abc}	Secondary winding three phase voltage
L_{1m}	Primary winding magnetizing inductance
L_{2m}	Secondary winding magnetizing inductance
L_{1l}	Primary winding leakage inductance
L_{2l}	Secondary winding leakage inductance
$L_{12_{max}}$	Peak mutual inductance between primary and secondary winding
θ_p	Electrical angular position of the primary winding current space vector
θ_s	Electrical angular position of the secondary winding current space vector
ω_p	Electrical angular frequency of the primary winding current space vector
ω_s	Electrical angular frequency of the secondary winding current space vector
θ_1	Electrical angular position of the primary winding d_1q_1 rotating reference frame
θ_2	Electrical angular position of the secondary winding d_2q_2 rotating reference frame
$\underline{\lambda}_{1r}$	Primary winding flux linkage space vector in the rotating reference frame
$\underline{\lambda}_{2r}$	Secondary winding flux linkage space vector in the rotating reference frame
$\underline{v}_{1r}$	Primary winding voltage space vector in the d_1q_1 rotating reference frame
$\underline{v}_{2r}$	Secondary winding voltage space vector in the d_2q_2 rotating reference frame
$\underline{i}_{1r}$	Primary winding current space vector in the d_1q_1 rotating reference frame
$\underline{i}_{2r}$	Secondary winding current space vector in the d_2q_2 rotating reference frame
$v_{1d,q}$	Primary winding $d-q$ axis voltage in the d_1q_1 rotating reference frame
$v_{2d,q}$	Secondary winding $d-q$ axis voltage in the d_2q_2 rotating reference frame
$i_{1d,q}$	Primary winding $d-q$ axis current in the d_1q_1 rotating reference frame
$i_{2d,q}$	Secondary winding $d-q$ axis current in the d_2q_2 rotating reference frame
$v_{1\alpha,\beta}$	Primary winding $\alpha-\beta$ axis voltage in the orthogonal $\alpha-\beta$ stationary reference frame
$v_{2\alpha,\beta}$	Secondary winding $\alpha-\beta$ axis voltage in the orthogonal $\alpha-\beta$ stationary reference frame
$i_{1\alpha,\beta}$	Primary winding $\alpha-\beta$ axis current in the orthogonal $\alpha-\beta$ stationary reference frame

$i_{2\alpha,\beta}$	Secondary winding$\alpha - \beta$ axis current in the orthogonal $\alpha - \beta$ stationary reference frame
$\lambda_{1d,q}$	Primary winding $d - q$ axis flux linkage in the d_1q_1 rotating reference frame
$\lambda_{2d,q}$	Secondary winding $d - q$ axis flux linkage in the d_2q_2 rotating reference frame
T_e	Developed electrical torque in the three phase reference frame
f_1	Primary winding electrical frequency
f_2	Secondary winding electrical frequency
f_{1ref}	Primary winding electrical frequency reference
$i_{2d_{ref}}$	Secondary winding d axis reference current in the d_2q_2 rotating reference frame
$i_{2q_{ref}}$	Secondary winding q axis reference current in the d_2q_2 rotating reference frame
$\omega_{m_{ref}}$	Mechanical rotor speed reference
n_m	Measured rotor mechanical speed in RPM
n_{ref}	Reference rotor mechanical speed in RPM
L_1	Primary winding self inductance
L_2	Secondary winding self inductance
L_{12}	Mutual inductance between primary and secondary windings
K_p	Proportional gain of PI controller
K_i	Integral gain of PI controller
K_1	Gain 1 of the DTSTSM controller
K_2	Gain 2 of the DTSTSM controller
T_s	Sampling time period used in DTSTSM controller
F_c	Cut-off frequency of the LPF
AC	Alternating Current
BDFIM	Brushless Doubly Fed Induction Machine
BDFM	Brushless Doubly Fed Machine
BDFRM	Brushless Doubly Fed Reluctance Machine
CNC	Computer Numeric Control
DAC	Digital to Analog Converter
DC	Direct Current
DFM	Doubly Fed Machine
DPC	Direct Power Control
DSP	Digital Signal Processor
DTC	Direct Torque Control

DTSTSM	Discrete Time Super Twisting Sliding Mode
EP	Evolutionary Programming
EV	Electric Vehicle
FOC	Field Oriented Control
GA	Genetic Algorithms
HOSM	Higher Order Sliding Mode
IIR	Infinite Impulse Response
IGBT	Insulated Gate Bipolar Transistor
IM	Induction Motor
LPF	Low Pass Filter
MMF	Magnetomotive Force
MIMO	Multi Input Multi Output
MPPT	Maximum Power Point Tracking
NdFeB	Neodymium Iron Boron
PI	Proportional Integral
PMSM	Permanent Magnet Synchronous Motor
PSO	Particle Swarm Optimization
PWM	Pulse Width Modulation
RPM	Revolutions Per Minute
SM	Synchronous Motor
SMC	Sliding Mode Control
SmCo	Samarium Cobalt
SRM	Switched Reluctance Motor
STA	Super Twisting Algorithm
SVPWM	Space Vector Pulse Width Modulation
SVM	Space Vector Model
SynRM	Synchronous Reluctance Motor
V/f	Volts per Hertz
VSC	Variable Structure Control
WECS	Wind Energy Conversion System

Epigraph

If I have seen further, it is by standing on the shoulders of giants.

- Isaac Newton

Chapter 1

Introduction

1.1 Background

Electrical energy plays a vital role in the modern society. Among all forms of energy, it is the most versatile and easiest to convert from one form to another like mechanical, thermal, chemical, or light. Additionally, it can be transported over long distances with minimal losses, especially through high voltage transmission lines [1]. These characteristics make electrical energy the most dominant and preferred form of energy across the globe.

With increasing industrialization, and urbanization the demand for electric energy has grown rapidly. This electricity consumption is projected to rise significantly in the coming decades, as illustrated in [2], which presents the long term outlook for electricity demand and generation in the Canadian province of Alberta.

However, this surge in electricity demand has led to the excessive consumption of fossil fuels for power generation which has not only accelerated the depletion of non-renewable resources but also contributed significantly to greenhouse gas emissions, environmental pollution, and global warming. These detrimental impacts have prompted governments, research institutions, and industries worldwide to prioritize sustainable and green energy solutions, as shown by the Clean Electricity Regulations published by the Government of Canada [3].

Consequently, there has been a global shift toward renewable energy sources such as solar and wind for electricity generation. In terms of consumption, the focus has turned to electric vehicles, energy efficient appliances, and electric motors that avoid the use of rare earth metals and permanent magnet resources that are both expensive and environmentally degrading to extract and process.

1.2 Electric Machines in Energy Systems

Electric machines, particularly electric motors and generators, are fundamental to both the production and utilization of electrical energy. They are found in almost every aspect of modern infrastructure from transportation and manufacturing to small scale household appliances.

Historically, the development of electric machines began with Michael Faraday's demonstration of electromagnetic induction in 1821, which laid the foundation for the first DC motors [4]. Despite their pioneering significance, early DC motors were expensive and not commercially viable. This limitation prompted the development of AC motors, which are more robust, efficient, and better suited to modern AC power grids [5]. Among these, the induction motor (IM) was the first widely adopted AC motor, followed by several others. Today, electric motors can be broadly categorized into two main types: AC and DC motors. Figure 1.1 shows the broad classification of the electric motors.

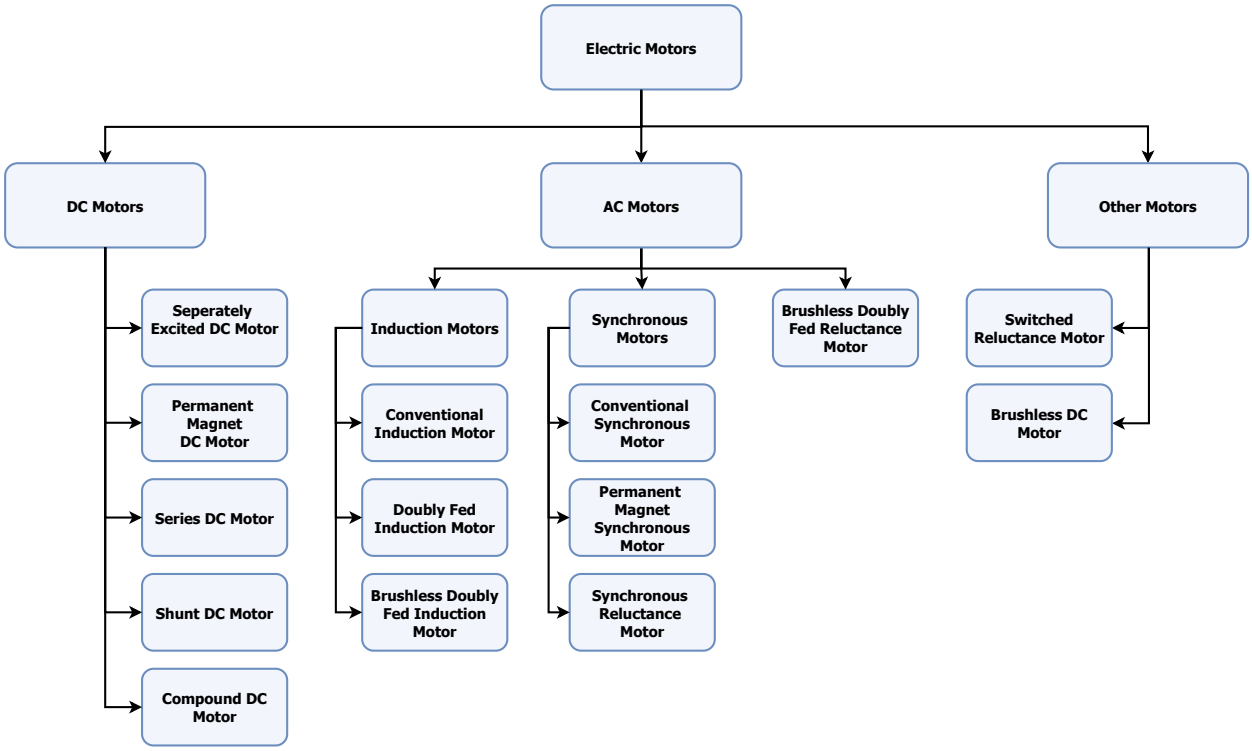

Figure 1.1: Classification of Electric Motors

In terms of energy consumption, the industrial sector is the largest consumer of electrical energy, largely through various electric motor driven variable speed drives employed in diverse applications such as electric traction, CNC machines, pumps, fans etc. Achieving efficient and precise control over the speed and torque of electric motors is important for the satisfactory operation of these drives. Hence, ongoing research has

focused on developing high performance electric motors. Additionally, designing effective control strategies to ensure precise speed control, and robustness against disturbances has also been a major research priority.

Initially, separately excited DC motors gained popularity due to their inherent decoupling of torque producing and flux producing current components, allowing for straightforward control [6]. In these motors, the armature winding on the rotor generates torque, while the field winding on the stator produces the magnetic field. This decoupling enables independent control of torque and flux. However, DC motors have notable disadvantages, including low torque density, high copper losses, and frequent maintenance requirements due to the presence of brushes and commutators, all of which reduce robustness and overall reliability. Consequently, AC motors have become the preferred choice in most applications.

Among AC motors, Induction Motors (IMs) are the most widely used. Induction motors quickly became widely adopted due to their simple and robust construction, self starting ability, low maintenance requirements, and lower cost [6]. Their self starting capability makes it possible to directly connect them to the power supply without the need for power converters, making them convenient for constant speed operations. However, induction motors also have certain drawbacks. These asynchronous motors operate at speeds below synchronous speed. This leads to induced currents in the rotor that causes rotor losses, reducing the motor efficiency [7]. Furthermore, an IM always operates at lagging power factor. These limitations paved the way for the development of synchronous motors that have higher efficiency [7].

Synchronous Motors (SMs) operate at synchronous speed and typically use an external DC excitation source for the rotor winding [6]. The configuration of the SM allows the motor to operate at varying power factors depending on the rotor excitation. Additionally, synchronous motors have relatively simple control algorithms based on supply frequency and voltage. Despite these advantages, the use of slip rings and brushes in the rotor structure reintroduces mechanical complexity and maintenance issues increasing the maintenance cost while also introducing rotor copper losses.

To resolve this, Permanent Magnet Synchronous Motors (PMSMs) were developed [8] by replacing the DC excited rotor with permanent magnets, commonly using rare earth magnets like Samarium Cobalt (SmCo) and Neodymium Iron Boron (NdFeB). PMSMs feature stator windings connected to an AC supply and permanent magnets mounted on the rotor [6]. This configuration eliminates the need for external DC excitation for the rotor and associated components like brushes and slip rings in the rotor structure, thereby eliminating high maintenance cost, reducing rotor losses and allowing for a more compact and efficient machine with high torque density. PMSMs also retain the advantages of synchronous motors and offer simpler control schemes. Yet, their dependence on rare earth magnets introduces several critical limitations like high cost and supply risk due to limited geographical availability [9], thermal demagnetization at high operating speeds and temperatures [10] and environmental impact associated with mining and processing of

rare earth elements [11] that raise concerns about sustainability and long term viability.

In light of these limitations, research has increasingly focused on developing electric machines that maintain high performance while eliminating dependence on permanent magnets. Among the alternatives, reluctance based machines such as Switched Reluctance Motors (SRMs) and Synchronous Reluctance Motors (SynRMs) have gained attention due to their simple rotor construction and absence of magnets [12, 13]. However, these machines often suffer from high torque ripple, poor power factor, increased acoustic noise, and require complex control and converter topologies [14].

To achieve better performance while maintaining cost and material efficiency, Doubly Fed Machines (DFMs) have emerged as a viable class of electric machines [15–17]. These machines offer greater controllability and flexibility in speed variation using partially rated power converters, which control only one of the two windings. This results in reduced power converter cost and lower power electronics stress. However, traditional DFMs use rotor windings, brushes, and slip rings bringing back issues of increased maintenance, rotor losses and reduced reliability [18].

To overcome these problems, Brushless Doubly Fed Machines (BDFMs) were developed [19], incorporating both windings on the stator and eliminating the need for brushes and slip rings in the rotor structure, leading to reduced maintenance and operational costs. The most commonly used BDFM variant has been the brushless doubly fed induction machine (BDFIM) [20], featuring two stator windings and a cage or wound rotor. Despite improvements, BDFIMs still experience rotor losses, similar to those of conventional IMs. Thus, to overcome this, the brushless doubly fed reluctance machine (BDFRM) was developed [21]. The BDFRM stands out as a highly promising candidate for advanced applications due to its unique structural and operational benefits.

A BDFRM consists of two stator windings, namely power winding and control winding and a reluctance rotor [21–23]. This design leads to several advantages. The absence of brushes and slip rings leads to low maintenance requirement. The two windings facilitates the use of a partially rated converter, reducing converter costs. The reluctance rotor eliminates the wound or cage rotor in the IM counterpart, resulting in minimal rotor losses, greater robustness, and no reliance on permanent magnets. Another distinctive feature of the BDFRM is its ability to operate across a wide speed range including sub-synchronous, synchronous, and super-synchronous speeds. Owing to the unique characteristics of a BDFRM, they can be operated as both a synchronous and an asynchronous machine depending upon the implemented control strategy for the energization of the stator windings.

The early development of BDFRMs was hindered by the limitations of initial prototypes, which exhibited low efficiency and poor power factor [22, 23]. However, recent research has shifted focus toward improving the machine's design to improve performance. As a result, newer prototypes have demonstrated significantly

improved torque density [24]. In addition, various rotor topologies have been explored to further improve overall performance [25–27]. Consequently, modern BDFRMs are now capable of operating across a wide speed range while maintaining suitable torque density and performance [24]. The development of BDFRMs over the years is further discussed in the next chapter.

1.3 Research Motivation

Electric motors account for a major portion of the global electrical energy consumption. Therefore, the development of high performance electric motors along with the design of their effective control strategies is essential. Over the years, several electric motor technologies have been developed, and investigated, including Direct Current (DC) motors, Induction Motors (IM), Synchronous Motors (SM), Permanent Magnet Synchronous Motors (PMSM), Switched Reluctance Motors (SRM), Synchronous Reluctance Motors (SynRMs), Doubly Fed Induction Motors (DFIM), Brushless Doubly Fed Induction Motors (BDFIM), and Brushless Doubly Fed Reluctance Motors (BDFRMs). Among these, the BDFRM stands out by offering several key advantages such as reduced rotor losses, low maintenance requirement, ability to operate with partially rated converter which significantly reduces converter cost, enhanced robustness, and no reliance on rare earth magnets.

These characteristic advantages offered by the BDFRM, makes it particularly suitable for variable speed applications with limited accessibility. Consequently, BDFRM has emerged as a highly attractive candidate for integration into wind energy conversion systems (WECS) and large scale variable speed pump drives. The doubly fed characteristic of the BDFRM is preferred for WECS application since it facilitates the variable speed operation of the wind turbine. Furthermore, the ability to operate with partially rated converters significantly reduces converter cost in a high power large scale WECS. Furthermore, BDFRM directly replaces the currently used Doubly Fed Induction Machine (DFIM) in the WECS as BDFRM is brushless, requires low maintenance and is more robust which is particularly more advantageous for offshore wind turbine generation systems with limited accessibility. Additionally, BDFRM can be directly coupled to the wind turbine as compared to the DFIM that requires a high ratio gear box. Lastly, the reluctance rotor used in BDFRM as compared to cage or wound rotor in DFIM, eliminates induced rotor current resulting in minimal rotor losses and reduced heating. Therefore, BDFRM proves to be a strong candidate for application in WECS.

As previously discussed, the negative environmental impact of electricity generation through conventional methods has led to a global paradigm shift towards greener electricity generation and consumption. WECS plays a significant role in this green transition. Since the BDFRM has demonstrated strong potential for use

in this domain, advancing research into its design, modeling, and control is increasingly important.

However, current BDFRM designs also present several challenges. These include lower efficiency and torque density compared to permanent magnet synchronous machines, poor operating power factor, and the presence of inherent nonlinearities and harmonic interactions that complicate control. Due to these limitations, BDFRMs have not yet been commercially adopted and remain primarily in the research and development stage.

Furthermore, since BDFRMs are relatively more recently developed, the control strategies for BDFRMs have not yet been explored as extensively when compared to more conventional machines. In particular, there has been very limited investigation into nonlinear control strategies for BDFRM control. Additionally, the impact of the inherent nonlinearities stemming from the unique operational characteristics of the BDFRM on various control strategies remains largely unexplored. Motivated by these gaps, this thesis aims to analyze the nonlinearities present in the BDFRM system and contribute to the development of advanced nonlinear control methodology for its effective operation and precise speed control.

1.4 Thesis Contribution

The main objective of this thesis is to investigate the challenges in the control of the BDFRM when using conventional linear controllers, and to subsequently evaluate the effectiveness of a nonlinear control strategy to regulate BDFRM current and achieve precise speed control across sub-synchronous, synchronous, and super-synchronous speed regions. The main contributions of this thesis include:

- Development of a Field Oriented Control (FOC) Strategy: This thesis develops a Field Oriented Control (FOC) strategy designed for a Brushless Doubly Fed Reluctance Machine (BDFRM). This approach employs a two converter based framework to ensure flexible and precise control of the machine's operation across the sub-synchronous, synchronous, and super-synchronous speed regions. A key aspect of this work involves a thorough analysis of the inherent nonlinearities and harmonics within the BDFRM system and a detailed investigation into how these factors influence the ultimate performance and stability of the designed control system.

- Implementation of DTSTSM Current Control: The research in this work further includes the design and implementation of Discrete Time Super Twisting Sliding Mode (DTSTSM) controllers specifically for the control of the BDFRM's secondary winding current. This advanced nonlinear control strategy is chosen for its superior robustness. The DTSTSM controller's effectiveness is evaluated and compared against the performance of more conventionally used Proportional Integral (PI) controllers. This

comparison focuses on validating the DTSTSM controller's enhanced ability to maintain precise current tracking and robustness in the presence of system nonlinearities.

- Optimization of DTSTSM Controller Gains via PSO: Finally, to enhance the performance of the implemented DTSTSM control, this thesis employs the Particle Swarm Optimization (PSO) algorithm. This metaheuristic optimization technique is used to automatically tune the DTSTSM controller gains with the objective of achieving minimal current tracking error. The effectiveness of this automated approach is validated by conducting a comparison between the performance of the PSO optimized controller and the manually tuned controller.

1.5 Thesis Organization

To achieve the objectives outlined above, this thesis is structured as follows:

- Chapter 1 serves as the foundation of the thesis. It begins by presenting the motivation for the study, followed by a broad overview of electric machines and their evolution. The chapter then introduces the Brushless Doubly Fed Reluctance Machine (BDFRM) as the subject of this Thesis. It then highlights the existing research gaps in the development of BDFRM control strategies. The chapter then concludes by outlining the original contributions this thesis makes in addressing these identified gaps.

- Chapter 2 reviews background research in BDFRM operation and control. It starts by explaining the physical structure and basic working principles of the BDFRM. The chapter then briefly reviews existing mathematical models of the BDFRM followed by the development of a complete Space Vector Model that serves as the basis for the control scheme. Existing BDFRM control strategies are reviewed and explained, this literature survey is then used to identify the gaps remaining in existing BDFRM control strategy research.

- Chapter 3 describes the proposed two converter based operational setup of the BDFRM used in this work. The mathematical torque expression based on the space vector model is developed and complete Field Oriented Control (FOC) scheme is presented. Discrete Time Super Twisting Sliding Mode (DTSTSM) controller is introduced and specific implementation for BDFRM current control is developed. Finally, the methodology for integrating the Particle Swarm Optimization (PSO) algorithm to automatically fine tune the DTSTSM controller gains is presented.

- Chapter 4 documents the experimental validation of the proposed control strategy. The experimental testrig and hardware implementation is described. The test cases and operating conditions under which

the proposed strategy was rigorously evaluated are presented. A thorough discussion of the results obtained, includes detailed analyses and performance comparisons that validate the effectiveness and robustness of the developed control scheme.

- Chapter 5 provides a clear and concise summary of the contributions made by this Thesis and presents the key points from the experimental results. Suggestions for possible future research directions are offered, outlining potential research opportunities for further exploration and detailing how the proposed BDFRM control system could be improved upon or extended in subsequent studies.

Chapter 2

BDFRM: Background and Theory

This chapter presents the fundamental principles of the BDFRM, emphasizing its unique structural and operational characteristics. The chapter then provides a brief overview of the evolution of BDFRM technology, starting from its early 20th-century origins to its most recent developments to utilize it's potential in the late 20th century. Following this historical development context, this chapter then shifts to mathematical modeling of the BDFRM where various approaches, such as steady state, dynamic and space vector models, are reviewed, followed by detailed space vector modeling of the BDFRM.

Finally, this chapter explores and provides an overview of various previously studied BDFRM control strategies such as scalar control, vector control, direct torque control, direct power control and sliding mode control methodologies. This overview is then followed by a discussion on alternative control approaches, highlighting recent research and innovations. Finally, based on the review of these already developed strategies and their limitations, a research gap is identified, setting a stage for the control strategy proposed in this research work, which will be presented in the next chapter.

2.1 BDFRM: Fundamentals

The BDFRM is a unique electrical machine that boasts the characteristic traits of a doubly fed machine and a reluctance machine. The unique structure and operational characteristics of the BDFRM makes it a potential solution for applications that require low maintenance and variable speed operation. Figure 2.1 shows a conceptual diagram for a typical BDFRM.

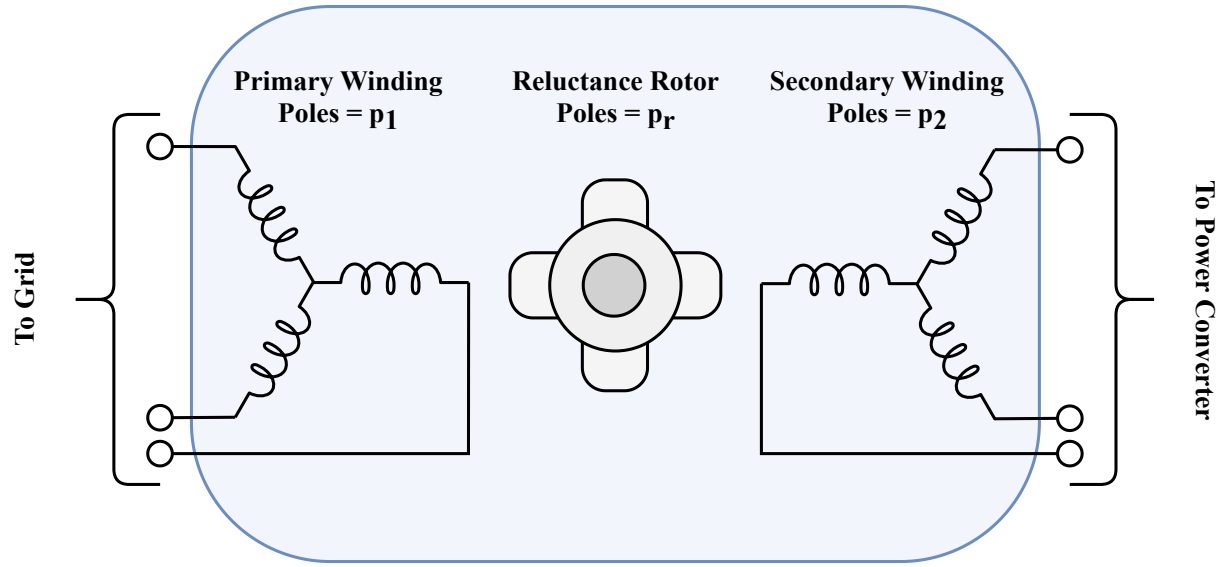

Figure 2.1: Conceptual diagram of a Brushless Doubly Fed Reluctance Machine

2.1.1 Structure of BDFRM

- The stator of the BDFRM consists of two windings, namely the Primary Winding (Winding 1) and the Secondary Winding (Winding 2). Typically the primary winding of the machine is connected directly to the grid supply and is responsible for providing the power needed to drive the machine and hence it may also be called the power winding, while the secondary winding is fed via a power converter that modulates the supply to the secondary winding in order to control the speed of the machine, and hence it is often called the control winding.

  The primary winding is wound with p_1 poles while the secondary winding is wound with p_2 poles. It is necessary for the two windings to be wound with different number of poles to ensure that there is no direct coupling between the two windings.

- The rotor in a BDFRM is a salient pole reluctance rotor. If the two stator windings are wound with different pole pairs, ideally there would be no coupling between them if the rotor has a round rotor structure. However, for the operation of BDFRM it is necessary for the two stator windings to be indirectly coupled through the rotor, which can be achieved through a reluctance rotor. Figure 2.2 shows the electromagnetic coupling concept between the two stator windings.

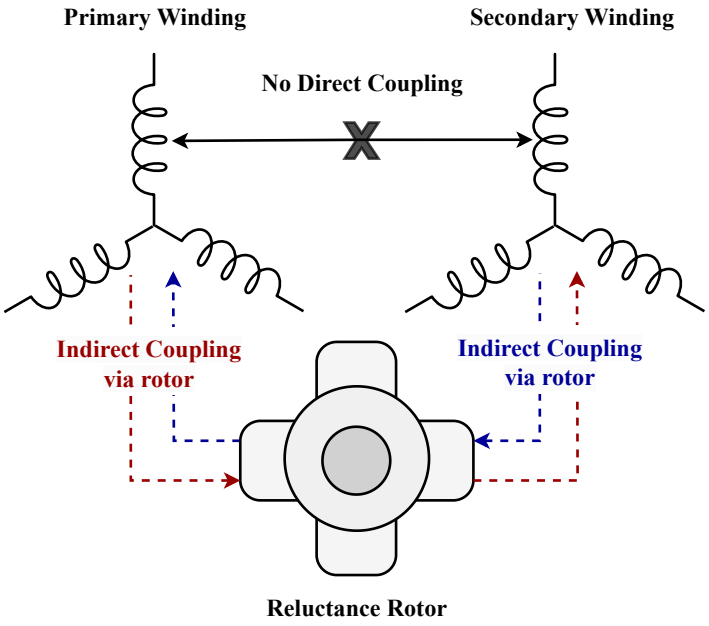

Figure 2.2: Electromagnetic Coupling between the two stator windings

This indirect coupling between the two stator windings occurs under the following condition [22]:

$$p_r = \frac{p_1 + p_2}{2} \quad , \quad \omega_m = \frac{\omega_1 + \omega_2}{p_r} \tag{2.1}$$

$$p_r = \pm\frac{p_1 - p_2}{2} \quad , \quad \omega_m = \pm\frac{\omega_1 - \omega_2}{p_r} \tag{2.2}$$

Here, p_1, p_2 and p_r are the primary winding, secondary winding and the rotor pole numbers respectively, ω_1 and ω_2 represent the electrical angular frequencies of the primary and secondary stator currents, and ω_m denotes the mechanical rotor speed. The relation in equation (2.2) has been shown to not provide desirable coupling between the two stator windings for certain pole combinations [28] and hence resulting in impractical design for those cases. Thus, we consider the relation outlined in equation (2.1).

2.1.2 Operating Principle

The basic principle of operation of a BDFRM is relatively simple and is similar to that of many flux modulating machines, including Vernier machines and flux switching machines. Two excitation sources are placed on the stator of the machine, with different pole numbers to ensure no direct coupling. These two excitation sources produce their respective MMFs. The salient pole reluctance rotor structure creates variable

reluctance paths for the magnetic flux in the machine, thereby modulating the stator mmf waveforms which results in the creation of flux density harmonics that link the two stator windings [22]. This indirect coupling and interaction between the two excitation sources produces torque on the rotor.

2.2 History of BDFRM

The fundamental concept of the BDFRM dates back to the early 20th century where the initial idea was introduced in the 1920s, primarily as a doubly fed machine with two stator windings operating at different frequencies [21]. Early developments were hindered by the limitations of materials and the complexity of controlling such machines.

Interest in BDFRM was revived in the 1970s and 1980s when advancements in power electronics, control theory, and materials allowed researchers to improve the machine's efficiency and performance [29, 30]. Over the following decades, BDFRM's unique attributes, such as the absence of brushes and slip rings and the ability to control power flow, made it a viable candidate for applications in wind energy conversion and variable speed drives. Thus, its development continued, with a number of papers [22, 23, 28, 31–53] published on analyzing the prototypes of the machine well into the 21st century.

2.3 BDFRM: Modeling

Over the years, various modeling approaches for BDFRM have been proposed. Early models, dating back to the early 1990s, focused on steady state performance. [54] introduced a steady state model of the BDFRM based on several approximations. Later, more detailed transient models emerged, such as those in [31, 39]. Building on this work, [22] proposed a dynamic model based on space vectors. Recently, advanced models using magnetic equivalent circuits [55] and reluctance networks [56] have also been introduced.

In this study, a space vector model will be employed for simulations, and hence, detailed space vector modeling for a BDFRM is discussed in this section. Furthermore, a brief overview of the mathematical frame transformations used while modeling the BDFRM is first presented. These same transformations are also used while employing the Field Oriented Control (FOC) strategy later discussed in the next chapter about the proposed control approach.

2.3.1 Mathematical Transforms

The process to transform three phase, time varying stator currents in the stationary $a-b-c$ reference frame ($I_{a,b,c}$) into time invariant stator currents in the orthogonal $d-q$ rotating reference frame ($I_{d,q}$) involves two

key steps:

1. **Clarke Transform**:

   This step converts the three phase, time varying system in the stationary $a-b-c$ reference frame into a two coordinate, time varying system in the stationary $\alpha-\beta$ reference frame. The Clarke transform takes the three phase time varying currents currents, i_a, i_b, i_c, and maps them onto two orthogonal components, i_α and i_β, in the stationary frame. i_α and i_β are also time varying. This transformation simplifies the representation of the three phase system by reducing the degrees of freedom from three to two, while preserving the system's time varying nature. Assuming that axis a and axis α are in the same direction, as seen in figure 2.3, we obtain:

$$\begin{aligned} i_\alpha &= i_a \\ i_\beta &= \frac{1}{\sqrt{3}} i_a + \frac{2}{\sqrt{3}} i_b \end{aligned} \tag{2.3}$$

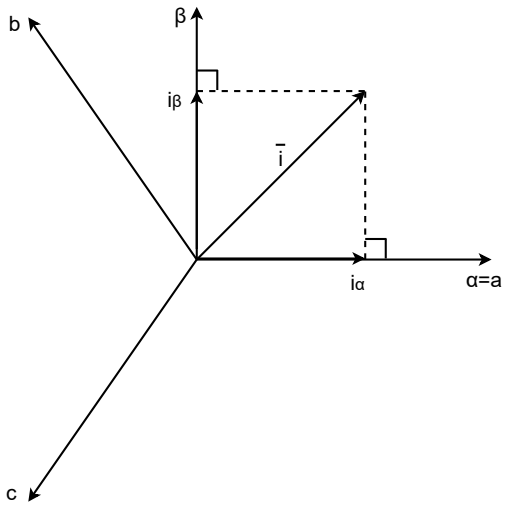

Figure 2.3: Clarke Transform

2. **Park Transform**:

   The second step involves converting the two coordinate, time varying current in the stationary $\alpha-\beta$ reference frame into a two coordinate, time invariant current in the $d-q$ rotating reference frame. Generally while employing field oriented control, the d axis represents the flux producing component of the stator current, and the q axis represents the torque producing component. Considering the d axis of the $d-q$ reference frame to be at angle θ from the $a=\alpha$ axis, as seen in figure 2.4, we obtain:

$$
\begin{aligned}
i_d &= i_\alpha \cos(\theta) + i_\beta \sin(\theta) \\
i_q &= -i_\alpha \sin(\theta) + i_\beta \cos(\theta)
\end{aligned}
\tag{2.4}
$$

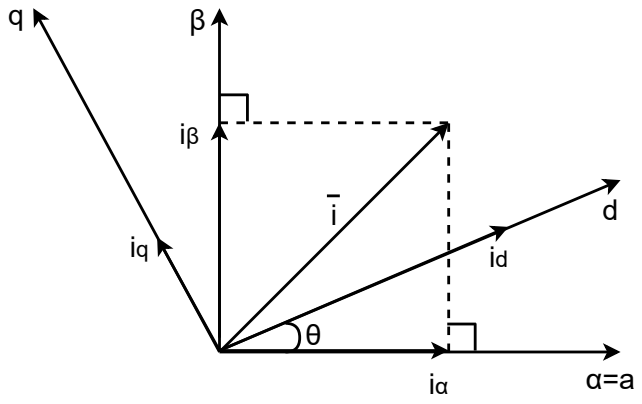

Figure 2.4: Park Transform

By using the knowledge of these frame transformations, space vector modeling of the BDFRM can be performed and field oriented control can be subsequently employed to control the speed of the motor.

2.3.2 Space Vector Modeling

A mathematical model for the Brushless Doubly Fed Reluctance Machine (BDFRM) using space vector modeling technique was first developed in [22]. This model provides a comprehensive framework for simulating and analyzing the dynamic behavior of BDFRM, making it a crucial step in the study of BDFRM control strategies and performance. The present research builds upon this foundational model, and hence, a detailed review of the approach taken by [22] is provided in this section.

To begin developing the model, it is first necessary to write the space vector voltage equations for the primary and the secondary winding in a stationary reference frame.

$$
\underline{v}_{1s} = r_1 \underline{i}_{1s} + \frac{d\underline{\lambda}_{1s}}{dt} \tag{2.5}
$$

$$
\underline{v}_{2s} = r_2 \underline{i}_{2s} + \frac{d\underline{\lambda}_{2s}}{dt} \tag{2.6}
$$

here, the subscripts ' 1 ' and ' 2 ' are used to denote the primary and the secondary windings respectively, the sub-subscript ' s ' is used to denote stationary reference frame and the underline ' _ ' is used to denote a

space vector. $\underline{v}, \underline{i}, \underline{\lambda}$ represent the voltage, current and the flux linkage space vector respectively. r represents the phase resistance.

Any space vector $\underline{x}$ can be obtained from it's respective instantaneous three phase $a-b-c$ reference frame values (x_{abc}) by applying the appropriate transformation in the following manner:

$$\underline{x} = \frac{2}{3}(x_a + a x_b + a^2 x_c) \tag{2.7}$$

Here, $a = e^{j\frac{2\pi}{3}}$ and $a^2 = e^{j\frac{4\pi}{3}}$

Now to derive the flux linkage expressions in three phase A-B-C reference frame, it is first necessary to establish an expression for the rotor electrical angle. The following equation defines the rotor electrical angle (θ_r) in terms of the rotor poles (p_r) and the rotor mechanical angle (θ_m):

$$\theta_r = p_r \theta_m \tag{2.8}$$

Now, with the knowledge of the rotor electrical angle , we can write the flux linkage expressions in the three phase $a-b-c$ reference frame for the primary (λ_{1abc}) and secondary winding (λ_{2abc}) as follows:

$$\begin{bmatrix} \lambda_{1a} \\ \lambda_{1b} \\ \lambda_{1c} \end{bmatrix} = \underbrace{\begin{bmatrix} L_{1a1a} & L_{1a1b} & L_{1a1c} \\ L_{1b1a} & L_{1b1b} & L_{1b1c} \\ L_{1c1a} & L_{1c1b} & L_{1c1c} \end{bmatrix}}_{L_{1\text{-}1}} \begin{bmatrix} i_{1a} \\ i_{1b} \\ i_{1c} \end{bmatrix} + \underbrace{\begin{bmatrix} L_{1a2a} & L_{1a2b} & L_{1a2c} \\ L_{1b2a} & L_{1b2b} & L_{1b2c} \\ L_{1c2a} & L_{1c2b} & L_{1c2c} \end{bmatrix}}_{L_{1\text{-}2}} \begin{bmatrix} i_{2a} \\ i_{2b} \\ i_{2c} \end{bmatrix}$$

$$\begin{bmatrix} \lambda_{2a} \\ \lambda_{2b} \\ \lambda_{2c} \end{bmatrix} = \underbrace{\begin{bmatrix} L_{2a2a} & L_{2a2b} & L_{2a2c} \\ L_{2b2a} & L_{2b2b} & L_{2b2c} \\ L_{2c2a} & L_{2c2b} & L_{2c2c} \end{bmatrix}}_{L_{2\text{-}2}} \begin{bmatrix} i_{2a} \\ i_{2b} \\ i_{2c} \end{bmatrix} + \underbrace{\begin{bmatrix} L_{2a1a} & L_{2a1b} & L_{2a1c} \\ L_{2b1a} & L_{2b1b} & L_{2b1c} \\ L_{2c1a} & L_{2c1b} & L_{2c1c} \end{bmatrix}}_{L_{2\text{-}1}} \begin{bmatrix} i_{1a} \\ i_{1b} \\ i_{1c} \end{bmatrix} \tag{2.9}$$

Here, i_{1abc} and i_{2abc} are the three phase $a-b-c$ reference frame primary and secondary winding currents respectively.

The matrices $[L_{1-1}]$ and $[L_{2-2}]$ are given as:

$$\begin{bmatrix} L_{1-1} \end{bmatrix} = \begin{bmatrix} L_{1m}+L_{1l} & -\frac{1}{2}L_{1m} & -\frac{1}{2}L_{1m} \\ -\frac{1}{2}L_{1m} & L_{1m}+L_{1l} & -\frac{1}{2}L_{1m} \\ -\frac{1}{2}L_{1m} & -\frac{1}{2}L_{1m} & L_{1m}+L_{1l} \end{bmatrix}$$

$$\begin{bmatrix} L_{2-2} \end{bmatrix} = \begin{bmatrix} L_{2m}+L_{2l} & -\frac{1}{2}L_{2m} & -\frac{1}{2}L_{2m} \\ -\frac{1}{2}L_{2m} & L_{2m}+L_{2l} & -\frac{1}{2}L_{2m} \\ -\frac{1}{2}L_{2m} & -\frac{1}{2}L_{2m} & L_{2m}+L_{2l} \end{bmatrix} \tag{2.10}$$

here, L_{1m} and L_{1l} are the primary winding magnetizing and leakage inductances respectively, and L_{2m} and L_{2l} are the secondary winding magnetizing and leakage inductances respectively.

The matrices $[L_{1-2}]$ and $[L_{2-1}]$ are given as:

$$[L_{1-2}] = [L_{2-1}] = \frac{1}{2}L_{12_{\max}} \begin{bmatrix} 1 & a^2 & a \\ a^2 & a & 1 \\ a & 1 & a^2 \end{bmatrix} e^{j\theta_r} + \frac{1}{2}L_{12_{\max}} \begin{bmatrix} 1 & a & a^2 \\ a & a^2 & 1 \\ a^2 & 1 & a \end{bmatrix} e^{-j\theta_r} \tag{2.11}$$

Here, $L_{12_{max}}$ is the peak mutual inductance between primary and secondary winding.

Substituting equations (2.10) and (2.11) in (2.9) and subsequently simplifying the equation we obtain:

$$\begin{bmatrix} \lambda_{1a} \\ \lambda_{1b} \\ \lambda_{1c} \end{bmatrix} = \begin{bmatrix} L_1 i_{1a} + \frac{1}{2}L_{12}\left[\underline{i}^*_{2s}e^{j\theta_r} + \underline{i}_{2s}e^{-j\theta_r}\right] \\ L_1 i_{1b} + \frac{1}{2}L_{12}\left[a^2\underline{i}^*_{2s}e^{j\theta_r} + a\underline{i}_{2s}e^{-j\theta_r}\right] \\ L_1 i_{1c} + \frac{1}{2}L_{12}\left[a\underline{i}^*_{2s}e^{j\theta_r} + a^2\underline{i}_{2s}e^{-j\theta_r}\right] \end{bmatrix}$$

$$\begin{bmatrix} \lambda_{2a} \\ \lambda_{2b} \\ \lambda_{2c} \end{bmatrix} = \begin{bmatrix} L_2 i_{2a} + \frac{1}{2}L_{12}\left[\underline{i}^*_{1s}e^{j\theta_r} + \underline{i}_{1s}e^{-j\theta_r}\right] \\ L_2 i_{2b} + \frac{1}{2}L_{12}\left[a^2\underline{i}^*_{1s}e^{j\theta_r} + a\underline{i}_{1s}e^{-j\theta_r}\right] \\ L_2 i_{2c} + \frac{1}{2}L_{12}\left[a\underline{i}^*_{1s}e^{j\theta_r} + a^2\underline{i}_{1s}e^{-j\theta_r}\right] \end{bmatrix} \tag{2.12}$$

here, $\underline{i}^*_{1s}, \underline{i}^*_{2s}$ are the complex conjugates of $\underline{i}_{1s}, \underline{i}_{2s}$ respectively,

$$L_1 = \frac{3}{2}L_{1m} + L_{1l} \tag{2.13}$$

$$L_2 = \frac{3}{2}L_{2m} + L_{2l} \tag{2.14}$$

$$L_{12} = \frac{3}{2} L_{12_{max}} \tag{2.15}$$

Applying the expression in equation (2.7) to obtain the primary and secondary winding flux linkage space vectors, we get:

$$\underline{\lambda}_{1s} = L_1 \underline{i}_{1s} + L_{12} \underline{i}^*_{2s} e^{j\theta_r} \tag{2.16}$$

$$\underline{\lambda}_{2s} = L_2 \underline{i}_{2s} + L_{12} \underline{i}^*_{1s} e^{j\theta_r} \tag{2.17}$$

Substituting equations (2.16) and (2.17) in (2.5) and (2.6) and performing the appropriate derivation, we obtain:

$$\underline{v}_{1s} = r_1 \underline{i}_{1s} + \left.\frac{d\underline{\lambda}_{1s}}{dt}\right|_{\theta_p \text{const}} + j\omega_p \underline{\lambda}_{1s} \tag{2.18}$$

$$\underline{v}_{2s} = r_2 \underline{i}_{2s} + \left.\frac{d\underline{\lambda}_{2s}}{dt}\right|_{\theta_s \text{const}} + j\omega_s \underline{\lambda}_{2s} \tag{2.19}$$

Here, θ_p, θ_s are the electrical angular positions and ω_p, ω_s are the electrical angular frequencies of the primary and secondary winding current space vectors in the stationary reference frame $(\underline{i}_{1s}, \underline{i}_{2s})$ respectively. These can be visualized in the figure 2.5 which details all the reference frames considered.

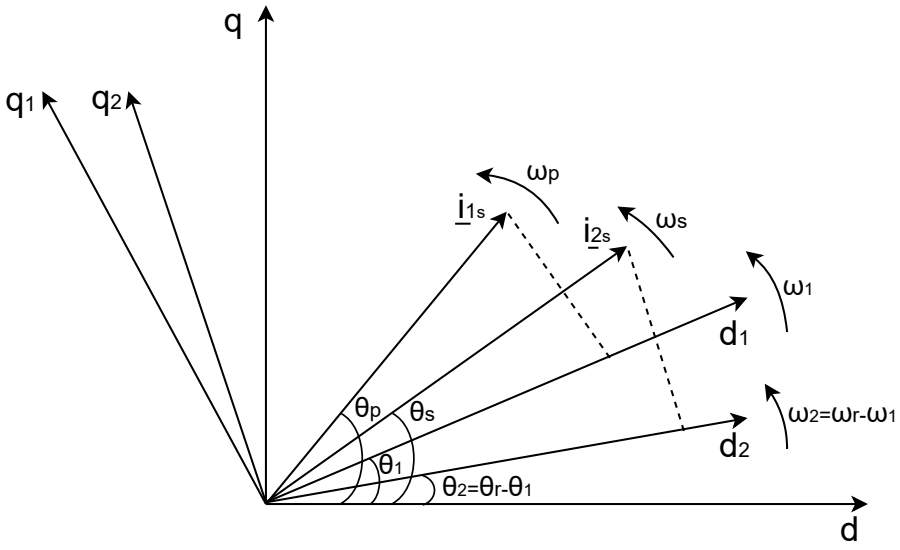

Figure 2.5: Reference frames and primary and secondary current vectors

Now that we have primary and secondary winding flux linkage and voltage space vectors in the stationary reference frame, we can convert them to rotating dq reference frame. Mapping the equation (2.16) to the $d_1 q_1$

reference frame which is assumed to be at an angle θ_1, by applying conventional reference frame conversion formulae, we obtain:

$$\underline{\lambda}_{1r} = (\underline{\lambda}_{1s})e^{-j\theta_1} \tag{2.20}$$

$$\underline{i}_{1r} = (\underline{i}_{1s})e^{-j\theta_1} \tag{2.21}$$

$$\begin{aligned} \tilde{\underline{i}}_{2r} &= (\underline{i}^*_{2s}e^{j\theta_r})e^{-j\theta_1} \\ &= \underline{i}^*_{2s}e^{j(\theta_r-\theta_1)} \\ &= [\underline{i}_{2s}e^{-j(\theta_r-\theta_1)}]^* \end{aligned} \tag{2.22}$$

Here, subscript ' r ' is used to denote rotating reference frame. Now by strategically selecting the angle of d_2q_2 reference frame as $\theta_2 = \theta_r - \theta_1$, onto which all the secondary winding space vectors are to be mapped, we obtain:

$$\underline{i}_{2r} = \underline{i}_{2s}e^{-j(\theta_r-\theta_1)} \tag{2.23}$$

Using this relation, $\tilde{\underline{i}}_{2r}$ in equation (2.22) can be rewritten as:

$$\tilde{\underline{i}}_{2r} = \underline{i}^*_{2r} \tag{2.24}$$

Now, by substituting (2.20), (2.21) and (2.24) in (2.16), the primary winding flux linkage in the primary winding d_1q_1 rotating reference frame can be written as:

$$\underline{\lambda}_{1r} = L_1\underline{i}_{1r} + L_{12}\underline{i}^*_{2r} \tag{2.25}$$

Similarly, the secondary winding flux linkage in the secondary winding d_2q_2 rotating reference can be derived to be:

$$\underline{\lambda}_{2r} = L_2\underline{i}_{2r} + L_{12}\underline{i}^*_{1r} \tag{2.26}$$

Using these flux linkage expressions, we can derive the primary and secondary winding voltage expressions in their respective arbitrary rotating dq reference frame as follows:

$$\begin{aligned} \underline{v}_{1r}e^{j\theta_1} &= r_1\underline{i}_{1r}e^{j\theta_1} + \frac{d}{dt}\left(\underline{\lambda}_{1r}e^{j\theta_1}\right) \\ &= r_1\underline{i}_{1r}e^{j\theta_1} + e^{j\theta_1}\frac{d\underline{\lambda}_{1r}}{dt} + j\omega_1\lambda_{1r}e^{j\theta_1} \end{aligned} \tag{2.27}$$

Therefore,

$$\underline{v}_{1r} = r_1 \underline{i}_{1r} + \frac{d\underline{\lambda}_{1r}}{dt} + j\omega_1 \underline{\lambda}_{1r} \tag{2.28}$$

In a similar way, the voltage expression for the secondary winding in the d_2q_2 reference frame can be derived as:

$$\underline{v}_{2r} = r_2 \underline{i}_{2r} + \frac{d\underline{\lambda}_{2r}}{dt} + j(\omega_r - \omega_1)\underline{\lambda}_{2r} \tag{2.29}$$

The voltage equations for the BDFRM in the dq form can be obtained by breaking equations (2.28) and (2.29) into their real and imaginary parts. The final dq equations for the BDFRM are given as follows:

$$\left.\begin{aligned} v_{1d} &= r_1 i_{1d} + \tfrac{d}{dt}\left(L_1 i_{1d} + L_{12} i_{2d}\right) + \omega_1 \left(L_{12} i_{2q} - L_1 i_{1q}\right) \\ v_{2d} &= r_2 i_{2d} + \tfrac{d}{dt}\left(L_2 i_{2d} + L_{12} i_{1d}\right) + \left(\omega_r - \omega_1\right)\left(L_{12} i_{1q} - L_2 i_{2q}\right) \\ v_{1q} &= r_1 i_{1q} + \tfrac{d}{dt}\left(L_1 i_{1q} - L_{12} i_{2q}\right) + \omega_1 \left(L_1 i_{1d} + L_{12} i_{2d}\right) \\ v_{2q} &= r_2 i_{2q} + \tfrac{d}{dt}\left(L_2 i_{2q} - L_{2s} i_{1q}\right) + \left(\omega_r - \omega_1\right)\left(L_2 i_{2d} + L_{12} i_{1d}\right) \end{aligned}\right\} \tag{2.30}$$

In this research work, the equations in (2.30) are used to construct the BDFRM model in Simulink. This model is then incorporated into the overall BDFRM drive model in Simulink, upon which the particle swarm optimization algorithm is applied to perform the required evaluations for obtaining the optimal results.

It is important to emphasize that the equations in (2.30) are derived after the assumption in equations (2.18) and (2.19) that the primary and secondary current space vectors contain only a single fundamental angular frequency component and rotate at that frequency in the stationary reference frame. In reality, however, the BDFRM currents include additional harmonic components due to inherent machine nonlinearities. Consequently, these equations do not capture the full dynamics of the machine, and the resulting Simulink based BDFRM model does not fully represent the real time behavior of the system. Therefore, the evaluations performed using this model and the optimal results produced by the optimization algorithm are not entirely accurate or fully reflective of the actual machine response.

2.4 BDFRM: Control

Effective control of the Brushless Doubly Fed Reluctance Machine (BDFRM) is essential for achieving desirable machine performance across various applications. Control of BDFRM systems primarily involves adjusting rotor speed and torque by manipulating the stator winding supply. Figure 2.6 shows a typical BDFRM drive system traditionally implemented.

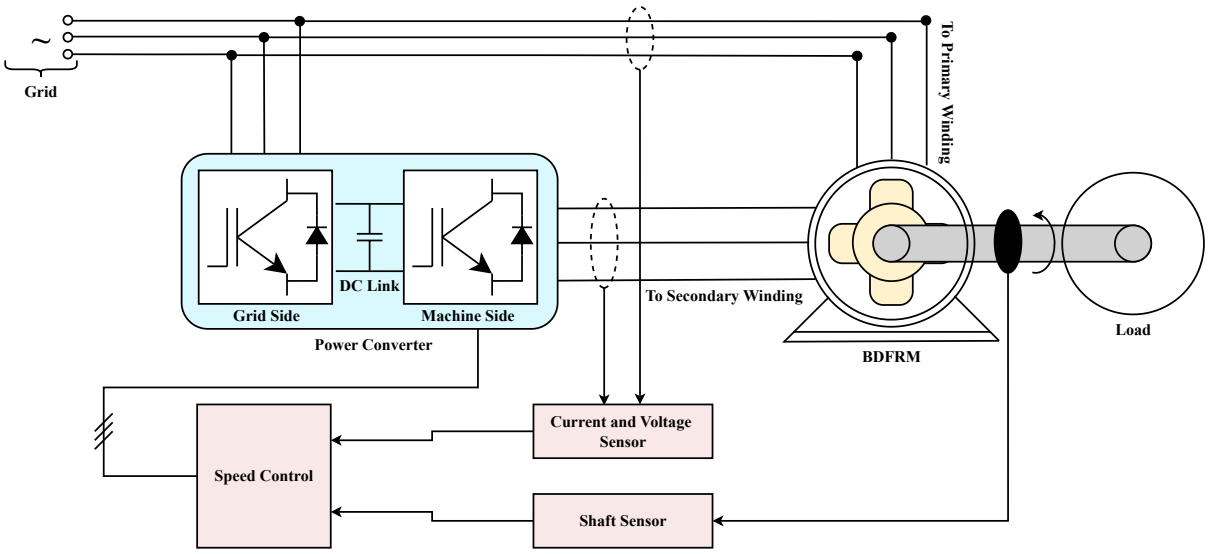

Figure 2.6: Typical BDFRM Drive

The control strategies for BDFRM have advanced considerably over the years, primarily driven by the demand for efficient and adaptable performance in variable speed applications, especially within renewable energy systems like wind turbines. Numerous studies, including [57–59], have reviewed and compared these evolving control strategies in detail. The following sections outline the various control strategies that have been proposed over the years.

2.4.1 Scalar Control

Scalar control is a straightforward control approach commonly employed in variable speed electric machines, including the Brushless Doubly Fed Reluctance Machine (BDFRM). In BDFRM, scalar control operates by adjusting the voltage and frequency applied to the machine without managing phase relationships or controlling individual magnetic field components, as would be done in vector control. This simplified approach is particularly suitable for applications where precise torque control and dynamic performance are not essential.

To implement scalar control in BDFRM, the voltage and frequency supplied to the secondary winding are adjusted to regulate the machine's speed, while the primary winding frequency remains fixed and synchronized with the grid. As the desired rotor speed changes, the frequency of the secondary winding is varied accordingly, as defined by equation (2.1). To prevent magnetic core saturation and ensure stable operation, the volts-per-hertz (V/f) ratio in the secondary winding is maintained constant. The basic schematic

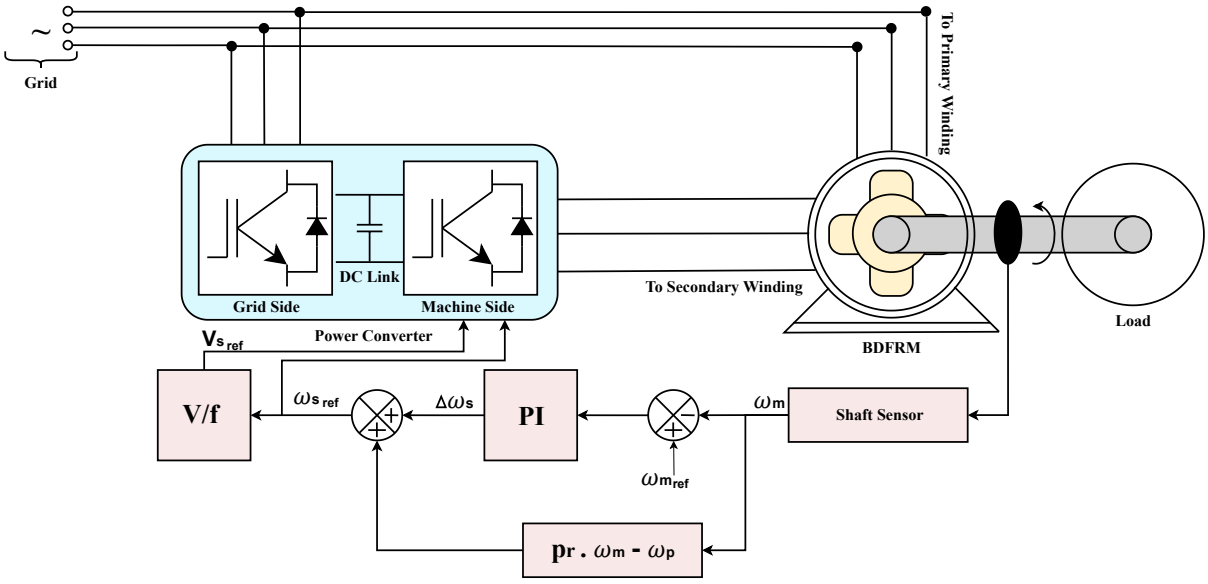

Figure 2.7: Scalar Control Schematic Diagram for BDFRM

diagram of a BDFRM drive system utilizing scalar control is shown in Figure 2.7.

As depicted in the schematic, the rotor's mechanical speed is measured using a speed sensor, which is then compared to a reference speed to produce a speed error. This error signal is processed by a Proportional-Integral (PI) controller to generate the required change in the reference frequency for the secondary winding. This required change is then combined with the current frequency of the secondary winding, derived from the measured rotor speed and the fixed frequency of the primary winding according to equation (2.1), to determine the new reference frequency for the secondary winding. To maintain a constant V/f ratio, the secondary winding reference voltage magnitude is also varied accordingly. These reference voltage and frequency values are then used to drive the inverter circuit.

Applications of scalar control in BDFRM for pump and wind energy systems are discussed in [60]. A sensorless approach to scalar control in BDFRM is presented by [61], providing an alternative for applications where speed sensors are not feasible. Additionally, an enhanced scalar control technique for wind driven BDFRM systems, aimed at improved performance, is proposed in [62]. In [63], scalar control is adapted for maximum power point tracking (MPPT) in wind driven BDFRM. Lastly, a closed loop scalar control strategy is explored in [64].

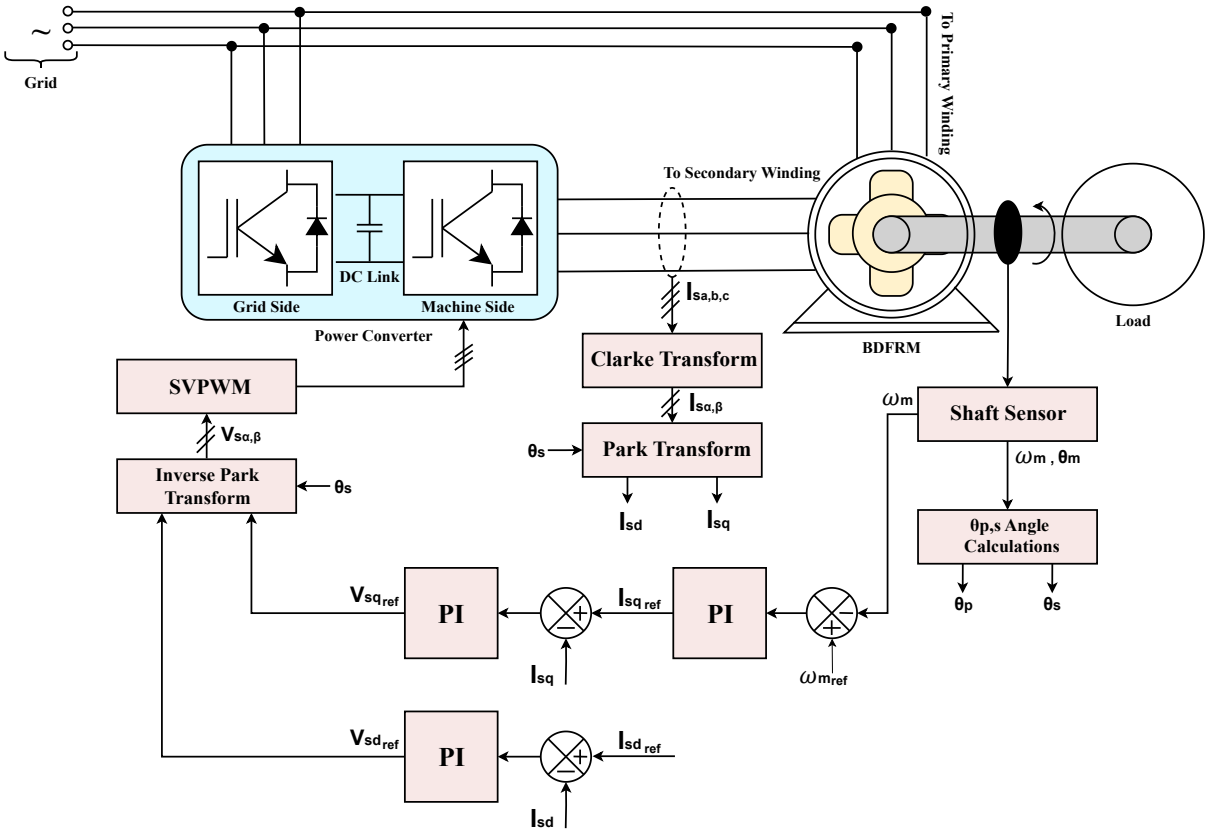

Figure 2.8: Vector Control Schematic Diagram for BDFRM

2.4.2 Vector Control/Field-Oriented Control

Vector control, also referred to as Field Oriented Control (FOC), is a widely used approach for controlling AC machines, including the BDFRM. In BDFRM applications, FOC enables independent control of torque and magnetic flux by decomposing the stator currents into two orthogonal components (direct-quadrature (d-q) axis). Typically, the primary winding of the BDFRM is connected directly to the grid, while the secondary winding receives variable voltage and frequency via a power converter. To control the BDFRM effectively, it is therefore necessary to regulate the current in the secondary winding. To implement FOC in a BDFRM, the three phase secondary winding current in the stationary a-b-c reference frame is transformed into a two coordinate rotating reference frame(d-q reference frame).

In the d-q frame, the magnetic flux producing component of the secondary current aligns with the direct axis (d-axis), while the torque producing component aligns with the quadrature axis (q-axis). This decoupling allows for independent manipulation: adjusting the q-axis current directly controls the torque without affecting the magnetic flux, while the d-axis current can adjust the magnetic flux independently of

the torque.

Through this independent control of d and q axis components, vector control facilitates precise torque control, smoother operation, and improved dynamic performance. The fundamental block diagram for vector control of the BDFRM is illustrated in figure 2.8.

Building on the advantages of vector control, a comparative analysis with scalar control for BDFRM is presented in [65], where the authors detail the underlying principles and performance distinctions of each approach. Further developments in vector control methods for BDFRM are proposed in [66–69], including the introduction of a novel sensorless FOC approach in [70]. Additionally, vector control techniques in grid-tied BDFRM systems, aimed at achieving Maximum Power Point Tracking (MPPT), are explored in [71]. This research work uses FOC to implement the proposed control strategy, and hence FOC will be further elaborated in Chapter 3.

2.4.3 Direct Torque Control

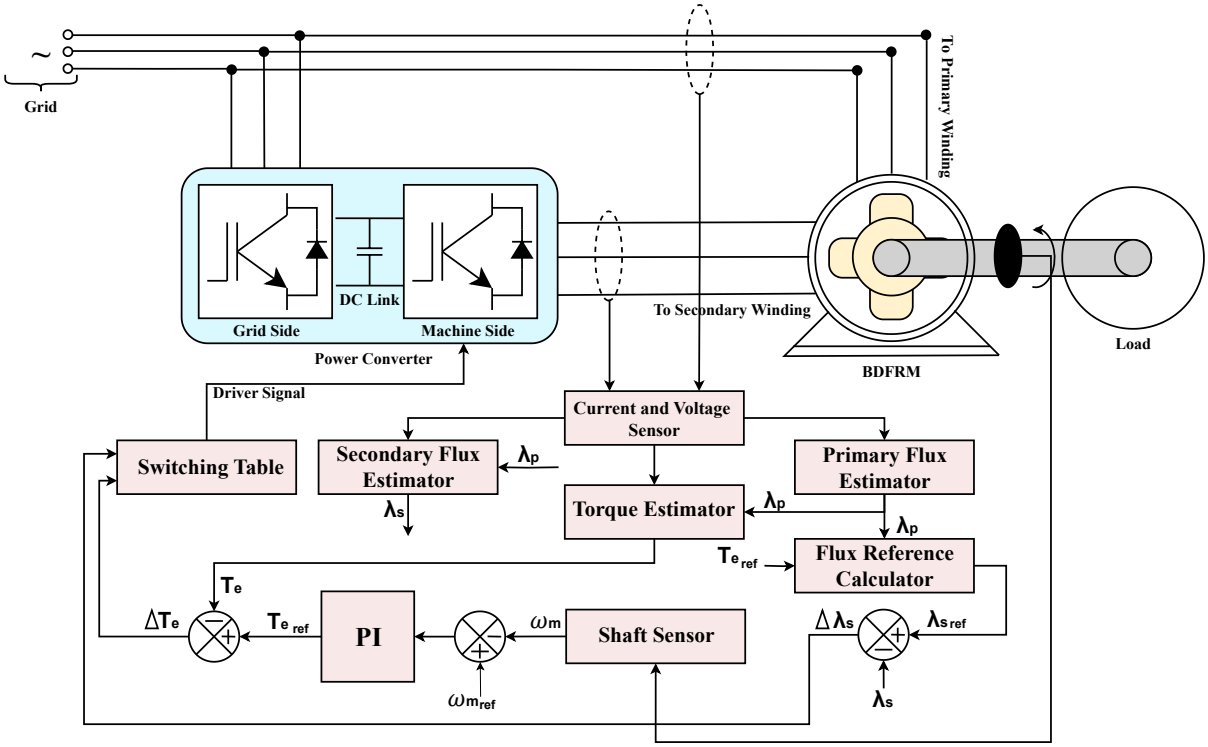

Figure 2.9: DTC Schematic Diagram for BDFRM

Direct Torque Control (DTC) is an advanced control method that offers rapid torque and flux control without the need for coordinate transformations or pulse width modulation (PWM). Instead, DTC directly regulates

the machine's stator voltages and currents by selecting optimal voltage vectors to apply to the BDFRM's secondary winding in real time. This method, based on instantaneous feedback, achieves fast and efficient control with minimal computational requirements. DTC selects these voltage vectors to bring the machine's torque and flux closer to their reference values, ensuring responsive and precise machine performance. Figure 2.9 shows a schematic diagram of a BDFRM drive with DTC.

In a BDFRM, Direct Torque Control (DTC) operates by first estimating flux and torque in real time based on voltage and current measurements from the primary and secondary windings. These estimated values are then compared with the reference values, generating error signals for both flux and torque. Using these error signals, DTC consults a predefined lookup table containing voltage vectors that can either increase or decrease torque and flux. Based on the signs and magnitudes of the errors, the control algorithm selects the most appropriate voltage vector from this table and applies it to the secondary winding through a power converter. To ensure stable operation, DTC utilizes hysteresis controllers that establish allowable error bands for torque and flux, maintaining the machine's operating point within a specified range. This minimizes unnecessary switching and helps sustain smooth performance.

Several studies have focused on advancing the practical implementation of DTC for BDFRM. For instance, [72, 73] provided a detailed exploration of the fundamental principles and implementation techniques of DTC. Building on this, [74] introduced an encoderless version of DTC, designed for applications with limited speed ranges. Additionally, to improve flux prediction during DTC, [75] proposed the use of a Sliding Mode Observer. Further refinements to DTC strategies, particularly for optimizing the performance of wind driven BDFRM systems, were presented in [76, 77].

2.4.4 Direct Power Control

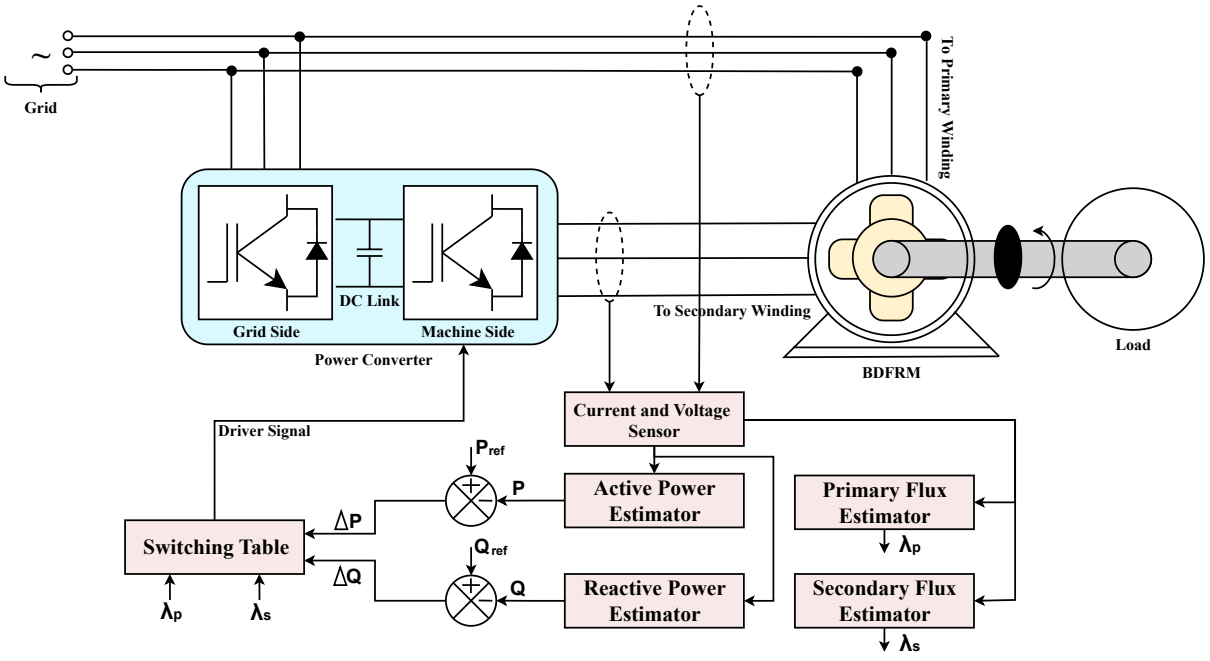

Figure 2.10: DPC Schematic Diagram for BDFRM

Direct Power Control (DPC) for Brushless Doubly Fed Reluctance Machines (BDFRM) is an advanced control strategy that directly regulates active and reactive power, in contrast to traditional methods like Vector Control or Direct Torque Control (DTC), which control torque and flux indirectly. DPC offers several advantages, such as improved dynamic performance and a simpler control structure. Similar to DTC, DPC manipulates the stator voltages and currents; however, its focus is on controlling the machine's active and reactive power consumption. This is achieved by selecting the appropriate voltage vectors to be fed to the secondary winding in real time, based on instantaneous feedback. The voltage vectors are chosen to adjust the machine's active and reactive power consumption toward the reference values. The fundamental block diagram for DPC of the BDFRM is illustrated in figure Figure 2.10.

In practice, DPC is implemented by first estimating the active and reactive power in real time using measurements of primary and secondary winding voltage and current. These estimates are then compared with the reference power values, and the resulting errors are calculated. A switching table (or lookup table) is then used to select the optimal voltage vector based on the power errors and flux position. The selected voltage vector is applied to the secondary winding by switching the inverter, which adjusts the magnetic field in the control winding and moves the active and reactive power closer to their reference values.

DPC offers the advantage of directly controlling the power exchanged between the machine and the grid, making it particularly beneficial for applications such as wind energy systems, where effective active and reactive power management is essential for optimizing energy capture, maintaining power quality, and supporting grid stability.

The concept of DPC for BDFRM was first introduced in [78, 79]. A model predictive approach to DPC was later explored in [80], and DPC for open winding BDFRM was further investigated in [81, 82].

2.4.5 Sliding Mode Control

Sliding Mode Control (SMC) is a robust nonlinear control strategy that is widely used in systems dominated by nonlinearities, model uncertainties, parameter variations, and external disturbances. The use of linear controllers like PI controllers in these kinds of systems yields very poor performance with the possibility of control system even going unstable. Thus nonlinear controller like SMC based controller provides a good alternative. The main idea behind SMC is to force the system trajectories i.e. drive the states of the system to reach and subsequently remain on a predefined surface in the state space, known as the sliding surface or switching surface. This sliding surface is chosen in a way such that, once the systems states or trajectories are on this surface, the system exhibits the desired dynamic behavior in presence of the system nonlinearities that is independent of the model uncertainties and disturbances. Following subsection details the controller equations and structure for a basic first order Sliding Mode Control [83].

First Order Sliding Mode control

Consider a dynamic system of the form:

$$\dot{x}(t) = f(x,t) + g(x,t)u(t) \tag{2.31}$$

where $x(t) \in \mathbb{R}^n$ is the state vector, $u(t) \in \mathbb{R}$ is the control input, and $f(x,t)$ and $g(x,t)$ are function of x, t.

The objective of the SMC is to design a controller output $u(t)$ such that the system states $x(t)$ track a desired reference $x_{ref}(t)$. A sliding surface $s(x,t)$ is defined as:

$$s(x,t) = e_{x(t)} = x(t) - x_{ref}(t) \tag{2.32}$$

where $e_{x(t)} = x(t) - x_{ref}(t)$ is the tracking error.

The controller output according to the SMC control law is given by:

$$u = u_{eq} + u_{sw} \tag{2.33}$$

where:

- u_{eq} (equivalent control) maintains the motion on the sliding surface.
- u_{sw} (switching control) drives the trajectories toward the surface.

To ensure that the system states will move toward the sliding surface, the following condition must be satisfied:

$$s\dot{s} < 0 \tag{2.34}$$

When this condition is satisfied, the system trajectories are guaranteed to reach the surface in finite time. A commonly used switching control u_{sw} to reach this condition is:

$$u_{sw} = -k\,\text{sign}(s) \tag{2.35}$$

where $k > 0$ is the switching gain and $\text{sign}(s)$ is given as:

$$\text{sign}\,(s) = \begin{cases} 1 & \text{if} \quad s > 0 \\ 0 & \text{if} \quad s = 0 \\ -1 & \text{if} \quad s < 0 \end{cases} \tag{2.36}$$

The equivalent control u_{eq} can be obtained by considering $\dot{s} = 0$ and solving for $u(t)$ as shown in the following equation:

$$\begin{aligned} \dot{s}(x,t) &= \dot{x}(t) - \dot{x}_{ref}(t) = 0 \\ \dot{x}(t) &= f(x,t) + g(x,t)u_{eq} = \dot{x}_{ref}(t) \end{aligned} \tag{2.37}$$

While the trivial first order Sliding Mode Control (SMC) provides robustness against system nonlinearities and model uncertainties, it also suffers from a major limitation known as the chattering phenomenon [84, 85]. This chattering arises due to high frequency switching of the control signal as the system state oscillates around the sliding surface. To overcome this chattering phenomenon, Higher Order Sliding Mode (HOSM) techniques were developed [85]. The basic idea of HOSM is to apply the first order SMC concept to higher order time derivatives of the sliding surface. For standard first order SMC, sliding surface $s = 0$ while $\dot{s}$ is

discontinuous. For an r^{th} order SMC, the equalities are given as:

$$s = \dot{s} = \ddot{s} = \cdots = s^{(r-1)} = 0 \tag{2.38}$$

By employing higher order SMC, the control action becomes continuous in the first derivative, thereby significantly reducing chattering. Higher order sliding mode control techniques have been investigated in [86] and [87]. Second order SMC with $s = 0$ and $\dot{s} = 0$ according to equation (2.38), is employed in [86] while continuous time super twisting algorithm is employed in [87]. SMC with super twisting algorithm is further discussed in detail in the next chapter since the research done in this thesis also uses super twisting algorithm with SMC.

2.4.6 Other Control Strategies

Over the past two decades, a wide range of control strategies and controllers have been developed to enhance the performance of Brushless Doubly Fed Reluctance Machine (BDFRM) drives, catering to the specific needs of various applications.

A notable approach is Reactive Power Control, which focuses on improving the control of reactive power to enhance system stability and efficiency. This method was proposed for BDFRM control in [88] and [89], where the authors explore techniques to regulate reactive power and improve the overall power factor of the system.

In the context of wind energy, Variable Structure Control (VSC) technique along with Lyapunov's theory is used to design a non linear Multi-Input Multi-Output (MIMO) controller for Brushless Doubly Fed Reluctance Generator based wind energy conversion systems in [90] as a means of ensuring robust performance despite system uncertainties and external disturbances.

Additionally, flatness based adaptive fuzzy control has been proposed in [91] as a method to address the uncertainties and nonlinearities in BDFRM systems. This control strategy leverages fuzzy logic principles to adapt to changing operating conditions and improve system performance by adjusting control parameters in real time.

These diverse control strategies underscore the growing interest in optimizing the performance of BDFRM for various applications, particularly in renewable energy and industrial systems, where reliability, robustness and precision are critical.

2.4.7 Limitations

The studies mentioned above exploring Scalar Control, Vector Control, Direct Torque Control, Direct Power Control and Reactive Power Control predominantly employ linear controllers like PI controllers for current control in their control structure, owing to their simplistic design, ease of implementation and low computational cost. However, PI based controllers struggle while dealing with the machine's nonlinearities and dominant harmonics in the stator currents leading to poor performance and control [92, 93]. Thus non linear control techniques provide an alternative solution to deal with the challenges imposed by linear control. However, the non linear control techniques including Variable Structure Control and Adaptive Fuzzy control discussed in studies mentioned above impose a heavy computational burden on the control system making their use not advisable. For this purpose, Sliding Mode Control technique emerges as the top non linear control technique. Furthermore, to overcome the issue of chattering imposed by sliding mode control, higher order sliding mode control techniques are used in practice. However, it is noteworthy that the studies mentioned above, which investigate higher order sliding mode control, primarily focus on the application of BDFRMs in large inertia wind energy systems and are limited to simulation studies. These works neither provide experimental validation nor examine the performance of the developed control strategies on low inertia BDFRM systems, such as BDFRM drives. Furthermore, the controllers developed in these studies are formulated in the continuous time domain, whereas practical implementations using Digital Signal Processors (DSPs) require discrete time controllers.

Therefore, to address the challenge of controlling a BDFRM, analyzing the difficulty in control caused by system harmonics and filling the research gap outlined above, the research work of this thesis will analyze the harmonics in the BDFRM system, analyze their impact on PI controller performance, investigate the performance and efficacy of a PI controller operating with a low pass filter, implement a discrete time super twisting sliding mode controller with optimally tuned gains from a particle swarm optimization algorithm as current controllers and compare and validate it's performance experimentally to the conventionally used PI controllers.

Chapter 3

Proposed Control Strategy

This chapter presents the proposed control strategy for employing an optimally tuned DTSTSM controller for the speed control of BDFRM. The chapter begins by discussing the two converter based operation theory employed in this research work, detailing the two distinct operational modes of the BDFRM achieved from the two converter implementation. These modes, namely open loop cascade induction mode and conventional BDFRM mode provide flexibility in operating the BDFRM and are suitable for different applications.

The chapter then explores the proposed control approach based on the BDFRM model developed in the previous chapter, focusing on achieving a linear relationship between torque and the control current to enable precise torque control, thereby enabling precise speed control. This proposed speed control involves a detailed Field Oriented Control (FOC) based control strategy to better facilitate the machine's torque and flux regulation by decoupling them, allowing for more precise speed control.

Following this, Discrete Time Super Twisting Sliding Mode (DTSTSM) controllers are discussed and their integration within the current control loops is discussed further in the chapter. This high order sliding mode controller provides smoother control and enhances reliability under nonlinearities and disturbances.

The final section of this chapter focuses on optimizing the controller gains of the DTSTSM controllers using Particle Swarm Optimization (PSO). By minimizing tracking errors in the current control loops, PSO ensures an optimal balance between fast response time and stability. The formulation of the optimization problem, as well as the algorithmic steps of PSO, are described in detail, providing a complete framework for the control strategy proposed in this research.

3.1 Two Converter based Operation Theory

In a two converter based operation of the BDFRM, the primary winding (Winding 1) and secondary winding (Winding 2) are powered by two separate power converters. This configuration allows for independent control of the voltage and frequency applied to each winding, enabling the BDFRM to operate in two distinct modes [94]:

1. **Open Loop Cascade Induction Mode**

   This mode is used for starting the BDFRM like a cascade induction motor. In this mode, the secondary converter is controlled to output zero voltage at its terminals, thereby effectively short circuiting the secondary winding. The primary winding is then energized with a gradually increasing frequency and voltage ramp using a constant V/f control scheme. This enables safe acceleration from standstill.

2. **Conventional BDFRM Mode**

   This mode is used to control the speed of the BDFRM. An FOC strategy is employed in this mode to achieve the speed control. After reaching a steady speed following startup of the BDFRM in the previous mode, it transitions into a closed loop speed control mode, where the primary winding remains energized by a fixed frequency and fixed voltage source, and the secondary winding supply is actively modulated to achieve precise speed regulation. The fixed frequency for the primary winding typically matches the grid frequency, while the secondary winding's frequency varies according to the motor's speed.

In this research, the BDFRM is always started using the open loop cascade induction mode wherein there is a set target speed but no closed loop speed control, and once the BDFRM reaches a steady speed, the machine is then transitioned into the closed loop standard BDFRM mode, in which the closed loop speed control is enabled to achieve precise speed control. This speed control is achieved by the control strategy proposed in this research work, which is outlined in detail in the next section.

3.2 Torque Expression and Control Approach

To show the control approach for BDFRM proposed in this research work, it is first crucial to develop the torque expression for the BDFRM. The torque expression gives important insights into the interaction between the stator currents and the magnetic field, which is necessary to develop a control strategy. [22] has developed the torque expression for the BDFRM in the rotating reference frame by employing space vector modeling. This subsection will continue on the review of the work done in [22] to derive the torque expression of a BDFRM in the rotating reference frame.

The generalized matrix Torque expression can be given as [22]:

$$T_e = \frac{1}{2} p_r [i]^T [G][i] \tag{3.1}$$

here, T_e is the developed electrical torque in the three phase reference frame, [i] is the instantaneous current vector and $[G] = \frac{d[L_{ij}]}{d\theta_r}$ where $[L_{ij}]$ is the machine inductance matrix. For a BDFRM:

$$[i]^T = [i_{1a}, i_{1b}, i_{1c}, i_{2a}, i_{2b}, i_{2c}] = [[i_{1abc}]^T, [i_{2abc}]^T] \tag{3.2}$$

$$[G] = \begin{bmatrix} [0] & \frac{d}{d\theta_r}[L_{1-2}] \\ \frac{d}{d\theta_r}[L_{2-1}] & [0] \end{bmatrix} \tag{3.3}$$

Substituting these in (3.1) we get,

$$T_e = p_r [i_{1abc}]^T \frac{d}{d\theta_r} [L_{1-2}][i_{2abc}] \tag{3.4}$$

Now substituting (2.11) in (3.4) and then solving the equation, we obtain:

$$T_e = j\frac{3}{4} p_r L_{12} [\underline{i}^*_{1s} \underline{i}^*_{2s} e^{j\theta_r} - \underline{i}_{1s} \underline{i}_{2s} e^{-j\theta_r}] \tag{3.5}$$

This developed electromagnetic torque expression is in terms of space vector quantities in the stationary reference frame. By mapping the primary winding space vectors to the d_1q_1 rotating reference frame and secondary winding space vectors to the d_2q_2 rotating reference frame, the torque can be represented in the rotating reference frame as follows:

$$T_e = j\frac{3}{4} p_r L_{12} [\underline{i}^*_{1r} \underline{i}^*_{2r} - \underline{i}_{1r} \underline{i}_{2r}] \tag{3.6}$$

This equation can be further simplified by using the flux linkage expressions in equations 2.25 and 2.26 and the torque can be represented as:

$$T_e = j\frac{3}{4} p_r [\underline{\lambda}_{1r} \underline{i}^*_{1r} - \underline{\lambda}^*_{1r} \underline{i}_{1r}] \tag{3.7}$$

On expanding $\underline{i}^*_{1r}$ from the equation 2.26 and using that, the torque equation can be represented in the rectangular form as follows:

$$T_e = \frac{3}{2} p_r \frac{L_{12}}{L_1} [\lambda_{1d} i_{2q} + \lambda_{1q} i_{2d}] \tag{3.8}$$

In the proposed control strategy, the primary winding voltage v_1 is applied along the q-axis of the stator

primary winding reference frame, thus, by first approximation, the resulting primary winding flux λ_1 will align with the d-axis. This simplifies the torque equation in (3.8) as follows:

$$T_e = \frac{3}{2} p_r \frac{L_{12}}{L_1} \lambda_{1d} i_{2q} \tag{3.9}$$

This simplified expression indicates that the torque T_e is directly proportional to the primary winding flux linkage (λ_{1d}) and the secondary winding q axis current (i_{2q}). Thus, controlling the machine's torque output can be achieved by modulating either λ_{1d} or i_{2q}. The control approach taken by this present research work involves modulation of i_{2q} while, λ_{1d} is maintained constant.

To achieve a linear relationship between torque and the control current i_{2q}, the proposed strategy involves maintaining λ_{1d} as a constant. This can be accomplished by recognizing that λ_{1d} is a function of both primary and secondary winding currents, given by:

$$\lambda_{1d} = L_1 i_{1d} + L_{12} i_{2d} \tag{3.10}$$

It can be observed from (3.10) that to maintain λ_{1d} as a constant, i_{1d} and i_{2d} must remain constant. Since, the primary winding is supplied with fixed voltage and fixed frequency, i_{1d} is ensured to be constant, and therefore, by setting a steady i_{2d} in the secondary winding (i_{2d} is set to 0 in this research work), the primary winding d-axis flux linkage λ_{1d} is maintained to be constant, which in turn allows the torque T_e to be linearly proportional to the q-axis secondary winding current i_{2q}.

To implement this control approach effectively, it is essential to decompose the stator current into its d-axis and q-axis components within a rotating reference frame. By breaking down the current into these orthogonal components, we can control each axis current independently, enabling precise regulation of torque and flux in the machine. This approach leverages Field Oriented Control (FOC), a widely used technique in motor control systems. Thus, the present research work employs FOC to implement the proposed control strategy. This FOC based control strategy in this two converter based framework is discussed thoroughly in the upcoming section of this chapter.

3.3 FOC based Control Strategy

3.3.1 FOC Fundamentals

FOC is a widely used control technique in AC machines. The basic principle of FOC revolves around transforming the stator currents into a rotating reference frame through specific mathematical transformations,

allowing independent control of the flux and torque components.

The logic behind FOC is to replicate the behavior of a DC motor, where the torque producing and flux producing currents are the rotor current and the stator excitation respectively. These two currents are decoupled and can be controlled independently. However, in an AC machine, this decoupling is not naturally present. The stator current in an AC machine inherently includes both torque producing and magnetic flux producing components, preventing direct independent control of torque and flux.

FOC overcomes this issue by decomposing the stator current into two separate components: one for torque production and the other for magnetic flux. This decomposition inherently decouples torque and flux control, enabling independent adjustment of each. To achieve this, the mathematical transformations outlined in the previous chapter namely, the Clarke and Park transforms are applied. These transformations convert the three phase time variant stator current in stationary $a-b-c$ reference frame to a time invariant space vector in orthogonal two coordinate $d-q$ (direct - quadrature axis) rotating reference frame, mimicking the control and operational characteristics of a DC motor. The q axis component of the stator current is generally responsible for torque production while the d axis component sets up the magnetic field in the machine.

3.3.2 Generalized FOC Control Scheme

The following block diagram depicts how FOC can be implemented on any machine:

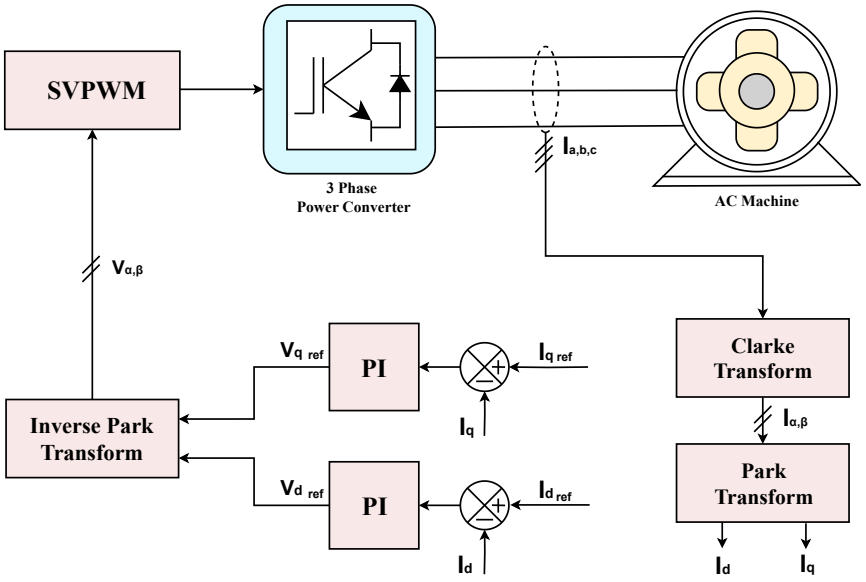

Figure 3.1: Generalized FOC Block Diagram

As shown in the figure, the first step in implementing Field-Oriented Control (FOC) is to measure the

phase currents of the motor, denoted as I_a and I_b. These phase currents are then fed into the Clarke and Park transform modules to map them to the $d-q$ rotating reference frame: I_d and I_q.

The I_d and I_q components represent the flux producing and torque producing current components, respectively. These currents are compared with their corresponding reference values: the flux reference for I_d and the torque reference for I_q. The comparison results in error signals, which are then fed to corresponding PI controllers. These controllers subsequently compute the reference stator voltages V_d and V_q in the $d-q$ reference frame.

Once the reference voltages V_d and V_q are determined, they are then fed to the inverse Park transform module to obtain the reference stator voltage vector in the stationary $(\alpha-\beta)$ reference frame V_α, V_β. This reference voltage vector is then fed to the SVPWM module which subsequently generates the gate signals for the three phase inverter that supplies the machine stator winding to control the motor's operation, ensuring precise control of torque and flux.

This process, involving Clarke and Park transformations, the control of current components, and the inverse transformations to generate the appropriate reference voltages, forms the core of Field Oriented Control, enabling effective and efficient operation of the motor.

3.3.3 FOC for BDFRM

The FOC based control strategy for BDFRM proposed in this work is detailed in the block diagram presented below in figure 3.2

Primary winding control loop

The primary winding frequency ($f_{1_{ref}}$) is fixed, the d-axis reference voltage (v_{1d}) is set to 0 and the q-axis reference voltage (v_{1q}) is determined based on the Volts-per-Hertz (V/f) ratio of the BDFRM. These reference voltages are then transformed via the inverse park transformation modules to obtain primary winding voltage vector ($v_{1\alpha,\beta}$), in the stationary reference frame. This voltage vector is then fed to the primary space vector pulse width modulation (SVPWM) module, which generates gate signals for the primary converter, supplying power to the primary winding of the BDFRM.

Secondary winding control loop

Secondary winding currents ($i_{2a,b}$) are measured through LEM current sensors, and passed through the Clarke and Park transformation modules to obtain the secondary winding d and q axis currents ($i_{2d,q}$). In case of operation without low pass filter, these currents are then compared with their corresponding

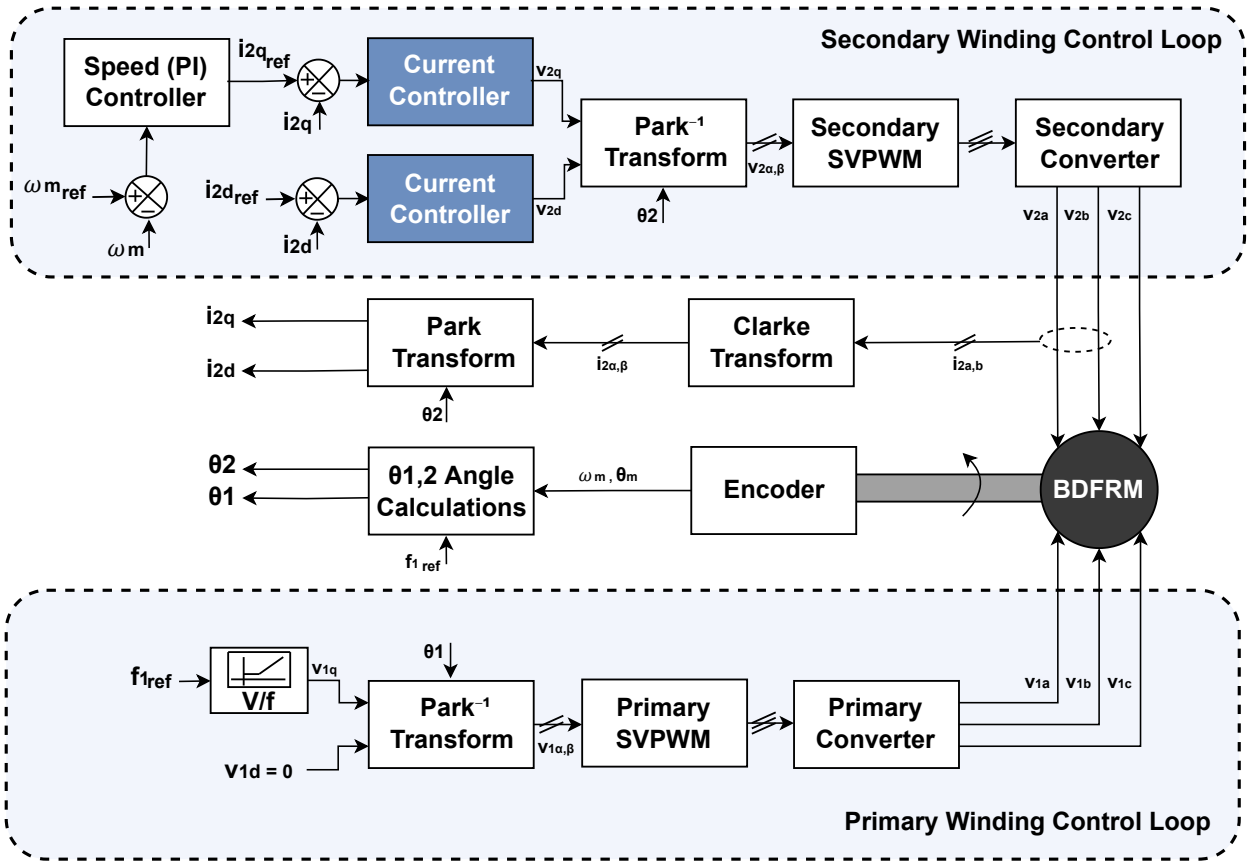

Figure 3.2: Block Diagram of the proposed control strategy

references ($i_{2d_{ref}}$ and $i_{2q_{ref}}$) directly. In case of operation with low pass filter, these currents are first fed to a filter, and the resulting filtered outputs are then compared with their corresponding references. The $i_{2d_{ref}}$ value is set to 0. Rotor speed is measured via an encoder and compared to the reference speed. The resulting error is input to the speed PI controller, which outputs $i_{2q_{ref}}$, i.e. torque component reference. The resulting current errors are fed to either PI or DTSTSM current controllers, depending on the one being implemented. The outputs from these current controllers serve as voltage references ($v_{2d,q}$), which are again transformed back into the stationary frame voltage vector ($v_{2\alpha,\beta}$) via inverse park transformation module and used by the SVPWM module to drive the secondary converter.

Electrical Angle Calculation:

It is important to note that the calculation of the electrical angles θ_1 and θ_2 for each winding's reference frame is essential for the Clarke and Park transform modules. These angles can be derived from the measured mechanical speed and position of the rotor by the following equations:

$$\theta_1 = \int \omega_1 * dt \tag{3.11}$$

$$\theta_m = \int \omega_m * dt \tag{3.12}$$

$$\theta_r = p_r \theta_m \tag{3.13}$$

$$\theta_2 = \theta_r - \theta_1 \tag{3.14}$$

Here, θ_1, θ_2 are the reference frame angles for the primary winding (d_1q_1) and the secondary winding (d_2q_2) reference frames respectively. The reference frames are shown in figure 2.5.

3.4 Discrete Time Super Twisting Sliding Mode Controller

Given the highly nonlinear dynamics of a BDFRM due to the harmonics present in the stator current, the use of traditional linear controllers, such as PI controllers, is not advisable because of their poor performance and instability in the face of the the non linear dynamics of the machine.

To better handle these dynamics while ensuring low computational cost, a nonlinear controller like the Sliding Mode Controller (SMC) can be employed to control the BDFRM stator current. SMCs are particularly advantageous in handling systems with significant nonlinearities because they force the system to follow a sliding surface, providing robustness against disturbances and parameter variations. However, despite their benefits, SMCs are notorious for a phenomenon known as chattering. Chattering refers to oscillations of finite magnitude and frequency that appear in the control output. This unwanted behavior arises due to the abrupt switching action of the controller and can lead to various issues such as reduced control accuracy, mechanical wear and tear, and noise, all of which degrade the system's performance, and hence, mitigating the chattering effect becomes essential.

To address this challenge, high order sliding mode control technique is employed in this research. Specifically, the Super Twisting Algorithm (STA) is used. The STA is a higher order sliding mode technique that smooths the control action thereby significantly mitigating the chattering effect. Furthermore, to support digital signal processor based implementation of the controller, the proposed controlloer is developed in discrete time domain.

Therefore, to summarize, this research work proposes and investigates the implementation of Discrete Time Super Twisting Sliding Mode (DTSTSM) controller for the control of BDFRM stator currents.

3.4.1 Generalized Controller Structure

This subsection presents the generalized DTSTSM controller structure detailing the sliding surface, and the control action taken from [95]:

The sliding surface s_k (where, k is the given sample instant) is given as,

$$s_k = e_k = i_k - i_k* \tag{3.15}$$

here, e_k is the current tracking error, i_k the measured current, and i_k^* the reference current.

Thereby, the control law of the DTSTSM controller is given as follows:

$$y_k = -K_1 \mid s_k \mid^{1/2} \text{sign}(s_k) + u_k \tag{3.16}$$

$$u_k = \gamma u_{k-1} - K_2 T_s \,\text{sign}(s_k) \tag{3.17}$$

here, y_k is the controller output, u_k is an auxiliary variable, γ is a fixed gain with a value between 0 to 1, K_1, K_2 are controller gains and T_s is the sampling time period.

The signal function (sign(s_k)) can be obtained as follows:

$$\text{sign}\,(s_k) = \begin{cases} 1 & \text{if} \quad s_k > 0 \\ 0 & \text{if} \quad s_k = 0 \\ -1 & \text{if} \quad s_k < 0 \end{cases} \tag{3.18}$$

The DTSTSM controller gains (K_1, K_2) have to be tuned so as to obtain the desired response from the controller and hence the overall system. In this research work, the DTSTSM controller is initially manually tuned and then later the controller gains K_1 and K_2 are selected using an offline Particle Swarm Optimization (PSO) algorithm. The performance of the controller with both these sets of gains is then subsequently compared. The next section will detail the process of PSO based DTSTSM gain tuning.

3.5 PSO based DTSTSM Controller Gain Design

The choice of controller gains directly influences the system's response characteristics, including the speed of response and the stability of the control action. A higher controller gain results in a faster system response. While this may seem advantageous, it comes at the cost of introducing larger peak overshoots and increased ripples in the current signal which can lead to increases error and instability. Therefore, a balance must be struck between the desired fast response time and the acceptable level of peak overshoot and ripple.

Achieving this balance is not straightforward, as it requires careful consideration of the trade-offs between system dynamics and performance. To address this, an optimization algorithm is employed to determine the optimal controller gains that satisfy the performance criteria. In the present research, the Particle Swarm Optimization (PSO) algorithm is utilized to tune the Discrete Time Super Twisting Sliding Mode (DTSTSM) controller gains.

3.5.1 Particle Swarm Optimization

Particle Swarm Optimization (PSO) is a metaheuristic inspired by the collective intelligence observed in nature, such as in bird flocking and fish schooling [96]. The underlying principle of PSO draws parallels to other evolutionary algorithms, such as Genetic Algorithms (GA) and Evolutionary Programming (EP). However, PSO distinguishes itself through its simplicity and ease of implementation, requiring relatively few parameters. Furthermore, PSO is highly versatile, capable of being applied to both discrete and continuous optimization problems. It is particularly well suited for tuning nonlinear controllers like DTSTSM.

PSO works by placing a swarm of N particles (candidate solutions) at random positions in the search space and computing the objective function for each particle. Over successive iterations, the positions of these particles are updated based on the following equations:

$$v_{k+1} = \underbrace{av_k}_{InertiaFactor} + \underbrace{b_1 r_1 (P_{best} - x_k)}_{CognitiveComponent} + \underbrace{b_2 r_2 (G_{best} - x_k)}_{SocialComponent} \tag{3.19}$$

$$x_{k+1} = x_k + v_{k+1} \tag{3.20}$$

where, v_k and x_k are the velocity and position of the particle at the k^{th} iteration, a is the inertia weight, b_1 and b_2 are the cognitive and social coefficients, respectively, r_1 and r_2 are random numbers between 0 and 1, P_{best}, G_{best} are the best known position of the particle and the entire swarm respectively up-to the current iteration[97].

3.5.2 PSO based Gain Design

The objective of the optimization problem is to minimize the sum of the current tracking error of the secondary winding currents, as shown in (3.21), by tuning the controller gain parameters:

Objective Function:

$$Minimize \sum_{t=0}^{t=T} e_{k(I_{2d})} + e_{k(I_{2q})} \tag{3.21}$$

where, $e_{k(I_{2d})}, e_{k(I_{2q})}$ are the secondary winding d and q axis current tracking errors respectively. This aims

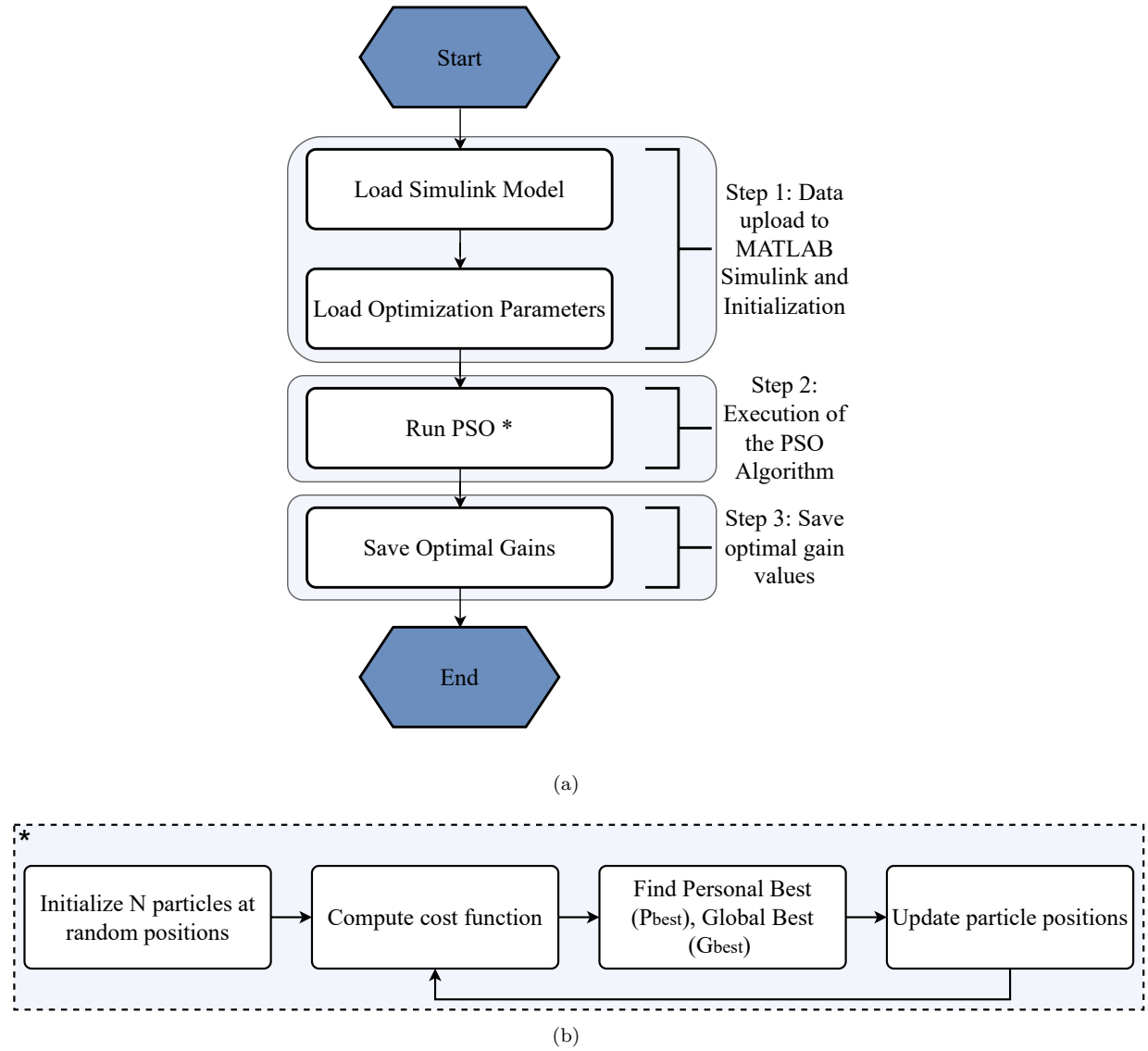

Figure 3.3: PSO-based gain design procedure (a) General procedure flowchart. (b) Detailed PSO algorithm flowchart.

to achieve minimum current tracking error between the secondary winding current reference and the actual secondary winding current.

Decision Variables:

The decision variables of this optimization problem are the controller gains for each current controller i.e

- Controller Gains for I_{2d} current controller: $K_{1(I_{2d})}, K_{2(I_{2d})}$
- Controller Gains for I_{2q} current controller: $K_{1(I_{2q})}, K_{2(I_{2q})}$

Constraints:

These controller gains are limited by upper and lower bounds. These limits are incorporated into the

optimization problem via constraints.

$$K_{1(I_{2d,q})min} \leq K_{1(I_{2d,q})} \leq K_{1(I_{2d,q})max} \tag{3.22}$$

$$K_{2(I_{2d,q})min} \leq K_{2(I_{2d,q})} \leq K_{2(I_{2d,q})max} \tag{3.23}$$

Optimization Algorithm:

Figure 3.3(a) illustrates the steps undertook to solve the optimization problem. First, a BDFRM simulation model is loaded onto MATLAB/Simulink software. This model is based on the $d-q$ reference frame BDFRM model equations derived in Chapter 2, with the machine parameters given in the next chapter. Next, the optimization parameters are set, them being: swarm size $N = 20$, inertia weight $a = 0.8$, and both cognitive and social coefficients $b_1 = b_2 = 2$. Then, the iterative PSO algorithm is executed, as shown in Fig. 3.3(b).

In the initial iteration ($k = 1$), the algorithm starts by assigning a random initial position within the solution space for each particle, while setting initial velocities to zero. The Simulink model is then run, and the fitness value for each particle is evaluated. Using these fitness values, each particle's Personal Best (P_{best}) and the Global Best (G_{best}) for the entire swarm are determined and updated.

Following this, the algorithm checks whether the termination condition has been met. If the condition is not satisfied, the iteration counter is incremented by one, and the process continues. From the second iteration onward, the position and velocity of each particle are updated based on the P_{best} and G_{best} values from the previous iteration according to the equations (3.19) and (3.20).

The algorithm continues iterating, incrementing the counter after each cycle, until the termination condition i.e. either reaching k_{max} iterations or achieving the desired fitness threshold is met. Once the termination criterion is satisfied, the algorithm concludes, and the best position known by the swarm is stored as the optimal controller gains.

Chapter 4

Experimental System and Results

This chapter provides an overview of the experimental setup used to perform the tests to validate the proposed control strategy outlined in the previous chapter. This chapter begins with providing the details of the experimental system and then moves towards discussing the various tests that have been performed, the results that were obtained and the subsequent observations that were made.

4.1 Experimental Setup

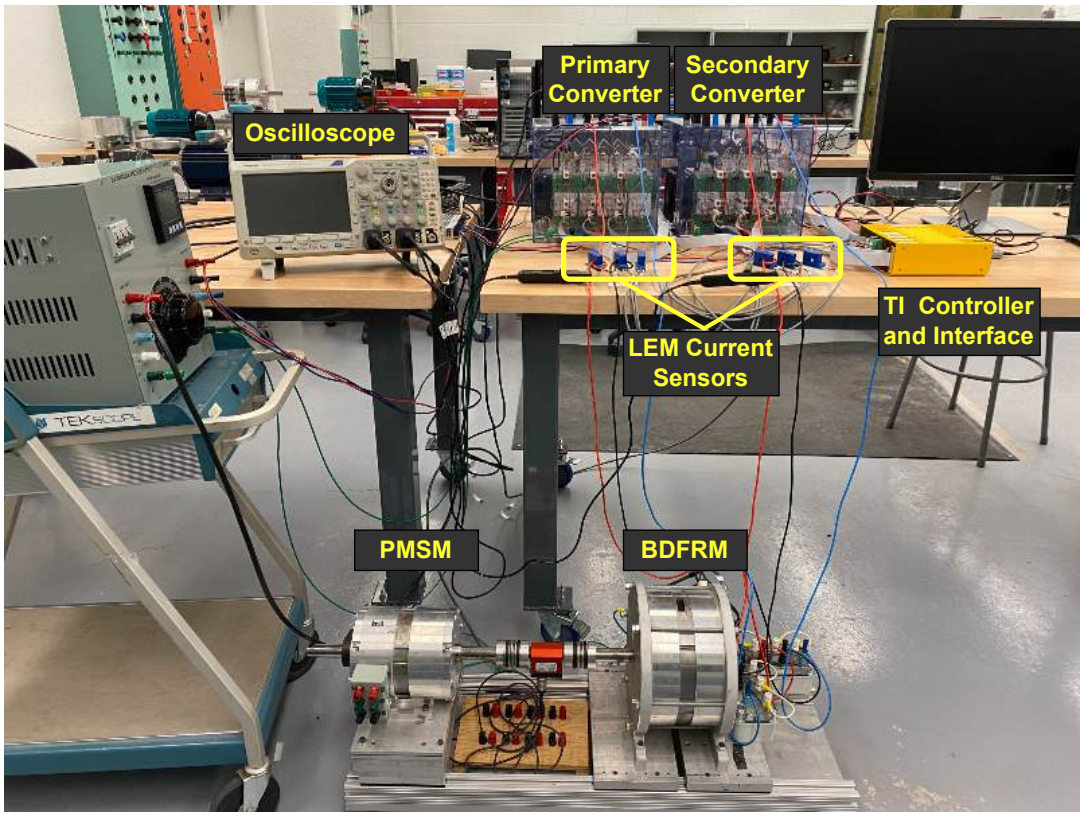

Figure 4.1: Experimental test rig

Figure 4.1 illustrates the experimental setup used for testing the BDFRM system. The rig features a BDFRM designed as per specifications in [25], with stator winding poles $p_1 = 8$, $p_2 = 4$, and rotor poles $p_r = 6$. Both stator windings are rated for 63 V (rms) phase voltage and 4.2 A (rms) current, with the primary side operating at a rated frequency of 100 Hz and overall power rating of 630 W. The electrical parameters of the machine are as follows: $R_1 = 2.8\ \Omega$, $R_2 = 4.05\ \Omega$, $L_1 = 0.0827$ H, $L_2 = 0.0398$ H, and mutual inductance $L_{12} = 0.0284$ H. The BDFRM shaft is mechanically coupled to a 1 kW permanent magnet synchronous machine (PMSM). To vary the load imposed by this PMSM on the BDFRM drive, the stator of this PMSM is connected to a 3 phase variable resistor bank and this resistance is varied.

The system is driven by two IGBT based Semikron Semiteach three phase converters (750 V DC max, 20 kW rating, 4400 μF DC-link capacitance) switching at a frequency of 10k Hz, controlled via a DSP based PwrCon platform from Denkinetic Pty Ltd. This control unit includes the Texas Instruments TMS320F28335 microcontroller. Key internal variables such as motor speed n_m, speed reference n_{ref}, secondary winding

q-axis current i_{2q}, secondary winding q-axis reference current $i_{2q_{ref}}$, secondary winding d-axis current i_{2d} and secondary winding d-axis reference current $i_{2d_{ref}}$ can be monitored in real time on an oscilloscope using DAC interface of the microcontroller..

Table 4.1: Test cases for Speed and Secondary Winding Current Controllers

Test Case	**Section**	**Mode**	**Speed Controller**	**Secondary Winding Current Controllers**	**LPF**	**Load (N.m)**	**Speed (RPM)**
1	4.2	Cascade	×	×	×	No load	0→600
2	4.3	BDFRM	PI	PI	×	No load	600
3	4.3	BDFRM	PI	PI	×	No load	400→800
4	4.3	BDFRM	PI	PI	×	0.77→1.65→2.55	1200
5	4.4	BDFRM	PI	PI	✓	No load	600
6	4.4	BDFRM	PI	PI	✓	No load	400→800
7	4.4	BDFRM	PI	PI	✓	0.77→1.65→2.55	1200
8	4.5	BDFRM	PI	DTSTSM (Manually tuned)	×	No load	400→800
9	4.5	BDFRM	PI	DTSTSM (Manually tuned)	×	0.77→1.65→2.55	1200
10	4.5	BDFRM	PI (re-tuned)	DTSTSM (Manually tuned)	×	No load	400→800
11	4.5	BDFRM	PI (re-tuned)	DTSTSM (Manually tuned)	×	0.77→1.65→2.55	1200
12	4.5	BDFRM	PI (re-tuned)	PI	×	No load	400→800
13	4.5	BDFRM	PI (re-tuned)	PI	×	0.77→1.65→2.55	1200
14	4.6	BDFRM	PI (re-tuned)	DTSTSM (PSO tuned)	×	No load	400→800
15	4.6	BDFRM	PI (re-tuned)	DTSTSM (PSO tuned)	×	0.77→1.65→2.55	1200

Each test performed on the BDFRM drive is described as a Test Case. In total 15 tests are performed on the test rig and hence total 15 Test Cases are detailed in this chapter along with their results and the observations made from those results. These test cases are classified amongst five broad categories with each category being dedicated to an individual section in the chapter. Thus, this section is followed by five sections, and each section entails certain number of test cases described, with total test cases amounting to 15. Each section is distinguished by mode of operation and the controller used for secondary winding

current control. Section 4.2 entails the tests run on the BDFRM test rig in open loop cascade induction mode, Section 4.3 includes the tests run on BDFRM in BDFRM mode, while using PI based current controllers for secondary winding current control without an LPF, Section 4.4 includes the tests performed on BDFRM in BDFRM mode, with PI based current controllers along with LPF implementation for secondary winding current control, Section 4.5 mainly consists of tests performed on the BDFRM test rig in BDFRM mode, with manually tuned DTSTSM based current controllers for secondary winding current control, and finally Section 4.6 details the tests performed on the BDFRM in BDFRM mode, with PSO tuned DTSTSM based current controllers for secondary winding current control. Lastly, this chapter ends with Section 4.7 that provides a summary of the results obtained from all test cases. An overview of the different test cases included in each section is presented in table 4.1. Complete details of each test case along with how the test is performed is described in detail in each section.

4.2 Open Loop Cascade Induction Mode: BDFRM Start-up

This section includes Test Case 1, where the BDFRM is operated under open loop cascade induction mode to start the motor from standstill and brought to a speed of 600 RPM under no-load condition.

4.2.1 Test Case 1

In this test case, the BDFRM is operated in open loop cascade induction mode. Thus, no speed control is employed. The secondary winding is short-circuited by controlling the secondary winding converter output to zero. On the primary winding, a frequency ramp ranging from 0 to 60 Hz along with a voltage ramp scaled according to the V/f ratio is applied to reach the target speed of 600 RPM through the primary winding converter. The speed response of the BDFRM from 0 to 600 RPM, during this startup, operating in the open loop cascade induction mode is shown in Figure 4.2.The machine speed (n_m) settles below the reference speed (n_{ref}) since it is an open loop operation and no speed control is employed. Furthermore, figure 4.3 illustrates the primary and secondary winding phase 'a' currents at 600 RPM reference speed. Significant harmonic content is evident in the secondary winding current.

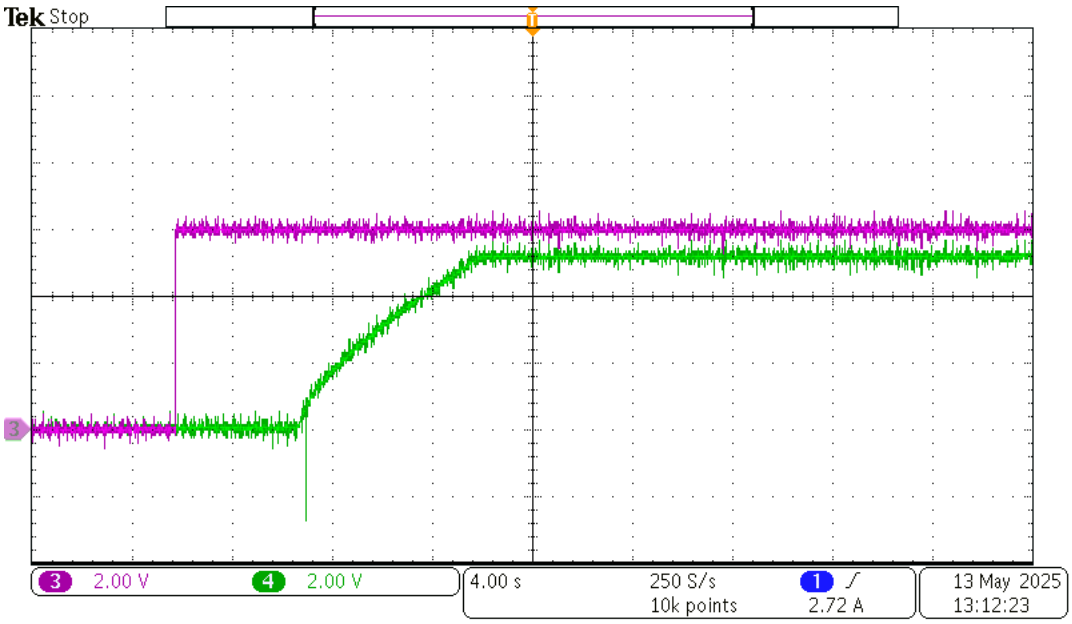

Figure 4.2: Test Case 1 - Speed Tracking: Channel 3 = n_{ref} (scale: 100 RPM = 1 V = 0.5 division), Channel 4 = n_m (scale: 100 RPM = 1 V = 0.5 division), (Time scale: 1 division = 4 s)

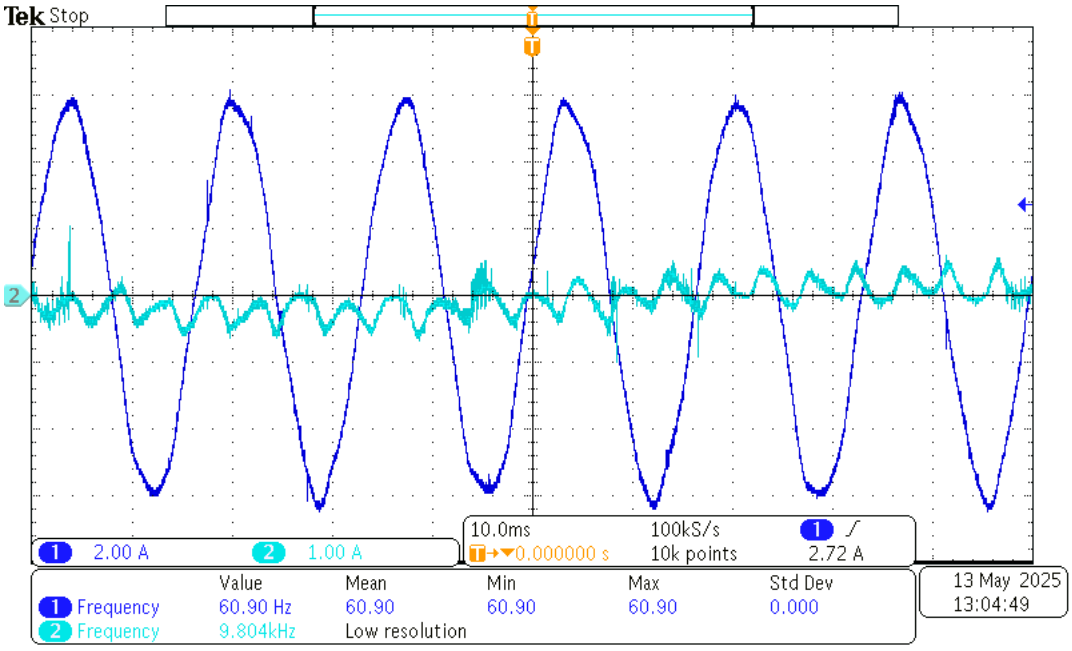

Figure 4.3: Test Case 1 - Phase a currents: Channel 1 = i_{1a} (scale: 2 A = 1 division), Channel 2 = i_{2a} (scale: 1 A = 1 division), (Time scale: 1 division = 10 ms)

4.3 BDFRM Mode: PI based Current Controller without LPF

This section includes Test Case 2, 3 and 4, where the BDFRM is operated in BDFRM mode and PI based current controllers are used for secondary winding current control without LPF implementation. These tests are performed to establish a baseline and benchmarks to which the subsequent test cases and their results will be compared. PI controller performance results are taken as benchmark for comparison because they are the conventionally used linear controllers in most applications.

4.3.1 Test Case 2

In this test case, the BDFRM is operated in BDFRM mode, and hence speed control is enabled. PI based controller is used for speed control. The gains of this speed PI controller are as follows: $K_p = 0.006$ and $K_i = 0.00025$. The primary winding is supplied with a constant voltage and constant frequency through the primary winding converter. The constant voltage and frequency applied to the primary winding are as follows: $V_{1d} = 0, V_{1q} = 87$ and $f_1 = 60$. The secondary winding supply is regulated to control the BDFRM speed. PI based current controllers are used to control the secondary winding current without LPF implementation in the current control loop. The gains of these PI based current controllers are as follows: $K_{p(I_{2d,q})} = 75$ and $K_{i(I_{2d,q})} = 50$. In this test case the BDFRM is operated at constant speed of 600 RPM. Thus, the frequency applied to the secondary winding is $f_2 = 0$Hz to satisfy the condition in the equation 2.1. Lastly, in this test case the BDFRM is operated under no-load.

Figure 4.4 shows the primary and secondary winding phase 'a' currents for test case 2, when the machine is at the steady state speed of 600 RPM. As seen in this figure, harmonic content still persists in the secondary winding current. To examine this further, the secondary winding current transformed into the rotating dq reference frame is analyzed.

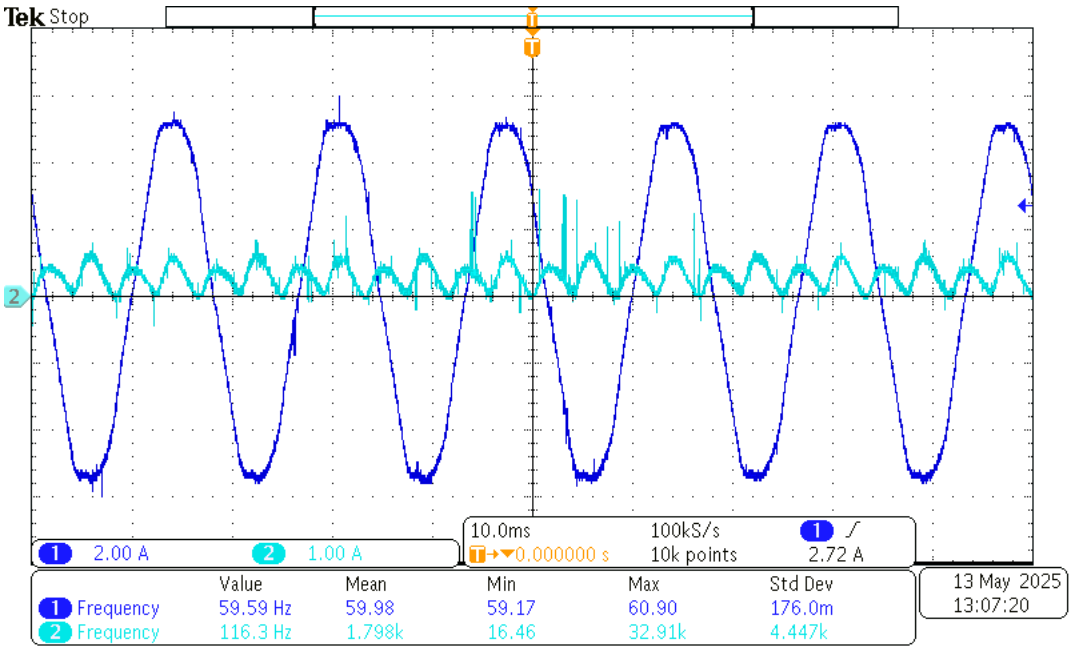

Figure 4.4: Test Case 2 - Phase a currents: Channel 1 = i_{1a} (scale: 2 A = 1 division), Channel 2 = i_{2a} (scale: 1 A = 1 division), (Time scale: 1 division = 10 ms)

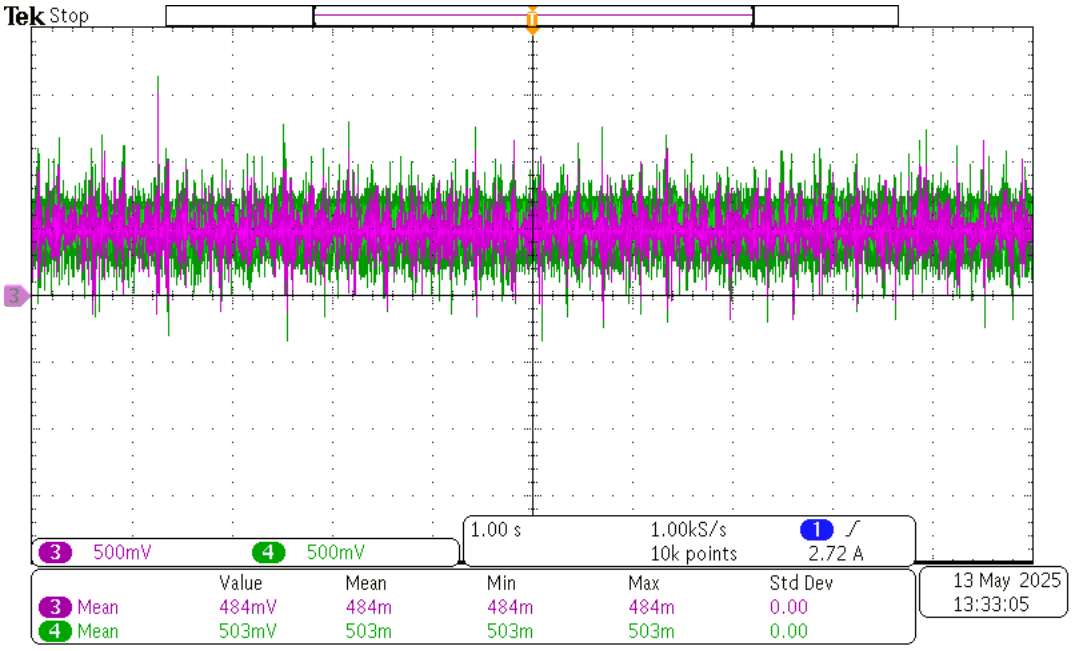

Figure 4.5: Test Case 2 - Secondary Winding q axis current: Channel 3 = $i_{2q_{ref}}$ (scale: 1 A = 1 V = 2 divisions), Channel 4 = i_{2q} (scale: 1 A = 1 V = 2 divisions), (Time scale: 1 division = 1 s)

As depicted in Fig. 4.5, the measured i_{2q} shows significant ripples around its mean value, which ideally

should be constant DC under steady-state operation. This ripple is a result of harmonics, which degrade the quality of the current control and adversely affect machine performance and speed response. These harmonics make the controller's objective to maintain i_{2q} at a constant reference, difficult to achieve. Furthermore, these fluctuations complicate PI controller tuning using conventional methods such as Ziegler-Nichols or manual adjustment, and the resulting tuned parameters are often not robust across different operating conditions. In some cases, the controller may even become unstable, potentially causing system faults.

Thus, it is very important to curb the negative impact of these harmonics on the control system by employing a low pass filter in conjunction with the PI controllers, or replacing the PI controllers altogether by non linear controller like a discrete time super twisting sliding mode controller. However, before employing these solution strategies, it is first essential to thoroughly inspect these harmonics and the subsequent challenges they impose on the control strategies of BDFRM. Therefore, the next subsection dives deeper into the harmonic analysis of the BDFRM.

4.3.2 Harmonic Analysis

To analyze the unwanted harmonics present in the secondary winding current of the BDFRM, spectral analysis of the i_{2q} waveform obtained in the BDFRM mode, under no load condition is performed at different speeds over the entire desired speed range of 400 to 800 RPM. Figure 4.6 shows the dominant harmonic components in i_{2q} current at different speeds ranging from 400 to 800 RPM. It can be observed that at

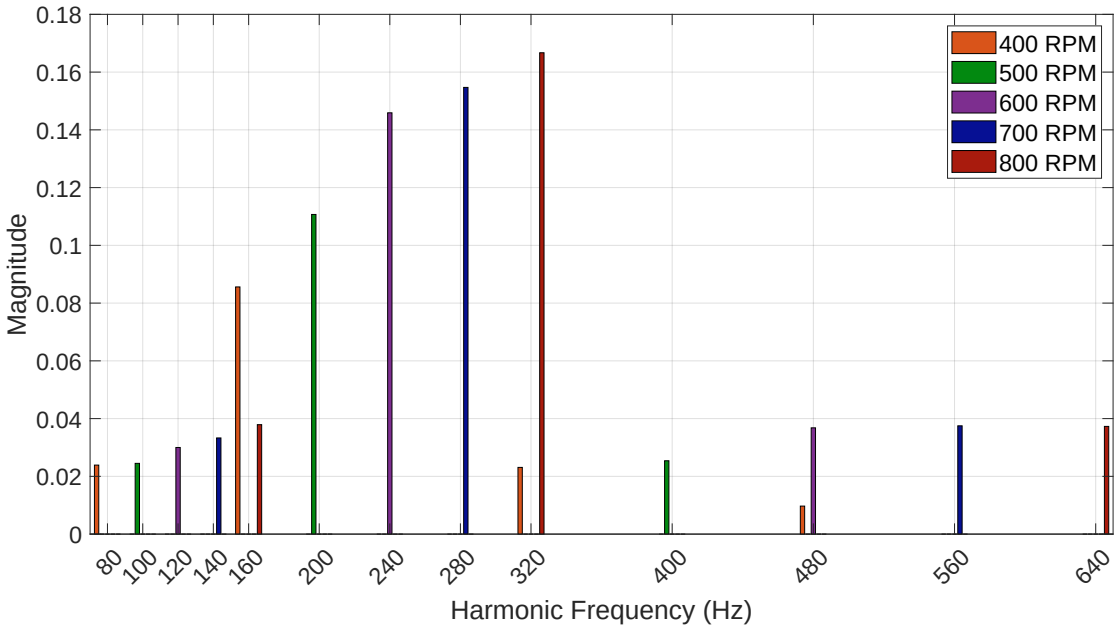

Figure 4.6: BDFRM Mode, with PI based current controller without LPF: Dominant harmonic components in i_{2q}

each speed, the dominant harmonics appear at multiples of the rotor electrical frequency ($f_r = \frac{p_r n_m}{60}$), i.e. harmonic frequencies $f_h = nf_r$, where $n = 2, 4, 8, 16...$ etc. The 4^{th} multiple of the rotor electrical frequency harmonic component ($4f_r$) is the most dominant, followed by $2f_r$ component. Thus, the remaining harmonic analysis is focused on these two components. Comparing with Figure 4.5 where the desired secondary winding current has a peak of 0.5 A, the magnitudes of the unwanted harmonics in Figure 4.6 are approaching 1/3 of the control value. It is also worth noting that these harmonics are in the secondary winding $d-q$ reference frame which is rotating at f_2 frequency. Thus, these harmonic components when observed in the secondary winding phase current in the stationary $a-b-c$ reference frame (as in figure 4.4) will appear at frequencies $nf_r - f_2$, where $n = 2, 4, 8, 16...$ etc.

Figure 4.7 shows the secondary winding control frequency ($|f_2|$) in the stationary reference frame, the 1^{st} and 2^{nd} significant harmonic component present in the secondary winding current, in both dq reference frame ($2f_r$ and $4f_r$) and stationary reference frame ($2f_r - f_2$ and $4f_r - f_2$) as functions of rotor speed.

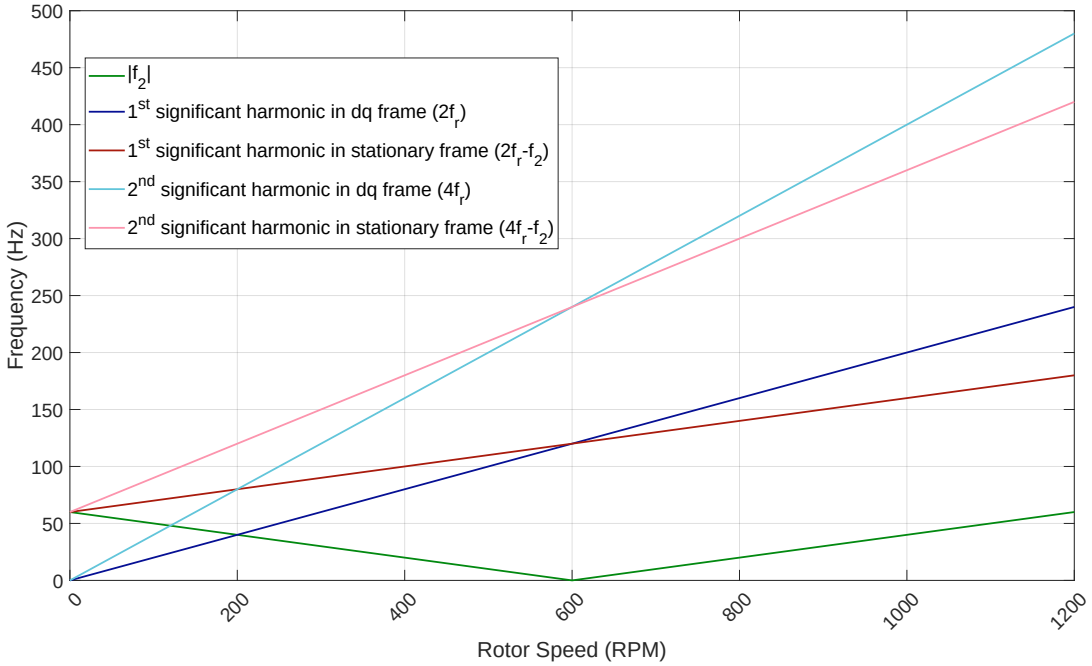

Figure 4.7: BDFRM Mode, with PI based current controller without LPF: Dominant harmonic components in i_2 in dq frame and stationary reference frame.

The secondary winding control frequency is always 0 Hz in the dq reference frame irrespective of the rotor speed. It can be noticed that for lower speeds, i.e. 0 to 200 RPM, in both reference frames, the unwanted current harmonic components in the secondary winding are at frequencies very close to the fundamental control frequency, with the harmonic frequencies being exactly equal to the control frequency (0 Hz in dq

frame, and 60 Hz in stationary frame) at 0 RPM or standstill condition. Thus, speed control of a BDFRM using a linear controller like a PI controller at lower speeds proves to be very difficult. However, for BDFRM speed in a band around the synchronous speed (400 to 800 RPM in our case), there is a significant gap between the control frequency and the harmonic frequencies, making it feasible to use a PI controller in conjunction with a low pass filter to attenuate the unwanted current harmonics before feeding it to the controller, thereby improving controller performance, aiding BDFRM speed control. Lastly upon the analysis of the harmonics present in secondary winding current of the BDFRM, it can be concluded that the harmonics make the use of linear controllers like PI controllers very difficult over the entire speed range, especially at the lower speeds. Thus, to affectively control the BDFRM without any additional filters, the use of a non linear controller like the DTSTSM controller offers an excellent alternative.

The following subsections further explore the test cases where the BDFRM is run in BDFRM mode, with PI based current controllers used for secondary winding control without LPF implementation to analyze the speed response with PI based current controllers.

4.3.3 Test Case 3

In this test case, the BDFRM is operated in BDFRM mode, and hence speed control is enabled. PI based controller is used for speed control. The gains of this speed PI controller are as follows: $K_p = 0.006$ and $K_i = 0.00025$. The primary winding is supplied with a constant voltage and constant frequency through the primary winding converter. The constant voltage and frequency applied to the primary winding are as follows: $V_{1d} = 0, V_{1q} = 87$ and $f_1 = 60$. The secondary winding supply is regulated to control the BDFRM speed. PI based current controllers are used to control the secondary winding current without LPF implementation in the current control loop. The gains of these PI based current controllers are as follows: $K_{p(I_{2d,q})} = 75$ and $K_{i(I_{2d,q})} = 50$. In this test case the BDFRM is operated under no-load. Lastly, in this test case, the speed of the BDFRM is varied from 400 RPM to 800 RPM. Thus, the frequency applied to the secondary winding is varied from $f_2 = -20$ Hz to $f_2 = +20$ Hz to satisfy the condition in the equation 2.1.

Figure. 4.8 presents the speed and current tracking performance of the BDFRM when subjected to this speed change.

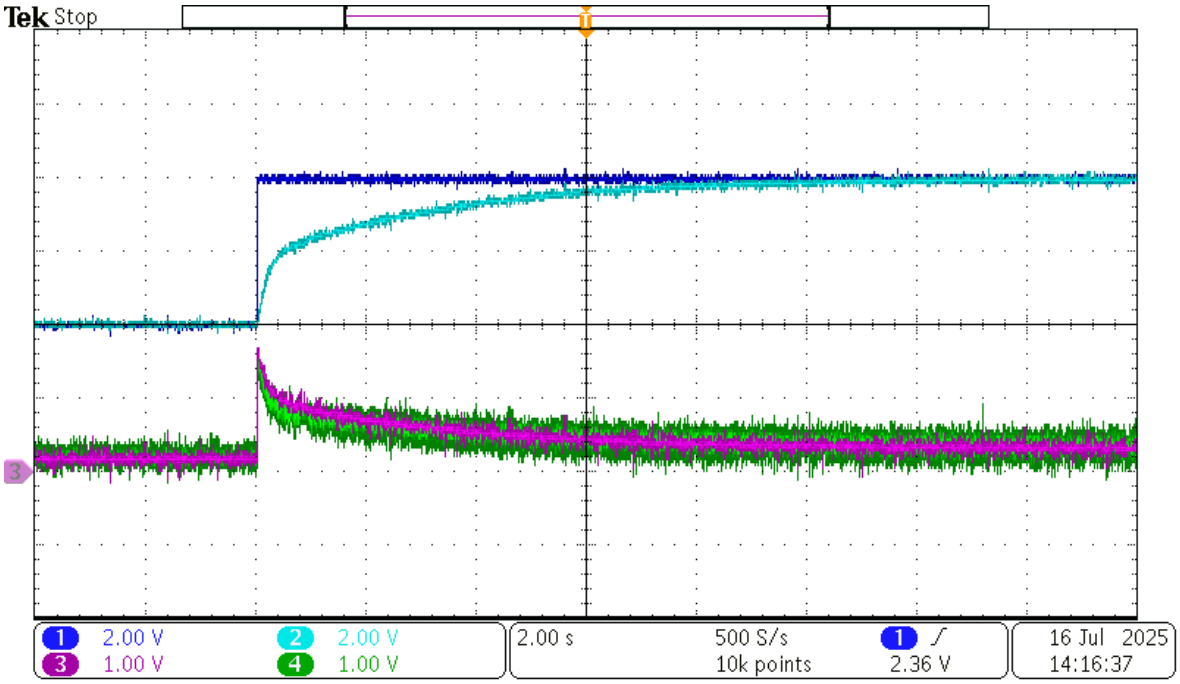

Figure 4.8: Test Case 3: Channel 1 = n_{ref} (scale: 100 RPM = 1 V = 0.5 division), Channel 2 = n_m (scale: 100 RPM = 1 V = 0.5 division), Channel 3 = $i_{2q_{ref}}$ (scale: 1 A = 1 V = 1 division), Channel 4 = i_{2q} (scale: 1 A = 1 V = 1 division), (Time scale: 1 division = 2 s)

The results clearly show that the speed response while employing PI controllers is very poor, with settling time exceeding 12 seconds, thereby highlighting the limitations of PI controller under harmonic dominant system.

4.3.4 Test Case 4

In this test case, the BDFRM is operated in BDFRM mode, and hence speed control is enabled. PI based controller is used for speed control. The gains of this speed PI controller are as follows: $K_p = 0.006$ and $K_i = 0.00025$. The primary winding is supplied with a constant voltage and constant frequency through the primary winding converter. The constant voltage and frequency applied to the primary winding are as follows: $V_{1d} = 0, V_{1q} = 87$ and $f_1 = 60$. The secondary winding supply is regulated to control the BDFRM speed. PI based current controllers are used to control the secondary winding current without LPF implementation in the current control loop. The gains of these PI based current controllers are as follows: $K_{p(I_{2d,q})} = 75$ and $K_{i(I_{2d,q})} = 50$. In this test case the BDFRM is operated at constant speed of 1200 RPM. Thus, the frequency applied to the secondary winding is $f_2 = +60$ Hz to satisfy the condition in the equation

2.1. Lastly, in this test case, the load on the BDFRM is varied from No-load (0.77 N-m)→1.65 N-m→2.55 N-m by varying the resistance value of the 3 phase resistor bank connected to the PMSM stator.

Figure. 4.9 presents the speed and current tracking performance of the BDFRM when subjected to this load change.

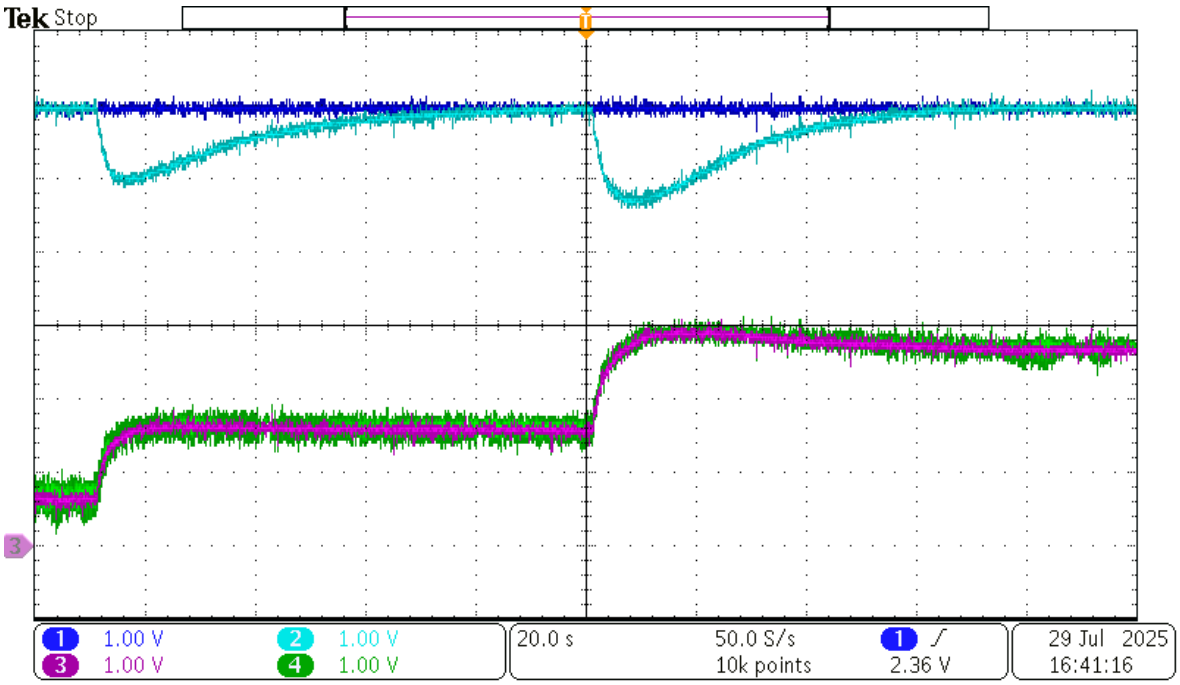

Figure 4.9: Test Case 4: Channel 1 = n_{ref} (scale: 200 RPM = 1 V = 1 division), Channel 2 = n_m (scale: 200 RPM = 1 V = 1 division), Channel 3 = $i_{2q_{ref}}$ (scale: 1 A = 1 V = 1 division), Channel 4 = i_{2q} (scale: 1 A = 1 V = 1 division), (Time scale: 1 division = 20 s)

It can be observed that on changing the load on the BDFRM while employing PI based current controller, the speed of the machine drops by over 300 RPM, and it takes over 65 seconds for the machine to recover and for the speed control to bring the machine back to it's original speed of 1200 RPM. Thereby further proving that the use of PI controller results in extremely poor performance for both constant load, speed change condition and constant speed, load change condition.

4.4 BDFRM Mode: PI based Current Controller with LPF

In this section, test cases 5,6 and 7 are presented. These test cases describe the tests performed on the BDFRM test rig in BDFRM mode, while PI based current controllers are used for secondary winding current control in conjunction with low pass filter implementation in the secondary winding current control

loop. The following subsection presents the details of the second order low pass filter implemented in the secondary winding current loop. This subsection will then be followed by the test cases.

4.4.1 Second Order Low Pass Filter Implementation

In this research work, to tackle the challenges imposed by harmonics present in the secondary winding current, a second order infinite impulse response (IIR) low pass filter (LPF) is implemented in the feedback path of the secondary winding current control loops, while still using PI controllers as the current controllers.

The standard form of second order IIR LPF is given as [98]:

$$\begin{aligned} y[n] =& B_0 x[n] + B_1 x[n-1] + B_2 x[n-2] \\ & - A_1 y[n-1] - A_2 y[n-2] \end{aligned} \tag{4.1}$$

where, $x[n]$ is the current input, $y[n]$ is the current output, B_0, B_1, B_2 are the feedforward coefficients and A_1 and A_2 are the feedback coefficients. These coefficients are designed so as to implement the desired cut-off frequency.

The lowest significant harmonic in the operating range occurs at 80 Hz, corresponding to 400 RPM. To effectively attenuate this harmonic, the filter cutoff frequency must be set below 80 Hz. Filter performance was evaluated at cutoff frequencies of 70 Hz, 60 Hz, 50 Hz, 40 Hz, 30 Hz, and 20 Hz. A cutoff frequency of 30 Hz was selected, as it successfully attenuates all lower frequency harmonics observed at 400 RPM. Frequencies above 30 Hz failed to fully suppress these harmonics, while lower value added unnecessary delay without significant benefit.

The following subsections will present the test cases in which the BDFRM is operated in BDFRM mode, with PI based current controllers for secondary winding current control along with second order low pass filter implemented in the secondary winding current control loop.

4.4.2 Test Case 5

In this test case, the BDFRM is operated in BDFRM mode, and hence speed control is enabled. PI based controller is used for speed control. The gains of this speed PI controller are as follows: $K_p = 0.006$ and $K_i = 0.00025$. The primary winding is supplied with a constant voltage and constant frequency through the primary winding converter. The constant voltage and frequency applied to the primary winding are as follows: $V_{1d} = 0$V , $V_{1q} = 87$V and $f_1 = 60$ Hz. The secondary winding supply is regulated to control the BDFRM speed. PI based current controllers are used to control the secondary winding current with LPF implementation in the current control loop. The gains of these PI based current controllers are as

follows: $K_{p(I_{2d,q})} = 75$ and $K_{i(I_{2d,q})} = 50$. The cut-off frequency of the second order LPF implemented in the secondary winding current control loop is $F_c = 30$ Hz. In this test case the BDFRM is operated at a constant speed of 600 RPM. Thus, the frequency applied to the secondary winding is $f_2 = 0$ Hz to satisfy the condition in the equation 2.1. Lastly, in this test case the BDFRM is operated under no-load.

Figure 4.10 shows the filtered secondary winding q axis current against the reference current.

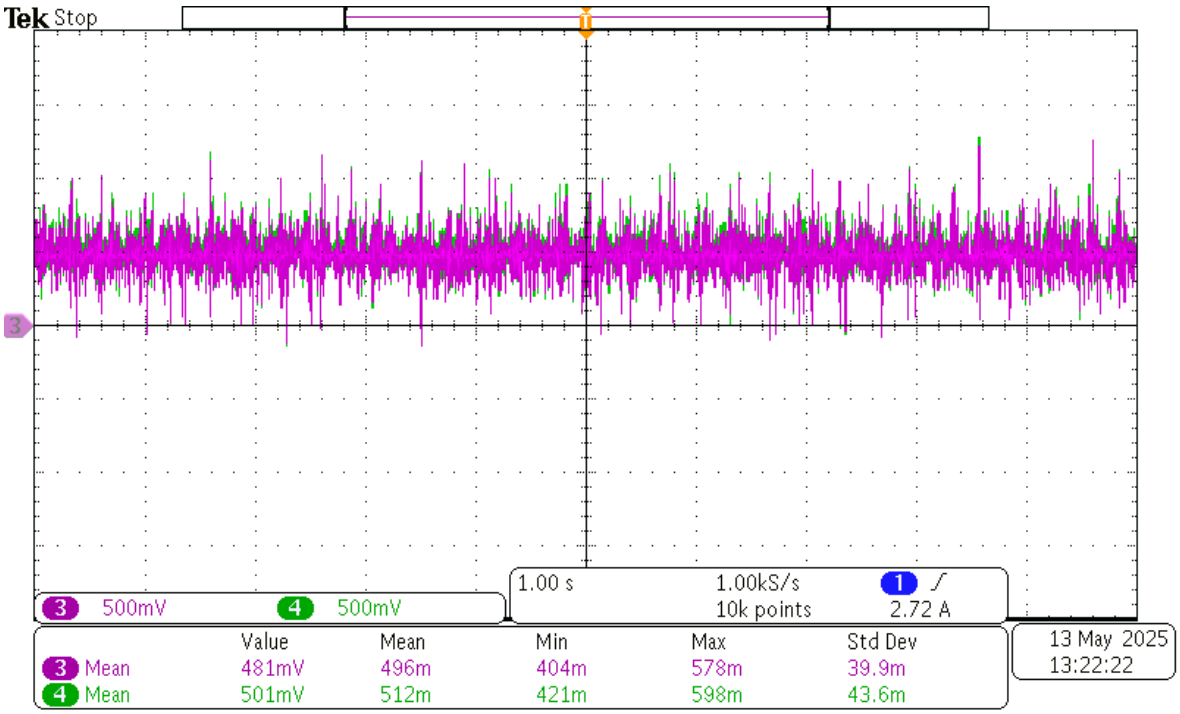

Figure 4.10: Test Case 5: Channel 3 = $i_{2q_{ref}}$ (scale: 1 A = 1 V = 2 divisions), Channel 4 = $i_{2q_{filtered}}$ (scale: 1 A = 1 V = 2 divisions), (Time scale: 1 division = 1 s)

Table 4.2 presents a comparative analysis of the PI based current controller performance with and without filtering, in terms of the average ripple in i_{2q} and $i_{2q_{filtered}}$, the mean error between i_{2q} and $i_{2q_{ref}}$, and the mean error between $i_{2q_{filtered}}$ and $i_{2q_{ref}}$ across various speeds.

Table 4.2: Comparison of Average Ripple and I_{2q} Error With and Without Filtering

Speed	**Average Ripple**		**Mean Error**	
(RPM)	**No Filter**	**With Filter**	**No Filter**	**With Filter**
400	0.0942	0.0704 (↓25.3%)	0.07292	0.028644 (↓60.7%)
500	0.1102	0.0711 (↓35.5%)	0.08736	0.028692 (↓67.2%)
600	0.1265	0.0684 (↓45.9%)	0.104224	0.02788 (↓73.3%)
700	0.1313	0.0716 (↓45.5%)	0.11216	0.030684 (↓72.6%)
800	0.1367	0.0705 (↓48.4%)	0.119296	0.03062 (↓74.3%)

It is evident from the results that the harmonic components in i_{2q} are effectively attenuated, showing a clear reduction in ripples and the current tracking error with filtering, especially at higher speeds, confirming substantial improvement in current regulation, simplifying PI controller tuning and enhancing dynamic performance.

4.4.3 Test Case 6

In this test case, the BDFRM is operated in BDFRM mode, and hence speed control is enabled. PI based controller is used for speed control. The gains of this speed PI controller are as follows: $K_p = 0.006$ and $K_i = 0.00025$. The primary winding is supplied with a constant voltage and constant frequency through the primary winding converter. The constant voltage and frequency applied to the primary winding are as follows: $V_{1d} = 0$V , $V_{1q} = 87$V and $f_1 = 60$Hz. The secondary winding supply is regulated to control the BDFRM speed. PI based current controllers are used to control the secondary winding current with LPF implementation in the current control loop. The gains of these PI based current controllers are as follows: $K_{p(I_{2d,q})} = 75$ and $K_{i(I_{2d,q})} = 50$. The cut-off frequency of the second order LPF implemented in the secondary winding current control loop is $F_c = 30$Hz. In this test case the BDFRM is operated under no-load. Lastly, in this test case, the speed of the BDFRM is varied from 400 RPM to 800 RPM. Thus, the frequency applied to the secondary winding is varied from $f_2 = -20$Hz to $f_2 = +20$Hz to satisfy the condition in the equation 2.1.

Figure. 4.11 presents the speed and current tracking performance of the BDFRM when subjected to this speed change.

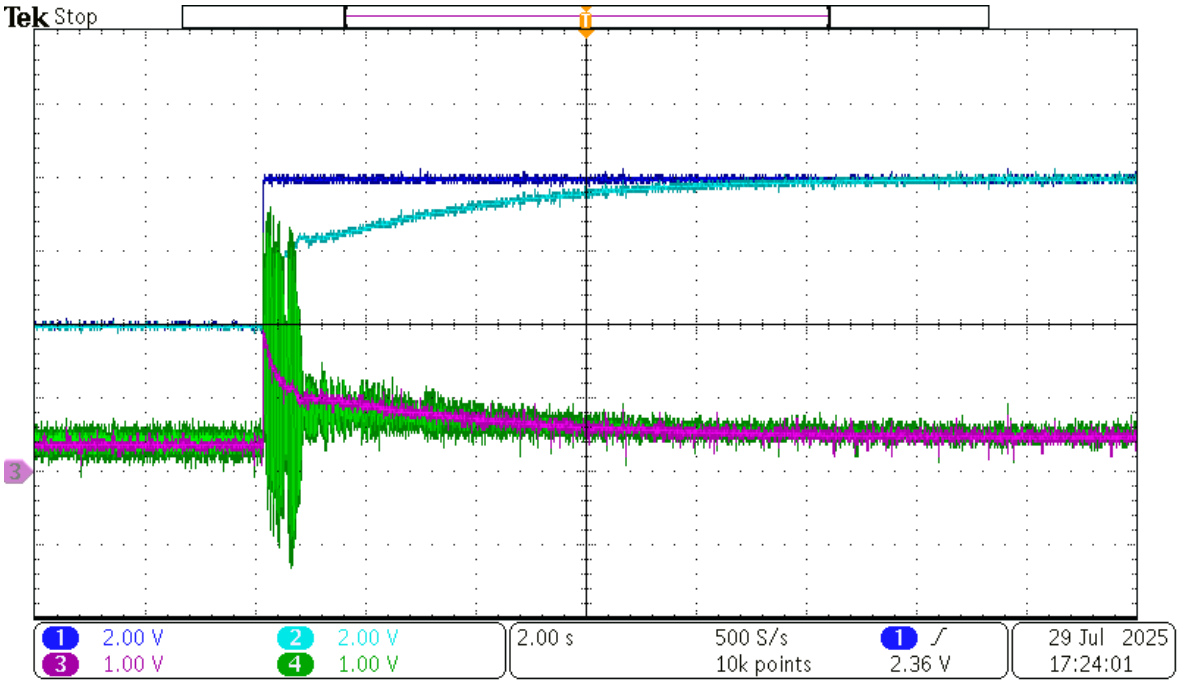

Figure 4.11: Test Case 6: Channel 1 = n_{ref} (scale: 100 RPM = 1 V = 0.5 division), Channel 2 = n_m (scale: 100 RPM = 1 V = 0.5 division), Channel 3 = $i_{2q_{ref}}$ (scale: 1 A = 1 V = 1 division), Channel 4 = i_{2q} (scale: 1 A = 1 V = 1 division), (Time scale: 1 division = 2 s)

It can be observed that the filtered response is slightly quicker and slightly improved speed tracking response is obtained with settling time of 10 s, thereby reducing the settling time of the speed response by 2 s as compared to the test case 3 with PI controller and no filter operation. However, the current tracking response shows large overshoots when the speed reference is changed.

4.4.4 Test Case 7

In this test case, the BDFRM is operated in BDFRM mode, and hence speed control is enabled. PI based controller is used for speed control. The gains of this speed PI controller are as follows: $K_p = 0.006$ and $K_i = 0.00025$. The primary winding is supplied with a constant voltage and constant frequency through the primary winding converter. The constant voltage and frequency applied to the primary winding are as follows: $V_{1d} = 0$V , $V_{1q} = 87$V and $f_1 = 60$Hz. The secondary winding supply is regulated to control the BDFRM speed. PI based current controllers are used to control the secondary winding current with LPF implementation in the current control loop. The gains of these PI based current controllers are as follows: $K_{p(I_{2d,q})} = 75$ and $K_{i(I_{2d,q})} = 50$. The cut-off frequency of the second order LPF implemented in

the secondary winding current control loop is F_c = 30Hz. In this test case the BDFRM is operated at a constant speed of 1200 RPM. Thus, the frequency applied to the secondary winding is f_2 = +60Hz to satisfy the condition in the equation 2.1. Lastly, in this test case, the load on the BDFRM is varied from No-load (0.77 N-m)→1.65 N-m→2.55 N-m by varying the resistance value of the 3 phase resistor bank connected to the PMSM stator.

Figure. 4.12 presents the speed and current tracking performance of the BDFRM when subjected to this load change. It can be observed that the speed recovery time for this test case is 60 seconds. Thus, the

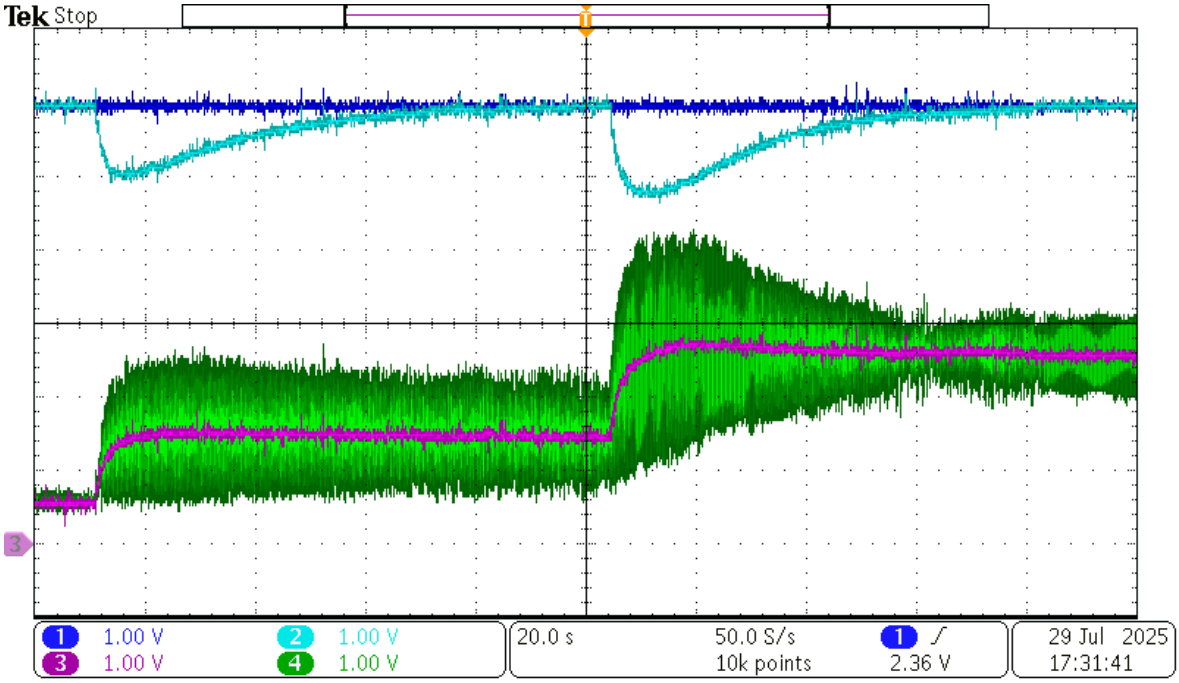

Figure 4.12: Test Case 7: Channel 1 = n_{ref} (scale: 200 RPM = 1 V = 1 division), Channel 2 = n_m (scale: 200 RPM = 1 V = 1 division), Channel 3 = $i_{2q_{ref}}$ (scale: 1 A = 1 V = 1 division), Channel 4 = i_{2q} (scale: 1 A = 1 V = 1 division), (Time scale: 1 division = 20 s)

speed tracking response here is similar to test case 4 where PI based current controllers were used without any filtering operation. However, the current tracking response for this test case as well shows very large overshoots and oscillations.

The oscillations observed in the secondary winding current for test cases 6 and 7 can be attributed to the presence of harmonic components in the secondary current. In these cases, the PI controller receives the filtered measured current, therefore, the harmonic induced oscillations are significantly attenuated before reaching the controller. As a result, the PI controller acts only on the fundamental component of the current and does not react to the harmonic oscillations that remain in the actual machine current.

In contrast, for test cases 3 and 4 where no filtering is applied, the PI controllers are driven by the unfil-

tered secondary current, which includes both the fundamental and the harmonic components. Consequently, the controllers attempt to regulate the entire signal, causing controlled overshoots and oscillatory behavior in the secondary winding current.

These substantial overshoots and oscillations demonstrate that employing PI controllers in conjunction with low pass filter to mitigate harmonic effects is not a viable control strategy for this system.

Thus, replacing the PI controller altogether by a non linear controller like the DTSTSM controller seems to be the only solution and hence, the performance of the DTSTSM controller in BDFRM control system will be further explored in the next sections.

4.5 BDFRM Mode: Manually Tuned DTSTSM based Current Controller

This section presents the test cases from 8 to 13. In these test cases, mainly the tests performed on the BDFRM test rig are in BDFRM mode, while DTSTSM based current controllers are used to control the secondary winding current of the BDFRM. The gains of these DTSTSM based current controllers in this section are selected through manual tuning process.

4.5.1 Test Case 8

In this test case, the BDFRM is operated in BDFRM mode, and hence speed control is enabled. PI based controller is used for speed control. The gains of this speed PI controller are as follows: $K_p = 0.006$ and $K_i = 0.00025$. The primary winding is supplied with a constant voltage and constant frequency through the primary winding converter. The constant voltage and frequency applied to the primary winding are as follows: $V_{1d} = 0$V , $V_{1q} = 87$V and $f_1 = 60$Hz. The secondary winding supply is regulated to control the BDFRM speed. DTSTSM based current controllers are used to control the secondary winding current. The gains of these DTSTSM based current controllers, selected through manual tuning, are as follows: $K_{1(I_{2d,q})} = 22$ and $K_{2(I_{2d,q})} = 3000$. The sampling frequency of these DTSTSM controllers is 20 kHz. In this test case the BDFRM is operated under no-load. Lastly, in this test case, the speed of the BDFRM is varied from 400 RPM to 800 RPM. Thus, the frequency applied to the secondary winding is varied from $f_2 = -20$Hz to $f_2 = +20$Hz to satisfy the condition in the equation 2.1.

Figure 4.13 displays the speed and current tracking performance of the BDFRM for the reference speed change.

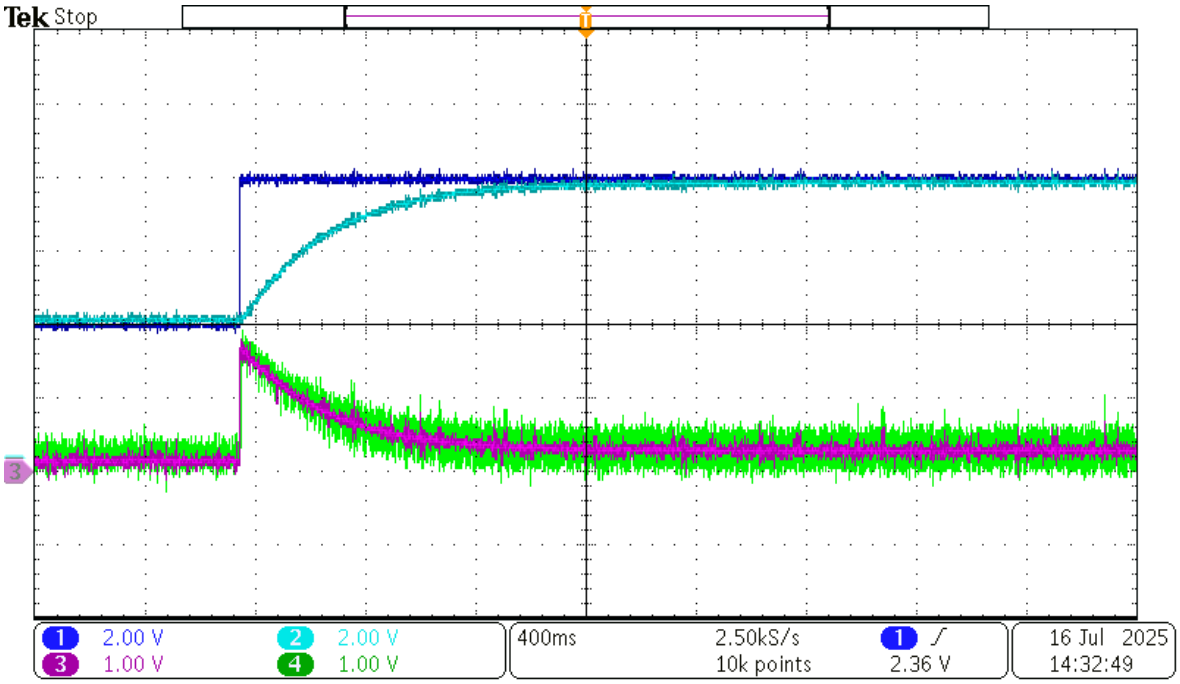

Figure 4.13: Test Case 8: Channel 1 = n_{ref} (scale: 100 RPM = 1 V = 0.5 division), Channel 2 = n_m (scale: 100 RPM = 1 V = 0.5 division), Channel 3 = $i_{2q_{ref}}$ (scale: 1 A = 1 V = 1 division), Channel 4 = i_{2q} (scale: 1 A = 1 V = 1 division), (Time scale: 1 division = 400 ms)

It can be observed that the machine exhibits significantly better performance with the settling time reduced to approximately 2 seconds. Thus, a reduction of 10 s is observed in the settling time of the speed response in case of manually tuned DTSTSM controller performance as compared to the test case 3 (PI controller performance with no filter).

4.5.2 Test Case 9

In this test case, the BDFRM is operated in BDFRM mode, and hence speed control is enabled. PI based controller is used for speed control. The gains of this speed PI controller are as follows: $K_p = 0.006$ and $K_i = 0.00025$. The primary winding is supplied with a constant voltage and constant frequency through the primary winding converter. The constant voltage and frequency applied to the primary winding are as follows: $V_{1d} = 0$V , $V_{1q} = 87$V and $f_1 = 60$Hz. The secondary winding supply is regulated to control the BDFRM speed. DTSTSM based current controllers are used to control the secondary winding current. The gains of these DTSTSM based current controllers, selected through manual tuning, are as follows: $K_{1(I_{2d,q})} = 22$ and $K_{2(I_{2d,q})} = 3000$. The sampling frequency of these DTSTSM controllers is 20 kHz. In

this test case the BDFRM is operated at a constant speed of 1200 RPM. Thus, the frequency applied to the secondary winding is $f_2 = +60$Hz to satisfy the condition in the equation 2.1. Lastly, in this test case, the load on the BDFRM is varied from No-load (0.77 N-m)→1.65 N-m→2.55 N-m by varying the resistance value of the 3 phase resistor bank connected to the PMSM stator.

Figure. 4.14 presents the speed and current tracking performance of the BDFRM when subjected to this load change.

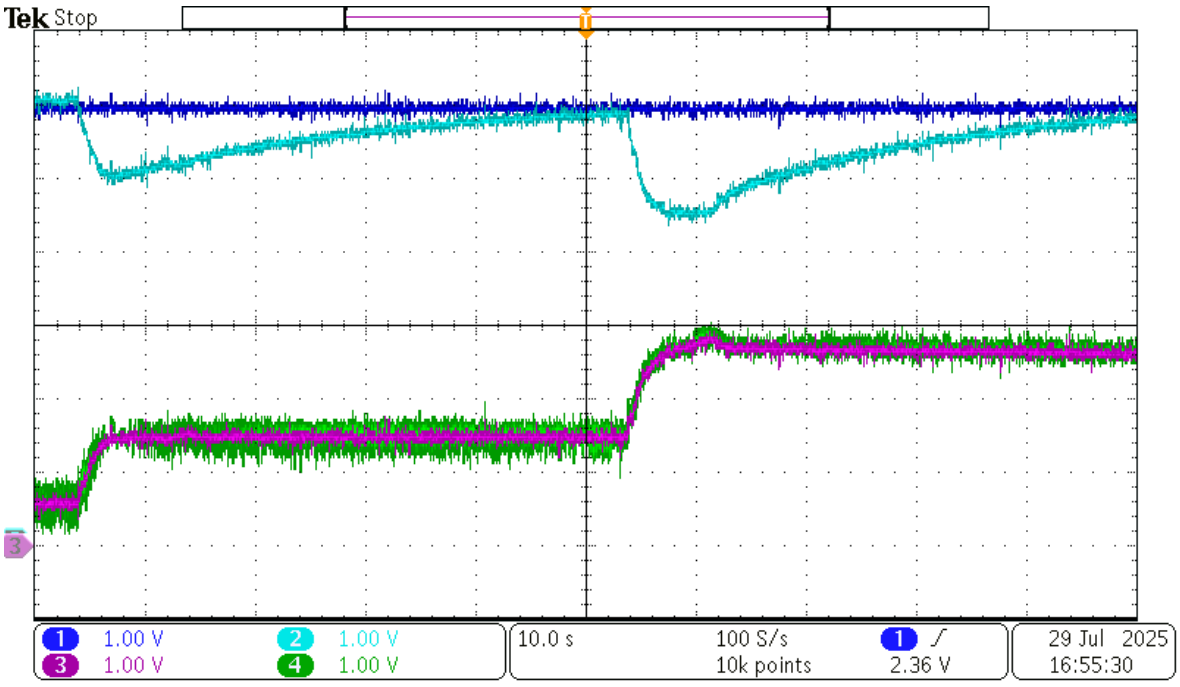

Figure 4.14: Test Case 9: Channel 1 = n_{ref} (scale: 200 RPM = 1 V = 1 division), Channel 2 = n_m (scale: 200 RPM = 1 V = 1 division), Channel 3 = $i_{2q_{ref}}$ (scale: 1 A = 1 V = 1 division), Channel 4 = i_{2q} (scale: 1 A = 1 V = 1 division), (Time scale: 1 division = 10 s)

The speed recovery time observed in this test case is still very high, i.e. 50 seconds. Thus, the speed response in this test case is also very slow, similar to test cases 4 and 7 where PI based current controllers were used. Thus, to further improve performance, the PI based speed controller is re-tuned through manual tuning process. The new speed PI controller gains selected after re-tuning are as follows: $K_p = 0.0075$ and $K_i = 0.0028$.

The BDFRM is once again tested in BDFRM mode, with manually tuned DTSTSM based current controllers used for secondary winding current control, and the re-tuned speed controller.

4.5.3 Test Case 10

In this test case, the BDFRM is operated in BDFRM mode, and hence speed control is enabled. PI based controller is used for speed control. The gains of this re-tuned speed PI controller are as follows: $K_p = 0.0075$ and $K_i = 0.0028$. The primary winding is supplied with a constant voltage and constant frequency through the primary winding converter. The constant voltage and frequency applied to the primary winding are as follows: $V_{1d} = 0$V , $V_{1q} = 87$V and $f_1 = 60$Hz. The secondary winding supply is regulated to control the BDFRM speed. DTSTSM based current controllers are used to control the secondary winding current. The gains of these DTSTSM based current controllers, selected through manual tuning, are as follows: $K_{1(I_{2d,q})} = 22$ and $K_{2(I_{2d,q})} = 3000$. The sampling frequency of these DTSTSM controllers is 20 kHz. In this test case the BDFRM is operated under no-load. Lastly, in this test case, the speed of the BDFRM is varied from 400 RPM to 800 RPM. Thus, the frequency applied to the secondary winding is varied from $f_2 = -20$Hz to $f_2 = +20$Hz to satisfy the condition in the equation 2.1.

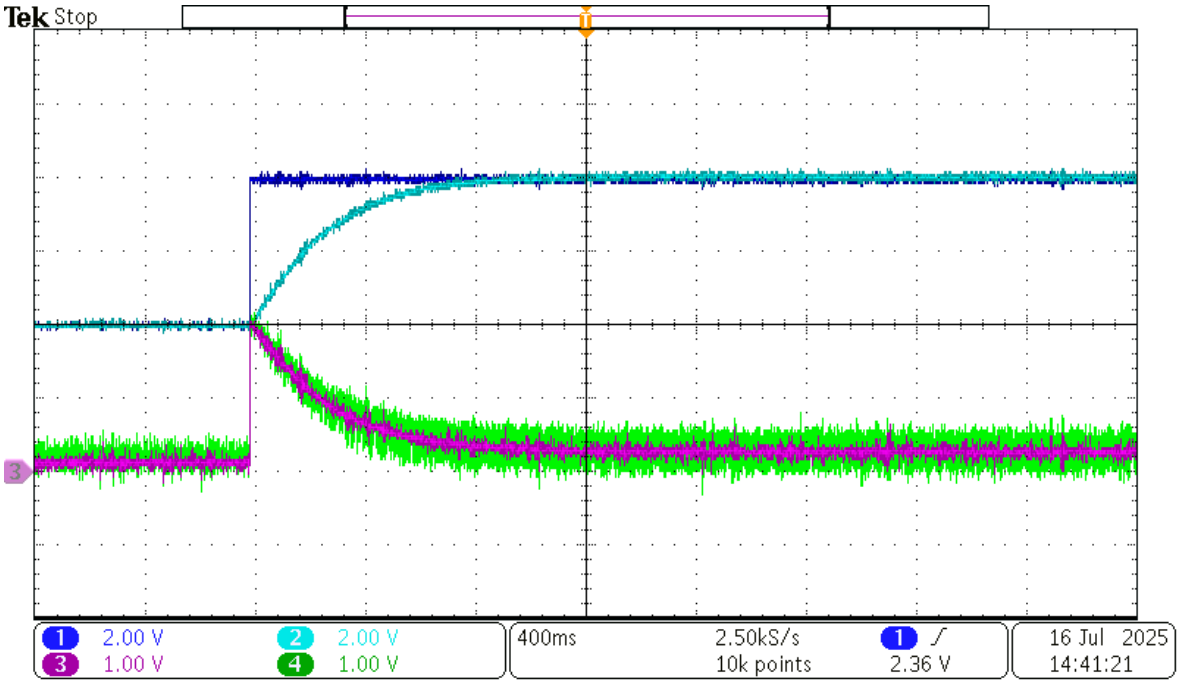

Figure 4.15: Test Case 10: Channel 1 = n_{ref} (scale: 100 RPM = 1 V = 0.5 division), Channel 2 = n_m (scale: 100 RPM = 1 V = 0.5 division), Channel 3 = $i_{2q_{ref}}$ (scale: 1 A = 1 V = 1 division), Channel 4 = i_{2q} (scale: 1 A = 1 V = 1 division), (Time scale: 1 division = 400 ms)

As shown in Fig. 4.15, re-tuning the speed controller further enhances the system response, reducing the settling time to only 0.8 seconds (11.2 seconds lower than test case 3), thereby making the response much

faster.

4.5.4 Test Case 11

In this test case, the BDFRM is operated in BDFRM mode, and hence speed control is enabled. PI based controller is used for speed control. The gains of this re-tuned speed PI controller are as follows: $K_p = 0.0075$ and $K_i = 0.0028$. The primary winding is supplied with a constant voltage and constant frequency through the primary winding converter. The constant voltage and frequency applied to the primary winding are as follows: $V_{1d} = 0$V , $V_{1q} = 87$V and $f_1 = 60$Hz. The secondary winding supply is regulated to control the BDFRM speed. DTSTSM based current controllers are used to control the secondary winding current. The gains of these DTSTSM based current controllers, selected through manual tuning, are as follows: $K_{1(I_{2d,q})} = 22$ and $K_{2(I_{2d,q})} = 3000$. The sampling frequency of these DTSTSM controllers is 20 kHz. In this test case the BDFRM is operated at a constant speed of 1200 RPM. Thus, the frequency applied to the secondary winding is $f_2 = +60$Hz to satisfy the condition in the equation 2.1. Lastly, in this test case, the load on the BDFRM is varied from No-load (0.77 N-m)→1.65 N-m→2.55 N-m by varying the resistance value of the 3 phase resistor bank connected to the PMSM stator.

Figure. 4.16 presents the speed and current tracking performance of the BDFRM when subjected to this load change.

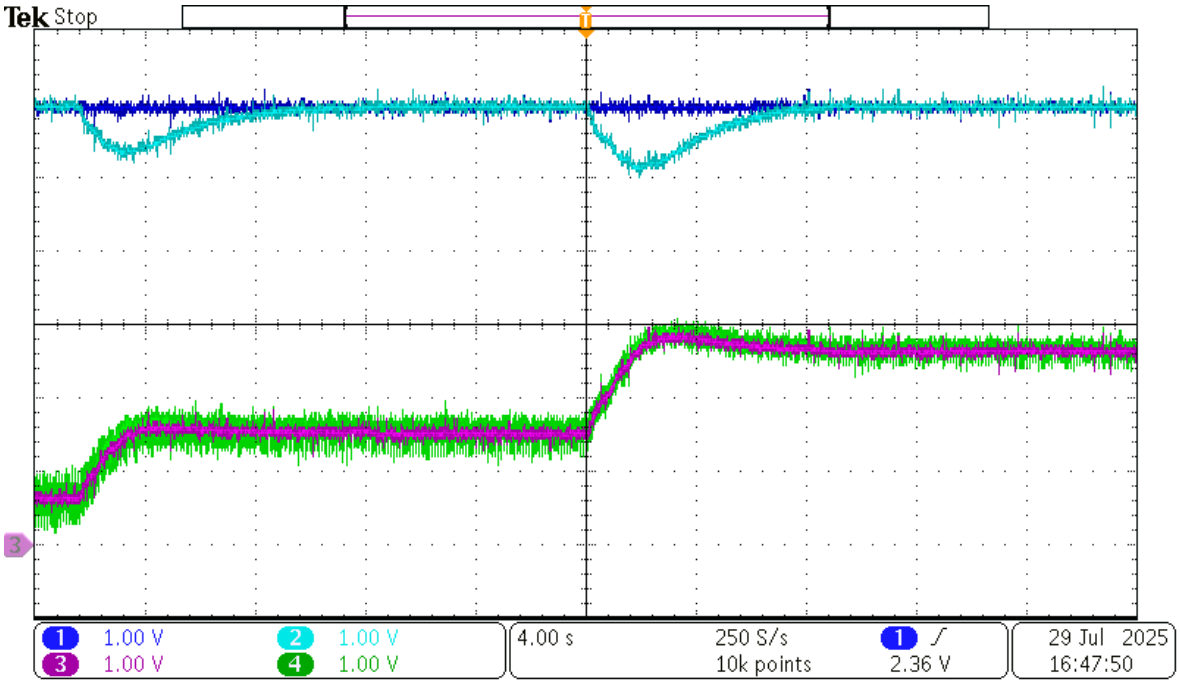

Figure 4.16: Test Case 11: Channel 1 = n_{ref} (scale: 100 RPM = 1 V = 0.5 division), Channel 2 = n_m (scale: 100 RPM = 1 V = 0.5 division), Channel 3 = $i_{2q_{ref}}$ (scale: 1 A = 1 V = 1 division), Channel 4 = i_{2q} (scale: 1 A = 1 V = 1 division), (Time scale: 1 division = 2 s)

It is very evident from the result that the speed tracking performance has significantly improved by a large margin, with the drop in BDFRM speed at changing load now being 175 RPM (reduced from over 300 RPM in Test case 4 and 7 with PI based current controller), and the speed recovery time taken for the machine to go back to it's original speed being only 8 seconds. Thus a reduction of 57 seconds is observed in the recovery time as compared to the test case 4 with PI based current controller.

The next subsections investigate the performance of the BDFRM control setup when this re-tuned speed controller with the new gains is paired with PI based current controllers.

4.5.5 Test Case 12

In this test case, the BDFRM is operated in BDFRM mode, and hence speed control is enabled. PI based controller is used for speed control. The gains of this re-tuned speed PI controller are as follows: $K_p = 0.0075$ and $K_i = 0.0028$. The primary winding is supplied with a constant voltage and constant frequency through the primary winding converter. The constant voltage and frequency applied to the primary winding are as follows: $V_{1d} = 0, V_{1q} = 87$ and $f_1 = 60$. The secondary winding supply is regulated to control the

BDFRM speed. PI based current controllers are used to control the secondary winding current without LPF implementation in the current control loop. The gains of these PI based current controllers are as follows: $K_{p(I_{2d,q})} = 75$ and $K_{i(I_{2d,q})} = 50$. In this test case the BDFRM is operated under no-load. Lastly, in this test case, the speed of the BDFRM is varied from 400 RPM to 800 RPM. Thus, the frequency applied to the secondary winding is varied from $f_2 = -20$Hz to $f_2 = +20$Hz to satisfy the condition in the equation 2.1.

Figure 4.17 displays the speed and current tracking performance of the BDFRM for the reference speed change.

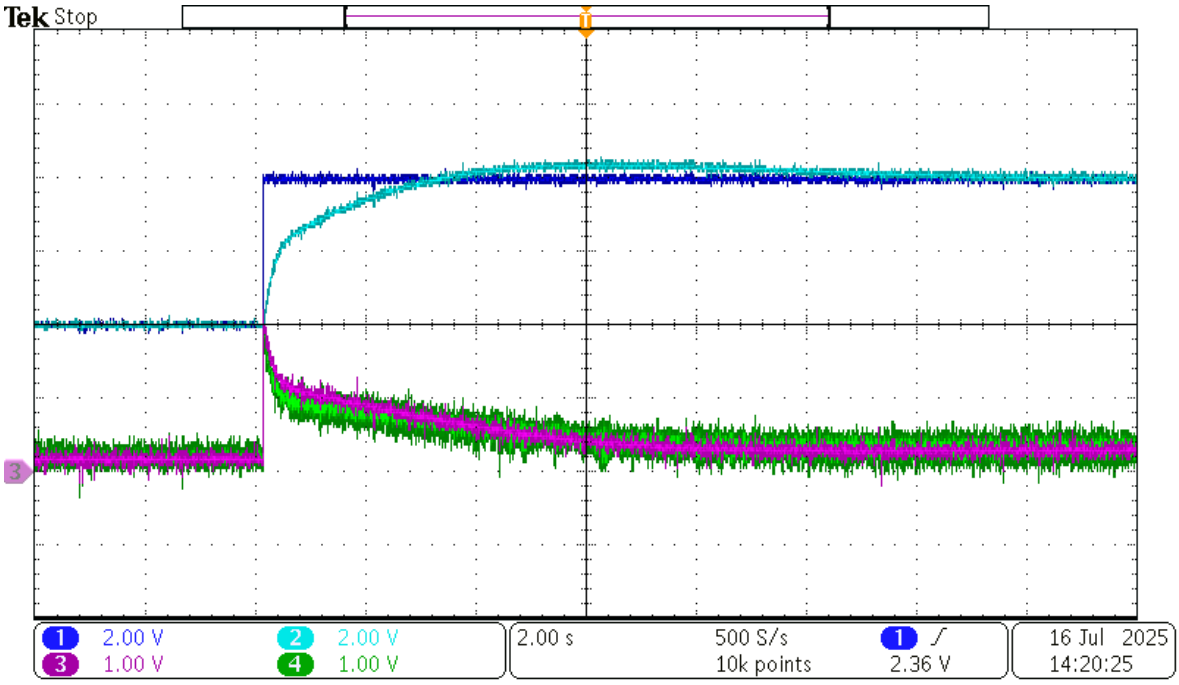

Figure 4.17: Test Case 12: Channel 1 = n_{ref} (scale: 100 RPM = 1 V = 0.5 division), Channel 2 = n_m (scale: 100 RPM = 1 V = 0.5 division), Channel 3 = $i_{2q_{ref}}$ (scale: 1 A = 1 V = 1 division), Channel 4 = i_{2q} (scale: 1 A = 1 V = 1 division), (Time scale: 1 division = 2 s)

The result reveals that the speed response deteriorates under PI control with re-tuned speed controller, with a peak overshoot of 35 RPM and an extended settling time of around 14 seconds. Thus, the speed trajectory has higher overshoot and is slower to settle.

4.5.6 Test Case 13

In this test case, the BDFRM is operated in BDFRM mode, and hence speed control is enabled. PI based controller is used for speed control. The gains of this re-tuned speed PI controller are as follows: $K_p = 0.0075$

and $K_i = 0.0028$. The primary winding is supplied with a constant voltage and constant frequency through the primary winding converter. The constant voltage and frequency applied to the primary winding are as follows: $V_{1d} = 0, V_{1q} = 87$ and $f_1 = 60$. The secondary winding supply is regulated to control the BDFRM speed. PI based current controllers are used to control the secondary winding current without LPF implementation in the current control loop. The gains of these PI based current controllers are as follows: $K_{p(I_{2d,q})} = 75$ and $K_{i(I_{2d,q})} = 50$. In this test case the BDFRM is operated at constant speed of 1200 RPM. Thus, the frequency applied to the secondary winding is $f_2 = +60$Hz to satisfy the condition in the equation 2.1. Lastly, in this test case, the load on the BDFRM is varied from No-load (0.77 N-m)→1.65 N-m→2.55 N-m by varying the resistance value of the 3 phase resistor bank connected to the PMSM stator.

When the same re-tuned speed controller is paired with PI-based current controllers with no filter, and the machine is tested for a load change at constant speed of 1200 RPM, the machine faults, indicating that the PI based current controller becomes unstable when paired with the re-tuned speed controller for a load change. Thereby, indicating the lack of robustness of the PI based current controller against changing speed controller gains, and proving that the results obtained in Test Cases 3 and 4 are the best results that can be obtained from PI based current controller with no filter for this BDFRM system.

4.6 BDFRM Mode: PSO Tuned DTSTSM based Current Controller

This section presents the test cases 14 and 15 where the tests are performed on the BDFRM in BDFRM mode, while DTSTSM based controllers are used to control the secondary winding current of the BDFRM. The gains of these controllers in this section are obtained from Particle Swarm Optimization algorithm. The following subsection provides details on the PSO based gain design applied and the resultant gains obtained from this algorithm. This subsection will then be followed by the test cases.

4.6.1 PSO based Gain Design

To ensure suitable dynamic responses and improved robustness against nonlinearities and disturbances, this research work proposes the use of Particle Swarm Optimization (PSO) algorithm to tune the Discrete Time Super Twisting Sliding Mode (DTSTSM) controller gains. By employing PSO for gain tuning, the present work ensures that the DTSTSM controllers are finely tuned to deliver the best possible performance while mitigating the typical issues of overshoot and ripple, contributing to the overall effectiveness and robustness of the BDFRM control system.

The detailed process of utilizing PSO to obtain the optimal controller gains is described in the previous chapter. After following that procedure, the optimal DTSTSM controller gains obtained from the PSO are: $K_{1(I_{2d})} = 43$, $K_{2(I_{2d})} = 40000$, $K_{1(I_{2q})} = 50$, and $K_{2(I_{2q})} = 50000$. The DTSTSM controllers are now configured with these optimal gains and the performance of the BDFRM control system with these optimally tuned DTSTSM controllers used as current controllers is further investigated in the next subsections.

4.6.2 Test Case 14

In this test case, the BDFRM is operated in BDFRM mode, and hence speed control is enabled. PI based controller is used for speed control. The gains of this re-tuned speed PI controller are as follows: $K_p = 0.0075$ and $K_i = 0.0028$. The primary winding is supplied with a constant voltage and constant frequency through the primary winding converter. The constant voltage and frequency applied to the primary winding are as follows: $V_{1d} = 0$V , $V_{1q} = 87$V and $f_1 = 60$Hz. The secondary winding supply is regulated to control the BDFRM speed. DTSTSM based current controllers are used to control the secondary winding current. The gains of these DTSTSM based current controllers, obtained through PSO based gain design, are as follows: $K_{1(I_{2d})} = 43$, $K_{2(I_{2d})} = 40000$, $K_{1(I_{2q})} = 50$, and $K_{2(I_{2q})} = 50000$. The sampling frequency of these DTSTSM controllers is 20 kHz. In this test case the BDFRM is operated under no-load. Lastly, in this test case, the speed of the BDFRM is varied from 400 RPM to 800 RPM. Thus, the frequency applied to the secondary winding is varied from $f_2 = -20$Hz to $f_2 = +20$Hz to satisfy the condition in the equation 2.1.

Figure 4.18 illustrates the speed and current tracking performance of the BDFRM for a reference speed change from 400 RPM to 800 RPM.

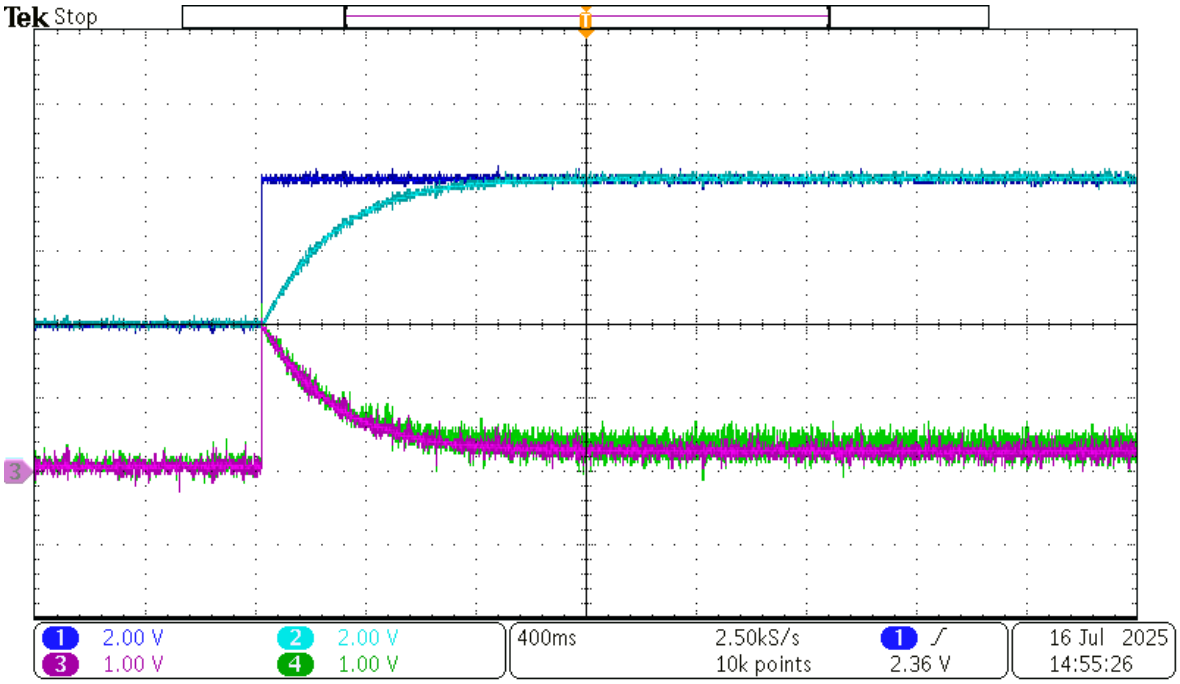

Figure 4.18: Test Case 14: Channel 1 = n_{ref} (scale: 100 RPM = 1 V = 0.5 division), Channel 2 = n_m (scale: 100 RPM = 1 V = 0.5 division), Channel 3 = $i_{2q_{ref}}$ (scale: 1 A = 1 V = 1 division), Channel 4 = i_{2q} (scale: 1 A = 1 V = 1 division), (Time scale: 1 division = 400 ms)

In this result, the observed settling time for the speed response is approximately 1 second. The settling time is reduced by 10 seconds as compared to test case 3. It is a good speed response but it is marginally slower than the response achieved using manually tuned gains. However, this configuration significantly enhances the quality of current tracking, as observed by a noticeable reduction in i_{2q} ripple.

While the PSO tuned DTSTSM controller provides improved current regulation, it exhibits slightly diminished performance in dynamic speed response. This could be attributed to the limitation of the PSO optimization process itself where the tuning was based on a model of the BDFRM described earlier in chapter 2, which does not incorporate the unwanted system harmonics. These omitted dynamics, illustrated in Fig. 4.6, introduce a discrepancy between the model based design and the actual experimental performance.

4.6.3 Test Case 15

In this test case, the BDFRM is operated in BDFRM mode, and hence speed control is enabled. PI based controller is used for speed control. The gains of this re-tuned speed PI controller are as follows: $K_p = 0.0075$ and $K_i = 0.0028$. The primary winding is supplied with a constant voltage and constant frequency through

the primary winding converter. The constant voltage and frequency applied to the primary winding are as follows: $V_{1d} = 0$V , $V_{1q} = 87$V and $f_1 = 60$Hz. The secondary winding supply is regulated to control the BDFRM speed. DTSTSM based current controllers are used to control the secondary winding current. The gains of these DTSTSM based current controllers, obtained through PSO based gain design, are as follows: $K_{1(I_{2d})} = 43$, $K_{2(I_{2d})} = 40000$, $K_{1(I_{2q})} = 50$, and $K_{2(I_{2q})} = 50000$. The sampling frequency of these DTSTSM controllers is 20 kHz. In this test case the BDFRM is operated at a constant speed of 1200 RPM. Thus, the frequency applied to the secondary winding is $f_2 = +60$Hz to satisfy the condition in the equation 2.1. Lastly, in this test case, the load on the BDFRM is varied from No-load (0.77 N-m)→1.65 N-m→2.55 N-m by varying the resistance value of the 3 phase resistor bank connected to the PMSM stator.

Figure. 4.19 presents the speed and current tracking performance of the BDFRM when subjected to this load change.

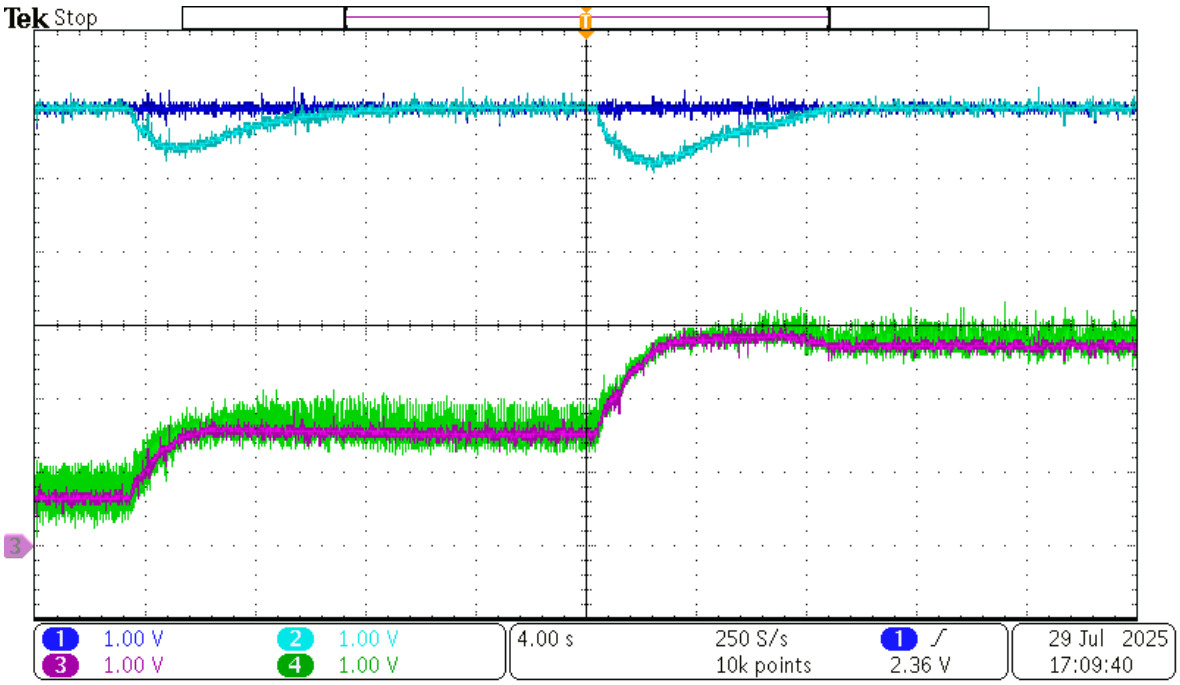

Figure 4.19: Test Case 15: Channel 1 = n_{ref} (scale: 100 RPM = 1 V = 0.5 division), Channel 2 = n_m (scale: 100 RPM = 1 V = 0.5 division), Channel 3 = $i_{2q_{ref}}$ (scale: 1 A = 1 V = 1 division), Channel 4 = i_{2q} (scale: 1 A = 1 V = 1 division), (Time scale: 1 division = 2 s)

From these results, it can be observed that the speed recovery time in this test case is approximately 9 seconds (reduced by 56 seconds as compared to test case 4), and the speed drop observed is approximately 175 RPM. Thus, the speed tracking response for PSO tuned DTSTSM based current controller for constant

speed, load change scenario is better than test case 4 with PI based current controller, however it is also marginally slower compared to manually tuned DTSTSM based current controller.

4.7 Summary of Results

This section provides a brief summary of the results obtained from all the test cases.

4.7.1 No-Load, Speed Change Tests

Table 4.3 summarizes the results obtained for the test cases, in which the BDFRM is operated in the BDFRM mode, at no-load and the reference speed is varied from 400 to 800 RPM, i.e. the test cases 3, 6, 8, 10, 12 and 14. The results are in terms of settling time and speed overshoot.

Table 4.3: Summary of Results (No-load, Speed Change Tests)

Test Case	Speed Controller	Current Controller	LPF	**No Load, Speed Change**	
				400 → 800 RPM	
				Settling Time	**Overshoot**
3	PI	PI	×	12 s	-
6	PI	PI	✓	10 s	-
8	PI	DTSTSM (Manually tuned)	×	2 s	-
10	PI (re-tuned)	DTSTSM (Manually tuned)	×	0.8 s	-
12	PI (re-tuned)	PI	×	16 s	35
14	PI (re-tuned)	DTSTSM (PSO tuned)	×	1 s	-

As it can be seen from the table, the best performance among all test cases for no-load, speed change condition is observed for test case 10. This test case corresponds to BDFRM operation in BDFRM mode with re-tuned PI based speed controller and manually tuned DTSTSM based current controllers used for secondary winding current control.

4.7.2 Constant Speed, Load Change Tests

Table 4.4 summarizes the results obtained for the test cases, in which the BDFRM is operated in the BDFRM mode, at 1200 RPM and the load on the machine is varied from No-load (0.77 N-m)→1.65 N-m→2.55 N-m, i.e. the test cases 4, 7, 9, 11, 13 and 15. The results are in terms of speed recovery time and speed drop.

Table 4.4: Summary of Results (Constant Speed, Load Change Tests)

Test Case	Speed Controller	Current Controller	LPF	**1200 RPM, Load Change**	
				0.77 → 1.65 → 2.55 N.m	
				Speed Recovery Time	**Speed Drop**
4	PI	PI	×	65 s	≅ 300 RPM
7	PI	PI	✓	60 s	≅ 300 RPM
9	PI	DTSTSM (Manually tuned)	×	50 s	≅ 300 RPM
11	PI (re-tuned)	DTSTSM (Manually tuned)	×	8 s	≅ 175 RPM
13	PI (re-tuned)	PI	×	Fault	Fault
15	PI (re-tuned)	DTSTSM (PSO tuned)	×	9 s	≅ 175 RPM

As it can be seen from the table, the best performance among all test cases for constant speed, load change condition is observed for test case 11. This test case corresponds to BDFRM operation in BDFRM mode with re-tuned PI based speed controller and manually tuned DTSTSM based current controllers used for secondary winding current control.

Thus, overall based on the results obtained for all the test cases for both no-load, speed change condition and constant speed, load change condition, it can be concluded that the BDFRM speed control response is most superior when manually tuned DTSTSM based current controllers are used for the secondary winding current control, along with re-tuned PI based speed controller for enhanced performance.

Chapter 5

Conclusion

This chapter provides a comprehensive summary of the motivation behind this research work, the experiments performed, the observations made, followed by concluding remarks.

5.1 Summary

This Thesis begins with an introduction to the BDFRM and understanding it's operation. Chapter 1 discusses the advantages offered by the BDFRMs compared to other conventionally used machines, and hence highlights the need for advancement in the research for BDFRM control.

In Chapter 2 a thorough literature review on the historical development of the machine is carried out, with a detailed description of the different control strategies proposed for BDFRM control over time. Space Vector Modeling is carried out to develop a model for the BDFRM which is subsequently used in this research work to perform simulations. Upon reviewing the past work carried out in the field of BDFRM control, a research gap is identified in which a simple, low computational cost effective non-linear control strategy like Sliding Mode Control for BDFRM had not been previously investigated for low inertia BDFRM drive systems and no experimental validation for such strategy had been previously done. Thus, as a conclusion to fill this research gap and provide significant contribution to advance the field of BDFRM control, this research work proposes the use of a Discrete Time Super-Twisting Sliding Mode Controller for current control of a BDFRM, to subsequently control the machine effectively.

Chapter 3 provides a detailed control strategy proposed to control the BDFRM, using the DTSTSM controller for the current control implementation. A detailed description of the two operating modes of the BDFRM, namely Open loop cascade Induction Mode and Conventional BDFRM mode, based on two converter based operation is presented, followed by the FOC based contol strategy to regulate the secondary

winding current to control the speed of the BDFRM is presented, along with detailed description of the DTSTSM controller that is to be implemented for the secondary winding current control. Furthermore, the gain design of the DTSTSM controllers is carried out using PSO, and the process of doing so is also outlined in this chapter.

Chapter 4 presents the experimental setup, followed by the tests that were carried out and the subsequent results that were obtained. Initially in Section 4.2, Test Case 1, the BDFRM is started in open loop cascade induction mode from standstill and the current waveforms for the secondary winding are analyzed. Followed by section 4.3 where the BDFRM is run in BDFRM mode using PI controllers for secondary winding current control without LPF, and the results from this test are used as a comparison benchmark onto which the results obtained from the proposed control strategy are compared. A thorough analysis of the harmonics present in the secondary winding current of the BDFRM is also performed, further highlighting the challenges faced by a linear controller like PI controller to regulate the machine current. This is followed by section 4.4, in which the BDFRM is operated in BDFRM mode, with PI controllers used as secondary winding current controllers along with Second Order Low Pass Filter implemented in the secondary winding current feedback loop to suppress the effects of the harmonics present before feeding them to the PI controllers. This section is then followed by section 4.5, in which the BDFRM is run in BDFRM mode using the proposed non linear DTSTSM controller as secondary winding current controllers to completely combat the challenge of dealing with the unwanted harmonics in the system, with the gains of these controllers being set through manual tuning. This is then followed by section 4.6, where BDFRM tests are performed by operating the machine in BDFRM mode, using the proposed DTSTSM controller as the secondary winding current controllers with the gain of these controllers obtained from the proposed PSO based gain design approach to obtain optimal performance. All of these sections outlined above consist of different test cases that include the information of the test being carried out, the results obtained from these tests and the observations made. Lastly the final section 4.7 of this chapter summarizes all the results for all the test cases.

5.2 Final Remarks

In section 4.2, from the results of test case 1, it can be concluded that significant harmonics are present in the secondary winding current of the BDFRM.

In section 4.3 which employs PI based current controllers without an LPF, the results from test case 2 indicate significant presence of harmonics in the secondary winding current and the frequencies of these harmonics change with the speed of the BDFRM. These harmonic frequencies approach the control frequency as speed lowers, with the harmonic frequencies being exactly the same as the control frequency at stand still

condition. Thereby, it is concluded that BDFRM control at lower speeds is the most challenging. Test case 3 (no-load, speed change) shows that the BDFRM exhibits poor speed response with a settling time exceeding 12 seconds, while test case 4 (constant speed, load change) also demonstrates poor performance with a speed recovery time of over 65 seconds. This demonstrates the inability of PI controllers to handle system nonlinearities and harmonics. The results obtained from test cases 3 and 4 serve as benchmarks for comparison, representing conventional PI control without LPF implementation.

In section 4.4 which employs PI based current controllers with an LPF, test case 5 shows that using a second order LPF in the current feedback loop reduces harmonic content fed to the PI controller, yielding smoother output with less ripple and steady state error. Test case 6 (no-load, speed change) demonstrates improved speed response with a reduced settling time of 10 seconds (2 seconds less than test case 3). In test case 7 (constant speed, load change), the speed tracking remains similar to test case 4 with a 60 second speed recovery time (5 seconds less than test case 4), though large oscillations in i_{2q} suggest possible instability under larger load changes. Overall, adding an LPF provides limited improvement, and the PI based current controllers still exhibit poor speed response.

In section 4.5, which employs manually tuned DTSTSM based current controllers, test case 8 (no-load, speed change) demonstrates a far superior speed response with a settling time of 2 seconds (10 seconds less than test case 3). In test case 9 (constant speed, load change), response remains comparable to test cases 4 and 7 with a speed recovery time of 50 seconds (15 seconds less than test case 4). To further enhance speed response, the PI based speed controller is re-tuned, as shown in test cases 10 and 11. Test case 10 (no-load, speed change) exhibits an even lower settling time of 0.8 seconds (11.2 seconds less than test case 3), while test case 11 (constant speed, load change) achieves a speed recovery time of 8 seconds (57 seconds less than test case 4). These results indicate that manually tuned DTSTSM current controllers provide far superior speed control compared to PI based controllers.

In the final section 4.6 which employs PSO tuned DTSTSM based current controllers, test case 14 (no-load, speed change) shows a settling time of 1 second (11 seconds less than test case 3) with low current tracking error, and test case 15 (constant speed, load change) shows a speed recovery time of 9 seconds (56 seconds less than test case 4). Thus, PSO tuned DTSTSM controllers outperform PI based controllers, though their performance is slightly inferior to manually tuned DTSTSM controllers due to the limitations of the BDFRM model run inside PSO, that neglect harmonic effects.

Overall, conventional linear PI based current controllers perform extremely poorly under harmonic rich conditions, such as in a BDFRM drive system. Adding low pass filters provides slight improvement for constant load, speed changing conditions, but significantly degrades performance under constant speed, load changing conditions, even indicating potential instability under large load changes. In contrast, the proposed

DTSTSM based current controller demonstrates far superior performance. The manually tuned DTSTSM achieves a settling time of 0.8 seconds and a speed recovery time of 8 seconds, offering excellent tracking and transient performance while maintaining stability across a wide range of gain values. These results establish the DTSTSM controller as a robust and effective alternative to conventional PI controllers, making it the ideal choice for BDFRM systems dominated by nonlinearities and harmonics.

Bibliography

[1] G. G. Karady and K. E. Holbert, *Electric Power System*, pp. 1–48. 2005.

[2] "2024 Long-Term Outlook."

[3] P. W. a. G. S. C. Government of Canada, "Canada Gazette, Part 2, Volume 158, Number 26: Clean Electricity Regulations," Dec. 2024. Last Modified: 2025-02-26 Publisher: Government of Canada, Public Works and Government Services Canada, Integrated Services Branch, Canada Gazette.

[4] E. G. Garrison, *History of Engineering and Technology: Artful Methods*. CRC Press, June 1998. Google-Books-ID: 5mvVElGudyYC.

[5] "Galileo Ferraris - Engineering Hall of Fame."

[6] S. J. Chapman, *Electric machinery fundamentals*. New York: McGraw-Hill Higher Education, 4th ed. ed., 2005.

[7] A. Boglietti, A. Cavagnino, M. Pastorelli, D. Staton, and A. Vagati, "Thermal analysis of induction and synchronous reluctance motors," *Industry Applications, IEEE Transactions on*, vol. 42, pp. 675 – 680, 06 2006.

[8] P. Pillay and R. Krishnan, "Modeling, simulation, and analysis of permanent-magnet motor drives. i. the permanent-magnet synchronous motor drive," *IEEE Transactions on Industry Applications*, vol. 25, pp. 265–273, 1989.

[9] B. Bilgin, J. W. Jiang, and A. Emadi, eds., *Switched Reluctance Motor Drives: Fundamentals to Applications*. Boca Raton: CRC Press, Apr. 2019.

[10] J. Gieras, "Design of permanent magnet brushless motors for high speed applications," *2014 17th International Conference on Electrical Machines and Systems, ICEMS 2014*, 01 2015.

[11] V. Balaram, "Rare earth elements: A review of applications, occurrence, exploration, analysis, recycling, and environmental impact," *Geoscience Frontiers*, vol. 10, no. 4, pp. 1285–1303, 2019.

[12] D. A. Staton, T. J. E. Miller, and S. E. Wood, "Maximising the saliency ratio of the synchronous reluctance motor," 1993.

[13] M. Krishnamurthy, C. Edrington, A. Emadi, P. Asadi, M. Ehsani, and B. Fahimi, "Making the case for applications of switched reluctance motor technology in automotive products," *Power Electronics, IEEE Transactions on*, vol. 21, pp. 659 – 675, 06 2006.

[14] Y. Okamoto, R. Hoshino, S. Wakao, and T. Tsuburaya, "Improvement of torque characteristics for a synchronous reluctance motor using mma-based topology optimization method," *IEEE Transactions on Magnetics*, vol. 54, pp. 1–4, 2018.

[15] L. Xu and W. Cheng, "Torque and reactive power control of a doubly fed induction machine by position sensorless scheme," *IEEE Transactions on Industry Applications*, vol. 31, no. 3, pp. 636–642, 1995.

[16] H. Chaal and M. Jovanovic, "Practical implementation of sensorless torque and reactive power control of doubly fed machines," *IEEE Transactions on Industrial Electronics*, vol. 59, no. 6, pp. 2645–2653, 2012.

[17] A. Stefani, A. Yazidi, C. Rossi, F. Filippetti, D. Casadei, and G.-A. Capolino, "Doubly fed induction machines diagnosis based on signature analysis of rotor modulating signals," *IEEE Transactions on Industry Applications*, vol. 44, no. 6, pp. 1711–1721, 2008.

[18] H. Li and Z. Chen, "Overview of different wind generator systems and their comparisons," *IET Renewable Power Generation*, vol. 2, pp. 123–138, June 2008. Publisher: The Institution of Engineering and Technology.

[19] F. Zhang, S. Yu, H. Wang, Y. Wang, and D. Wang, "Overview of research and development status of brushless doubly-fed machine system," *Chinese Journal of Electrical Engineering*, vol. 2, no. 2, pp. 1–13, 2016.

[20] R. Li, A. Wallace, and R. Spee, "Dynamic simulation of brushless doubly-fed machines," *IEEE Transactions on Energy Conversion*, vol. 6, no. 3, pp. 445–452, 1991.

[21] L. Hunt, "The cascade induction motor," *Journal of the Institution of Electrical Engineers*, vol. 52, pp. 406–426, Mar. 1914.

[22] R. Betz and M. Jovanovic, "Introduction to the Space Vector Modeling of the Brushless Doubly Fed Reluctance Machine," *Electric Power Components and Systems - ELECTR POWER COMPON SYST*, vol. 31, pp. 729–755, Aug. 2003.

[23] R. Betz and M. Jovanovic, "The brushless doubly fed reluctance machine and the synchronous reluctance machine-a comparison," *IEEE Transactions on Industry Applications*, vol. 36, pp. 1103–1110, July 2000. Conference Name: IEEE Transactions on Industry Applications.

[24] E. M. Schulz and R. E. Betz, "Use of doubly fed reluctance machines in wind power generation," in *2006 12th International Power Electronics and Motion Control Conference*, pp. 1901–1906, 2006.

[25] R. S. Rebeiro and A. M. Knight, "Characterization of a ducted rotor brushless doubly fed reluctance machine," *IEEE Transactions on Energy Conversion*, vol. 34, no. 1, pp. 79–87, 2019.

[26] S. Khaliq, M. Modarres, T. A. Lipo, and B.-I. Kwon, "Design of Novel Axial-Flux Dual Stator Doubly Fed Reluctance Machine," *IEEE Transactions on Magnetics*, vol. 51, pp. 1–4, Nov. 2015. Conference Name: IEEE Transactions on Magnetics.

[27] S. Khaliq, S. Atiq, T. A. Lipo, and B.-I. Kwon, "Rotor pole optimization of novel axial-flux brushless doubly fed reluctance machine for torque enhancement," *IEEE Transactions on Magnetics*, vol. 52, no. 7, pp. 1–4, 2016.

[28] A. M. Knight, R. E. Betz, and D. G. Dorrell, "Design and Analysis of Brushless Doubly Fed Reluctance Machines," *IEEE Transactions on Industry Applications*, vol. 49, pp. 50–58, Jan. 2013. Conference Name: IEEE Transactions on Industry Applications.

[29] A. Broadway, "Cageless induction machine," *Proceedings of the Institution of Electrical Engineers*, vol. 118, pp. 1593–1600, Nov. 1971. Publisher: The Institution of Engineering and Technology.

[30] A. Broadway and L. Burbridge, "Self-cascaded machine: a low-speed motor or high-frequency brushless alternator," *Proceedings of the Institution of Electrical Engineers*, vol. 117, pp. 1277–1290, July 1970. Publisher: The Institution of Engineering and Technology.

[31] L. Xu, F. Liang, and T. Lipo, "Transient model of a doubly excited reluctance motor," *IEEE Transactions on Energy Conversion*, vol. 6, pp. 126–133, Mar. 1991. Conference Name: IEEE Transactions on Energy Conversion.

[32] Y. Fan, K. Chau, and S. Niu, "Development of a New Brushless Doubly Fed Doubly Salient Machine for Wind Power Generation," *IEEE Transactions on Magnetics*, vol. 42, pp. 3455–3457, Oct. 2006.

[33] O. Ojo and Z. Wu, "Synchronous operation of a dual-winding reluctance generator," *IEEE Transactions on Energy Conversion*, vol. 12, no. 4, p. 357, 1997.

[34] R. Betz and M. Jovanovic, "Theoretical analysis of control properties for the brushless doubly fed reluctance machine," *IEEE Transactions on Energy Conversion*, vol. 17, pp. 332–339, Sept. 2002. Conference Name: IEEE Transactions on Energy Conversion.

[35] Y. Liao, L. Xu, and L. Zhen, "Design of a doubly fed reluctance motor for adjustable-speed drives," *IEEE Transactions on Industry Applications*, vol. 32, pp. 1195–1203, Sept. 1996. Conference Name: IEEE Transactions on Industry Applications.

[36] E. Schulz and R. Betz, "Optimal rotor design for brushless doubly fed reluctance machines," in *38th IAS Annual Meeting on Conference Record of the Industry Applications Conference, 2003.*, vol. 1, pp. 256–261 vol.1, Oct. 2003.

[37] D. Dorrell, I. Scian, E. Schulz, R. Betz, and M. Jovanovic, "Electromagnetic Considerations in the Design of Doubly-Fed Reluctance Generators for use in Wind Turbines," pp. 4272–4277, Dec. 2006.

[38] L. Xu, L. Zhen, and E.-H. Kim, "Field-orientation control of a doubly excited brushless reluctance machine," *IEEE Transactions on Industry Applications*, vol. 34, pp. 148–155, Jan. 1998. Conference Name: IEEE Transactions on Industry Applications.

[39] F. Liang, L. Xu, and T. A. Lipo, "d-q ANALYSIS OF A VARIABLE SPEED DOUBLY AC EXCITED RELUCTANCE MOTOR," *Electric Machines & Power Systems*, vol. 19, pp. 125–138, Mar. 1991.

[40] S. Williamson, A. Ferreira, and A. Wallace, "Generalised theory of the brushless doubly-fed machine. Part 1: Analysis," in *IEE Proceedings - Electric Power Applications*, vol. 144, p. 111, 1997. ISSN: 13502352 Issue: 2 Journal Abbreviation: IEE Proc., Electr. Power Appl.

[41] R. A. McMahon, P. C. Roberts, X. Wang, and P. J. Tavner, "Performance of BDFM as generator and motor," *IEE proceedings. Electric power applications.*, vol. 153, Mar. 2006. Publisher: IET.

[42] L. Xu, B. Guan, H. Liu, L. Gao, and K. Tsai, "Design and control of a high-efficiency Doubly-Fed Brushless machine for wind power generator application," in *2010 IEEE Energy Conversion Congress and Exposition*, pp. 2409–2416, Sept. 2010. ISSN: 2329-3748.

[43] I. Scian, D. Dorrell, and P. Holik, "Assessment of Losses in a Brushless Doubly-Fed Reluctance Machine," *IEEE Transactions on Magnetics*, vol. 42, pp. 3425–3427, Oct. 2006. Conference Name: IEEE Transactions on Magnetics.

[44] E. Schulz and R. Betz, "Impact of winding and gap flux density harmonics on brushless doubly fed reluctance machines," in *Second International Conference on Power Electronics, Machines and Drives (PEMD 2004).*, vol. 2, pp. 487–491 Vol.2, Mar. 2004. ISSN: 0537-9989.

[45] P. J. Tavner, M. Jagiela, T. Chick, and E. Abdi-Jalebi, "A Brushless Doubly Fed Machine for use in an Integrated Motor/Converter, Considering the Rotor Flux," in *2006 3rd IET International Conference on Power Electronics, Machines and Drives - PEMD 2006*, pp. 601–605, Apr. 2006.

[46] A. M. Knight, R. E. Betz, and D. Dorrell, "Design principles for brushless doubly fed reluctance machines," in *IECON 2011 - 37th Annual Conference of the IEEE Industrial Electronics Society*, pp. 3602–3607, Nov. 2011. ISSN: 1553-572X.

[47] D. G. Dorrell, A. M. Knight, and R. E. Betz, "Issues with the design of brushless doubly-fed reluctance machines: Unbalanced magnetic pull, skew and iron losses," in *2011 IEEE International Electric Machines & Drives Conference (IEMDC)*, pp. 663–668, May 2011.

[48] S. Tohidi, M. R. Zolghadri, H. Oraee, and A. Oraee, "Dynamic modeling of a wind turbine with brushless doubly fed induction generator," in *2012 3rd Power Electronics and Drive Systems Technology (PEDSTC)*, pp. 490–494, Feb. 2012.

[49] S. Shao, E. Abdi, and R. McMahon, "Low-Cost Variable Speed Drive Based on a Brushless Doubly-Fed Motor and a Fractional Unidirectional Converter," *IEEE Transactions on Industrial Electronics*, vol. 59, pp. 317–325, Jan. 2012. Conference Name: IEEE Transactions on Industrial Electronics.

[50] M. Ruviaro, F. Runcos, N. Sadowski, and I. M. Borges, "Analysis and Test Results of a Brushless Doubly Fed Induction Machine With Rotary Transformer," *IEEE Transactions on Industrial Electronics*, vol. 59, pp. 2670–2677, June 2012. Conference Name: IEEE Transactions on Industrial Electronics.

[51] R. S. Rebeiro, "Design, Analysis, Implementation and Operation of a Brushless Doubly Fed Reluctance Motor Drive," June 2018.

[52] R. S. Rebeiro and A. M. Knight, "Two-Converter-Based Frequency-Sharing Operation and Control of a Brushless Doubly Fed Reluctance Motor Drive," *IEEE Transactions on Industry Applications*, vol. 55, pp. 5873–5880, Nov. 2019. Conference Name: IEEE Transactions on Industry Applications.

[53] S. Agrawal, A. Province, and A. Banerjee, "An Approach to Maximize Torque Density in a Brushless Doubly Fed Reluctance Machine," *IEEE Transactions on Industry Applications*, vol. 56, pp. 4829–4838, Sept. 2020. Conference Name: IEEE Transactions on Industry Applications.

[54] Y. Liao, L. Zhen, and L. Xu, "Design of a doubly-fed reluctance motor for adjustable speed drives," in *Proceedings of 1994 IEEE Industry Applications Society Annual Meeting*, vol. 2, pp. 305–312 vol.1, Oct. 1994.

[55] M.-F. Hsieh, Y.-H. Chang, and D. G. Dorrell, "Design and Analysis of Brushless Doubly Fed Reluctance Machine for Renewable Energy Applications," *IEEE Transactions on Magnetics*, vol. 52, pp. 1–5, July 2016. Conference Name: IEEE Transactions on Magnetics.

[56] E. D. Fankem, C. J. Kendeg Onla, W. Xiaoyan, A. Dountio, and Y. Effa, "Modelling of brushless doubly fed reluctance machines based on reluctance network model," *IET Electric Power Applications*, vol. 15, June 2021.

[57] F. Zhang, S. Yu, H. Wang, Y. Wang, and D. Wang, "Overview of research and development status of brushless doubly-fed machine system," *Chinese Journal of Electrical Engineering*, vol. 2, pp. 1–13, Dec. 2016. Conference Name: Chinese Journal of Electrical Engineering.

[58] M. Jovanovic, "Brushless Doubly Fed Reluctance Machines: An Emerging Technology," *International Journal of Emerging Electric Power Systems*, vol. 8, Jan. 2007. Publisher: De Gruyter.

[59] O. Sadeghian, S. Tohidi, B. Mohammadi-Ivatloo, and F. Mohammadi, "A Comprehensive Review on Brushless Doubly-Fed Reluctance Machine," *Sustainability*, vol. 13, p. 842, Jan. 2021. Number: 2 Publisher: Multidisciplinary Digital Publishing Institute.

[60] M. Jovanovic, R. Betz, and J. Yu, "The use of doubly fed reluctance machines for large pumps and wind turbines," *IEEE Transactions on Industry Applications*, vol. 38, pp. 1508–1516, Nov. 2002. Conference Name: IEEE Transactions on Industry Applications.

[61] M. Jovanovic, "Sensored and sensorless speed control methods for brushless doubly fed reluctance motors," *IET Electric Power Applications*, vol. 3, pp. 503–513, Nov. 2009. Publisher: The Institution of Engineering and Technology.

[62] M. Hassan and M. Jovanovic, "Improved scalar control using flexible DC-Link voltage in Brushless Doubly-Fed Reluctance Machines for wind applications," in *2012 2nd International Symposium On Environment Friendly Energies And Applications*, pp. 482–487, June 2012.

[63] M. G. Mousa, S. M. Allam, and E. M. Rashad, "Maximum power tracking of a grid-connected wind-driven Brushless Doubly-Fed Reluctance Generator using scalar control," in *2015 IEEE 8th GCC Conference & Exhibition*, pp. 1–6, Feb. 2015.

[64] T. Taluo, L. Ristić, and M. Jovanović, "Performance Analysis of Brushless Doubly Fed Reluctance Machines," in *2019 20th International Symposium on Power Electronics (Ee)*, pp. 1–6, Oct. 2019.

[65] M. Jovanovic, R. Betz, J. Yu, and E. Levi, "Aspects of vector and scalar control of brushless doubly fed reluctance machines," in *4th IEEE International Conference on Power Electronics and Drive Systems. IEEE PEDS 2001 - Indonesia. Proceedings (Cat. No.01TH8594)*, vol. 2, pp. 461–467 vol.2, Oct. 2001.

[66] M. Jovanovic and R. Betz, "Slip power recovery systems based on brushless doubly fed reluctance machines," in *Proceedings of the Power Conversion Conference-Osaka 2002 (Cat. No.02TH8579)*, vol. 3, pp. 987–992 vol.3, Apr. 2002.

[67] S. Ademi and M. Jovanovic, "High-efficiency control of brushless doubly-fed machines for wind turbines and pump drives," *Energy Conversion and Management*, vol. 81, pp. 120–132, May 2014.

[68] S. Ademi, M. G. Jovanović, and M. Hasan, "Control of Brushless Doubly-Fed Reluctance Generators for Wind Energy Conversion Systems," *IEEE Transactions on Energy Conversion*, vol. 30, pp. 596–604, June 2015. Conference Name: IEEE Transactions on Energy Conversion.

[69] S. Ademi and M. G. Jovanović, "Vector Control Methods for Brushless Doubly Fed Reluctance Machines," *IEEE Transactions on Industrial Electronics*, vol. 62, pp. 96–104, Jan. 2015. Conference Name: IEEE Transactions on Industrial Electronics.

[70] S. Ademi and M. Jovanović, "A novel sensorless speed controller design for doubly-fed reluctance wind turbine generators," *Energy Conversion and Management*, vol. 120, pp. 229–237, July 2016.

[71] M. G. Mousa, S. M. Allam, and E. M. Rashad, "A comparative study of vector-control strategies for maximum wind-power extraction of a grid-connected wind-driven brushless doubly-fed reluctance generator," *Australian Journal of Electrical and Electronics Engineering*, vol. 14, pp. 1–11, Apr. 2017. Publisher: EA Website _eprint: https://doi.org/10.1080/1448837X.2017.1410964.

[72] M. JOVANOVIC, J. YU, and E. LEVI, "Direct Torque Control of Brushless Doubly Fed Reluctance Machines," *Electric Power Components and Systems*, vol. 32, pp. 941–958, Oct. 2004. Publisher: Taylor & Francis _eprint: https://doi.org/10.1080/15325000490257791.

[73] M. Jovanovic, J. Yu, and E. Levi, "Real-time implementation of direct torque control scheme for brushless doubly-fed reluctance motors," in *Second International Conference on Power Electronics, Machines and Drives (PEMD 2004).*, vol. 2, pp. 752–757 Vol.2, Mar. 2004. ISSN: 0537-9989.

[74] M. Jovanovic, J. Yu, and E. Levi, "Encoderless direct torque controller for limited speed range applications of brushless doubly fed reluctance motors," *IEEE Transactions on Industry Applications*, vol. 42, pp. 712–722, May 2006. Conference Name: IEEE Transactions on Industry Applications.

[75] H. Chaal, M. Jovanovic, and K. Busawon, "Sliding Mode Observer based direct torque control of a Brushless Doubly-Fed Reluctance Machine," in *2009 IEEE Symposium on Industrial Electronics & Applications*, vol. 2, pp. 866–871, Oct. 2009.

[76] W. K. Song and D. G. Dorrell, "Improved Direct Torque Control method of brushless doubly-fed reluctance machines for wind turbine," in *2013 IEEE International Symposium on Industrial Electronics*, pp. 1–5, May 2013. ISSN: 2163-5145.

[77] W. K. Song and D. G. Dorrell, "Implementation of improved direct torque control method of brushless doubly-fed reluctance machines for wind turbine," in *2014 IEEE International Conference on Industrial Technology (ICIT)*, pp. 509–513, Feb. 2014.

[78] H. Chaal and M. Jovanovic, "Direct Power Control of Brushless Doubly-Fed Reluctance Machines," in *5th IET International Conference on Power Electronics, Machines and Drives (PEMD 2010)*, pp. 1–6, Apr. 2010.

[79] H. Chaal and M. Jovanovic, "Power control of brushless doubly-fed reluctance drive and generator systems," *Renewable Energy*, vol. 37, pp. 419–425, Jan. 2012.

[80] M. Moazen, R. Kazemzadeh, and M.-R. Azizian, "Model-based predictive direct power control of brushless doubly fed reluctance generator for wind power applications," *Alexandria Engineering Journal*, vol. 55, pp. 2497–2507, Sept. 2016.

[81] S. Jin, L. Shi, L. Zhu, W. Cao, T. Dong, and F. Zhang, "Dual Two-Level Converters Based on Direct Power Control for an Open-Winding Brushless Doubly-Fed Reluctance Generator," *IEEE Transactions on Industry Applications*, vol. 53, pp. 3898–3906, July 2017. Conference Name: IEEE Transactions on Industry Applications.

[82] F. Zhang, L. Zhu, S. Jin, X. Su, S. Ademi, and W. Cao, "Controller Strategy for Open-Winding Brushless Doubly Fed Wind Power Generator With Common Mode Voltage Elimination," *IEEE Transactions on Industrial Electronics*, vol. 66, pp. 1098–1107, Feb. 2019.

[83] V. Utkin, "Variable structure systems with sliding modes," *IEEE Transactions on Automatic Control*, vol. 22, no. 2, pp. 212–222, 1977.

[84] V. I. Utkin, *Sliding Modes in Control and Optimization*. Berlin, Heidelberg: Springer, 1992.

[85] . . Introduction, "Higher-Order Sliding Modes: L. Fridman and A. Levant," in *Sliding Mode Control In Engineering*, CRC Press, 2002. Num Pages: 50.

[86] F. Valenciaga, "Second order sliding power control for a variable speed-constant frequency energy conversion system," *Energy Conversion and Management*, vol. 51, no. 12, pp. 3000–3008, 2010.

[87] O. Oualah, D. Kerdoun, and A. Boumassata, "Super-twisting sliding mode control for brushless doubly fed reluctance generator based on wind energy conversion system," *Electrical Engineering & Electromechanics*, pp. 86–92, Mar. 2023.

[88] H. Chaal and M. Jovanovic, "Toward a Generic Torque and Reactive Power Controller for Doubly Fed Machines," *IEEE Transactions on Power Electronics*, vol. 27, pp. 113–121, Jan. 2012. Conference Name: IEEE Transactions on Power Electronics.

[89] H. Chaal and M. Jovanovic, "Practical Implementation of Sensorless Torque and Reactive Power Control of Doubly Fed Machines," *IEEE Transactions on Industrial Electronics*, vol. 59, pp. 2645–2653, June 2012. Conference Name: IEEE Transactions on Industrial Electronics.

[90] F. Valenciaga and P. F. Puleston, "Variable Structure Control of a Wind Energy Conversion System Based on a Brushless Doubly Fed Reluctance Generator," *IEEE Transactions on Energy Conversion*, vol. 22, pp. 499–506, June 2007. Conference Name: IEEE Transactions on Energy Conversion.

[91] G. Rigatos, P. Siano, and S. Ademi, "Flatness-based adaptive fuzzy control of brushless doubly-fed reluctance machines," in *2017 IEEE 26th International Symposium on Industrial Electronics (ISIE)*, pp. 1913–1920, June 2017. ISSN: 2163-5145.

[92] O. Oualah, D. Kerdoun, and A. Boumassata, "Super-twisting sliding mode control for brushless doubly fed reluctance generator based on wind energy conversion system," *Electrical Engineering & Electromechanics*, pp. 86–92, Mar. 2023.

[93] F. Valenciaga and C. Evangelista, "2-Sliding active and reactive power control of a wind energy conversion system," *IET Control Theory & Applications*, vol. 4, pp. 2479–2490, Nov. 2010. Publisher: The Institution of Engineering and Technology.

[94] A. Singh, F. P. Scalcon, and A. M. Knight, "Challenges in the control of brushless doubly fed reluctance machines," in *2025 IEEE Industry Applications Society Annual Meeting (IAS)*, pp. 1–7, 2025.

[95] F. P. Scalcon, G. Fang, R. P. Vieira, H. A. Gründling, and A. Emadi, "Discrete-time super-twisting sliding mode current controller with fixed switching frequency for switched reluctance motors," *IEEE Transactions on Power Electronics*, vol. 37, no. 3, pp. 3321–3333, 2022.

[96] J. Kennedy and R. Eberhart, "Particle swarm optimization," in *Proceedings of ICNN'95 - International Conference on Neural Networks*, vol. 4, pp. 1942–1948 vol.4, 1995.

[97] Y. Shi and R. Eberhart, "A modified particle swarm optimizer," in *1998 IEEE International Conference on Evolutionary Computation Proceedings. IEEE World Congress on Computational Intelligence (Cat. No.98TH8360)*, pp. 69–73, 1998.

[98] J. D. Broesch, *Digital Signal Processing: Instant Access.* Elsevier, 2008.